Li-growth and SEI engineering for anode-free Li-metal rechargeable batteries

Document license:
TAVERNE

DOI:
10.1016/j.ensm.2023.02.036

Document status and date:
Published: 01/03/2023

Document Version:
Publisher's PDF, also known as Version of Record (includes final page, issue and volume numbers)

Please check the document version of this publication:

• A submitted manuscript is the version of the article upon submission and before peer-review. There can be important differences between the submitted version and the official published version of record. People interested in the research are advised to contact the author for the final version of the publication, or visit the DOI to the publisher's website.
• The final author version and the galley proof are versions of the publication after peer review.
• The final published version features the final layout of the paper including the volume, issue and page numbers.

Link to publication

Li-growth and SEI engineering for anode-free Li-metal rechargeable batteries: A review of current advances

Baolin Wu [a,b], Chunguang Chen [c,d,*], Luc H.J. Raijmakers [a], Jin Liu [c,d], Dmitri L. Danilov [a,e], Rüdiger-A. Eichel [a,b], Peter H.L. Notten [a,e,f,*]

[a] *Forschungszentrum Jülich (IEK-9), D-52425, Jülich, Germany*
[b] *RWTH Aachen University, D-52074 Aachen, Germany*
[c] *LNM, Institute of Mechanics, Chinese Academy of Sciences, Beijing 100190, China*
[d] *School of Engineering Sciences, University of Chinese Academy of Sciences, Beijing 100049, China*
[e] *Eindhoven University of Technology, P.O. Box 513, 5600 MB, Eindhoven, the Netherlands*
[f] *University of Technology Sydney, Broadway, Sydney, NSW 2007, Australia*

A B S T R A C T

Li-metal battery systems are attractive for next-generation high-energy batteries due to their high theoretical specific capacity and Li-metal's low redox potential. Anode-free Li-metal batteries (AFLBs) have a higher energy density than conventional Li-metal batteries because the anode material is absent in the pristine state. An additional advantage is that the battery production costs are relatively low due to simplified anode coating processing, which makes AFLBs favorable for large-scale industrial production. Despite these advantages, commercializing AFLBs remains challenging because of the high reactivity of Li-metal and dendrite-growth issues at the anode side. The chemical and physical properties of solid-electrolyte interphase (SEI) formed at Li-metal anodes determine the Li-ion transport kinetics, Li-metal deposition behavior, and overall cycling performance. The key to resolving these issues is to grow a homogeneous Li-metal and design a stable SEI. Many approaches, such as electrolyte optimization and artificial layers design, have been developed to guide a uniform Li-metal growth and form a stable SEI, facilitating rapid Li-ion transport and suppressing Li-dendrite growth and other undesirable side reactions. An overview of these discoveries and developments in Li-growth and SEI engineering and insights into the intrinsic mechanisms of battery performance, presented in this review, is, therefore, of great interest to the battery research community.

1. Introduction

Advanced battery systems with high energy density, prolonged cycle life, and low costs promote the rapidly growing electric vehicle industry [1]. After three-decades of development, Li-ion batteries (LIBs) technology based on the Li-ion intercalation mechanism has reached a specific energy density of about 260 Wh kg^{-1} at the battery level. This technology quickly approaches its theoretical limit of 300 Wh kg^{-1} [2]. Unfortunately, currently developed batteries cannot cope with the growing demand of the future EV market, which requires specific energy densities of more than 500 Wh kg^{-1} [3]. Developing high-energy-density battery systems has received and still receives much interest in academia and industry [4].

Li-metal is considered the most promising anode material for next-generation batteries because of its high theoretical capacity (3860 mAh g^{-1}), low density (0.534 g cm^{-3}), and low electrochemical potential (3.040 V *vs.* standard hydrogen electrode) [5]. However, using excess Li-metal anodes in Li-metal batteries raises various practical

limitations due to its high reactivity, limited reversibility, and non-planar plating/stripping behavior, leading to irreversible losses of active Li-metal and electrolyte [6].

Minimizing Li-metal use would increase the potential energy density of Li-metal batteries to its highest-level format of anode-free Li-metal batteries (AFLBs) [6]. In AFLBs, the anode host is completely absent in the pristine state. A bare anode current collector (commonly Cu) is used as a Li-deposition substrate, schematically shown in Fig. 1a. After the first charging process, the plated Li-metal on the current collectors will function as anode material during the subsequent battery cycling. Because of the lack of an anode host material (or Li-metal electrode), AFLBs have the following advantages in comparison with conventional Li-ion or Li-metal batteries [7,8]:

1) The Li-metal amount in AFLBs is less than in Li-metal batteries. Pure Li-metal is not present in the Earth's crust. Extraction from Li-minerals and purification considerably increases the primary cost of raw materials. In this regard, manufacturing AFLBs results in a

List of notations

Notation	Definition
AFLBs	Anode-free Li-metal batteries
SEI	Solid-electrolyte interphase
LIB	Li-ion battery
CE	Coulombic efficiency
CEI	Cathode electrolyte interface
EC	Ethylene carbonate
PC	Propylene carbonate
DEC	Diethyl carbonate
DMC	Dimethyl carbonate
DME	Dimethyl ether
DOL	1,3-dioxolane
FDMB	Fluorinated 1,4-dimethoxylbutane
DMB	1,4-dimethoxylbutane
HFE	1,1,2,2 tetrafluoroethyl 2,2,3,3-tetrafluoropropyl ether
EMC	Ethyl methyl carbonate
FEC	Fluoroethylene carbonate
TTE	1, 1, 2, 2-tetrafluoroethyl-2, 2, 3, 3-tetrafluoropropyl ether
VC	Vinylene carbonate
PDA	Polydopamine
GO	Graphene oxide
PAN	Polyacrylonitrile
PVDF	Poly(vinylidene fluoride)
LiBOB	Lithium bis(oxalate)borate
LiDFOB	Lithium difluoroxalate borate
LiFSI	Lithium bis(difluorosulfonyl)imide
LiTFSI	Lithium bis(trifluoromethylsulfonyl)imide
LPSCl	Li_6PS_5Cl
LGPS	$Li_{10}GeP_2S_{12}$
OCV	Open-circuit voltage
CV	Cyclic voltammetry
EIS	Electrochemical impedance spectroscopy
NCM	$LiNi_xCo_yMn_zO_2$
NCM532	$LiNi_{0.5}Mn_{0.3}Co_{0.2}O_2$
NCM111	$LiNi_{0.3}Mn_{0.3}Co_{0.3}O_2$
NCM811	$LiNi_{0.8}Mn_{0.1}Co_{0.1}O_2$
NCM622	$LiNi_{0.6}Mn_{0.2}Co_{0.2}O_2$
LFP	$LiFePO_4$
LCO	$LiCoO_2$
NCA	$LiNi_xCo_yAl_zO_2$
LiPON	Lithium phosphorus oxynitride
LLZO	Lithium Lanthanum Zirconate Oxide
LATP	Lithium Aluminum Titanium Phosphate
PEO	Polyethylene oxide
SSE	Solid-state electrolytes
LLZTO	$Li_{6.75}La_3Zr_{1.75}Ta_{0.25}O_{12}$
3D	Three-dimensional
PVD	Physical vapor deposition
CVD	Chemical vapor deposition
PLD	Pulsed Laser Deposition
ALD	Atomic Layer Deposition
XPS	X-ray photoelectron spectroscopy
FTIR	Fourier-transformed infrared spectroscopy
NMR	Nuclear magnetic resonance
SIMS	Secondary ion mass spectroscopy
AFM	Atomic Force Microscopy
TXM	Transmission X-ray microscopy
TEM	Transmission electron microscopy
OM	Optical microscopy
EPR	Electron paramagnetic resonance
ICP–MS	Inductively coupled plasma mass spectrometry
FBG	Fiber Bragg grating
LEDs	Local excessive deposits

lower cost per kWh due to the absence of Li-metal in the pristine battery state.

2) AFLBs can be easily produced using the current LIBs manufacturing processes. The absence of unnecessary anode slurry pasting and drying processes significantly reduces the material and energy consumption during battery fabrication.

3) In addition to the high negative-to-positive electrode capacity ratio (N/P), a maximum (equilibrium) battery voltage output is achieved. Furthermore, the absence of a Li-metal anode in the pristine cell reduces the mass of the whole battery, allowing it to exhibit a higher energy density.

Due to the above advantages, AFLBs have been highly attractive for developing advanced battery systems with higher energy density (Fig. 1b-c). Various cathode materials have been applied to fabricate innovative AFLBs with excellent specific energy density, such as $LiFePO_4$||Cu (336 Wh kg^{-1}), $LiNi_{0.5}Mn_{0.3}Co_{0.2}O_2$||Cu (485 Wh kg^{-1}), $LiCoO_2$||Cu (506 Wh kg^{-1}) and $LiNi_{0.8}Mn_{0.1}Co_{0.1}O_2$||Cu (575 Wh kg^{-1}) [10]. Despite the impressive advantages, the anode-free design was previously thought to be unpractical due to poor cycling performance and low cell Coulombic efficiency (CE), particularly for those batteries utilizing nonaqueous liquid electrolytes [11]. Poor cycling performance and CE were generally observed for Li-metal plating/stripping on planar Cu-substrates in carbonate electrolytes [12]. The energy barrier hinders the Li- nucleation and growth process due to the higher overpotential required for Li-nucleation on the Cu-substrates, which results in non-uniform Li-deposition and the growth of Li-dendrites and dead Li metal [13]. In addition, the plated Li metal reacts strongly with the nonaqueous liquid electrolyte, forming thick SEI layers and consuming many Li-ions and solvent molecules. The formed SEI layers significantly influence the battery cycling performance. If the as-formed SEI is unstable and cannot sufficiently protect the plated Li-metal, the subsequent Li-metal deposits will be continuously exposed to the electrolyte. That results in further SEI formation, poor CE performance, and short cycle life.

Constructing a highly-stable passivation artificial-layer is therefore essential for suppressing continuous side reactions at the Li-metal/ electrolyte interface, allowing smooth Li-ion transportation and limiting Li-dendrite growth [14,15]. Ideal SEI should be thin, homogeneous, mechanically stable, electrically insolating, ionically conductive, and (electro)chemically stable.

Intensive efforts have been devoted to designing and tuning the properties of the formed Li-metals and SEI layers, which can mainly be divided into two groups (as summarized in Fig. 2): Electrolyte design and current collector modification. In the first approach, optimizing the electrolyte composition is a popular strategy for growing uniform Li-metals and designing the most optimum SEI, resulting in low cost and high effectiveness [16]. Electrolyte engineering involves the selection of solvents, Li-salts, additives, and manipulating electrolyte salt concentration [17]. The second approach focuses on regulating the lithiophilicity of the anode current collector toward Li-metal, such as hetero-atom doping [18] and lithiophilic coating with thin film deposition techniques [19] to reduce the energy barrier for Li-nucleation for more homogeneous Li-deposition [20] and form more stable SEI layers. Alternatively, three-dimensional (3D)-structured current collectors with an enlarged surface area could be helpful in this approach to improve the battery (dis)charge kinetics [21]. Several reviews have summarized current achievements in AFLBs in recent years [6,8,11,22]. However,

most reviews demonstrate strategies to improve battery performance without discussing details of Li-nucleation and SEI formation process.

In this review, the mechanism of Li-metal growth and SEI formation are presented in Section 2 to reveal the original reasons for the rapid capacity degradation and low CE in AFLBs. It is followed by a description of common approaches in SEI engineering, including electrolyte optimization in Section 3, current-collectors design in Section 4, and cycling conditions settings in Section 5. The influence of these strategies on SEI formation and cycling performance of AFLBs will be evaluated. Followed with advanced characterization techniques for high-energy AFLBs are presented in Section 6. Finally, future aspects of Li-growth and SEI engineering methods for high-energy AFLBs are discussed in Section 7. Such a thorough evaluation will be significantly helpful in guiding future developments of AFLBs with a high specific capacity, high safety, and extended cycle life.

2. Mechanisms

The cycling performance of AFLBs highly depends on the Li-metal plating/stripping processes and the SEI formation behaviors at the anode side. In the early stage of the first charge cycle, Li-metal is plated on the surface of the anode current collectors (Fig. 3a). On the surface of the as-deposited Li-metal, SEI is simultaneously readily formed due to the thermodynamic instability of Li-metal in the electrolyte [30]. The formed SEI layer operates as a physical protection barrier for the underlying Li-metal anodes by insulating the electron's movement yet permitting Li-ion transfer [31]. The subsequent stripping process unavoidably involves a mechanical fracture of the fragile SEI due to localized stress [32]. During further plating, Li-metal tends to deposit

along the cracks and defects. That aggravates the formation of wire-wrap micro-structured Li-metal, also called mossy Li-metal [33]. At the macro level, the mossy morphology accelerates the parasitic SEI formation, resulting in severe electrolyte depletion and electronic separation of Li-metal from current collectors [34]. The morphology and uniformity of the deposited Li-metals directly affect the stability of formed SEI, which influence the cycling performance of the cells. Therefore, understanding the mechanisms of Li-deposition and SEI formation and exploring their influence on cycling degradation is vital for designing high-performance AFLBs.

2.1. Li-nucleation and growth on anode current collectors

AFLBs are fabricated with fully lithiated Li-rich cathodes stacked with separators and current collectors, as schematically shown in Fig. 3a. During the initial charge, the Li-ions from the cathode are extracted and deposited on the current collectors as Li-metal anode. In contrast with most conventional Li-metal batteries, the Li-source in AFLBs is provided only by the cathode material. The overall capacity and energy density of AFLBs depend on the applied cathode materials [38]. Therefore, high-capacity cathode materials, such as $LiNi_xCo_yMn_zO_2$ (NCM), $LiNi_xCo_yAl_zO_2$ (NCA), and Li_2S, significantly improve the battery energy density [39,40].

The most significant difference between AFLBs and standard Li-metal batteries lays in the initial Li-metal deposition process (Fig. 3b) [36]. In AFLBs, Li-ions migrate from the cathode to the anode and are reduced with electrons to form the initial Li-nuclei at the surface of the anode current collector. In a standard Li-metal battery, that reduction occurs at the Li-metal surface. The property of initial Li-nucleation is

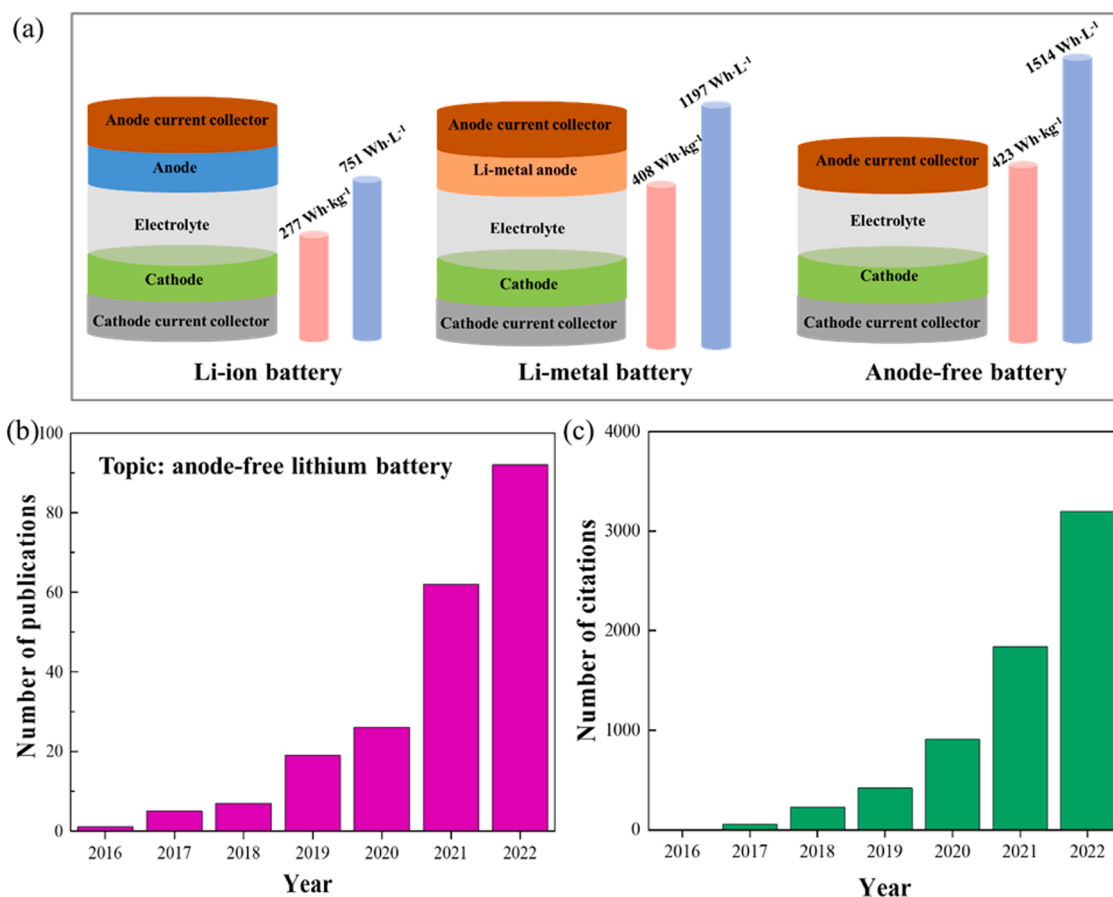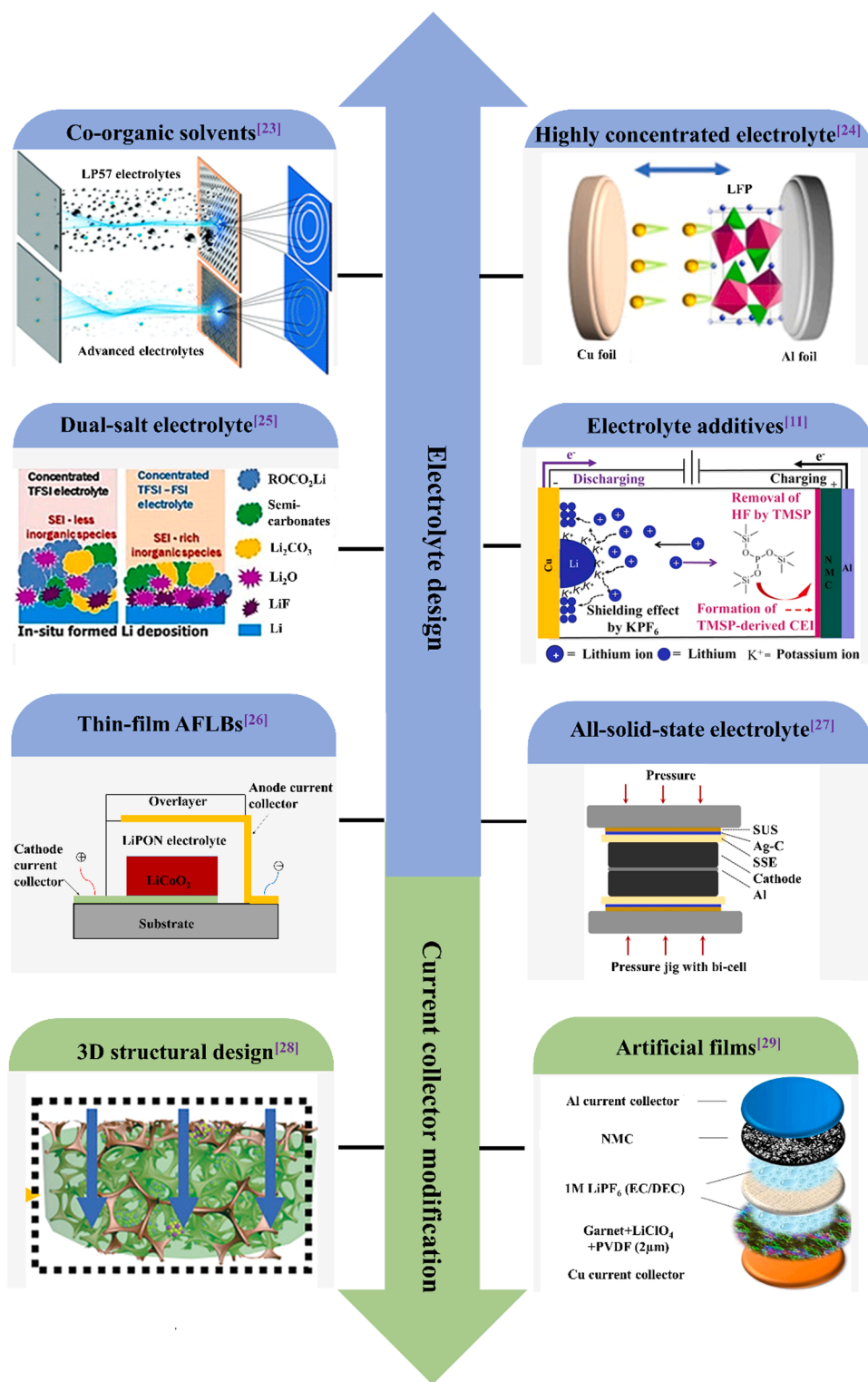**Fig. 1.** (a) Schematic representation of various cell configurations with Gravimetric energy density (Wh·kg^{-1}) and volumetric energy density (Wh·L^{-1}). Reproduced with permission [9]. Copyright 2021, Wiley-VCH GmbH; (b) Literature distribution of AFLB-based research on the website of Web of Science, and (c) the corresponding number of citations.

Fig. 2. Current main research methods on AFLB. Co-organic solvents: Reproduced with permission [23]. Copyright 2022, Royal Society of Chemistry; High-concentration electrolytes: Reproduced with permission [24]. Copyright 2016, Wiley-VCH GmbH; Dual-salt electrolytes: Reproduced with permission [25]. Copyright 2019, IOP Publishing; Electrolyte additives: Reproduced with permission [12]. Copyright 2027, IOP Publishing; Thin-film AFLIBs: Reproduced with permission [26]. Copyright 2000, IOP; All-solid-state electrolyte: Reproduced with permission [27]. Copyright 2020, Springer Nature; 3D Current-collectors design: Reproduced with permission [28]. Copyright 2022, Wiley-VCH; Artificial films: Reproduced with permission [29]. Copyright 2019, Elsevier.

essential for the final Li-metal morphology, which further influences the cycling stability of the complete AFLBs. Li-nucleation is thermodynamically driven by the Li-ion-concentration-induced Gibbs free energy, transforming from a super-saturated solution to a saturated solution at the current collectors/electrolyte interface [41].

Guided by these considerations, Pei et al. [13] investigated the Li-nucleation and growth processes on Cu current collectors by combining the observed nucleation overpotential and plateau overpotential in a three-electrode electrochemical cell during the Li-electrodeposition. The authors found that the Li-nuclei size is inversely proportional to the overpotentials. Smaller nuclei seeds and nonuniform Li-morphologies can accelerate electrolyte consumption and SEI formation due to the high specific surface area. However, compared to nucleation at a Li-metal surface, a higher overpotential is required for Li-nucleation on Cu, resulting in a less uniform Li-metal morphology. Optimizing current collectors to reduce the Li-nucleation overpotential is an effective method to improve the Li-metal morphology and, consequently, the cycling performance. Yan *et al*
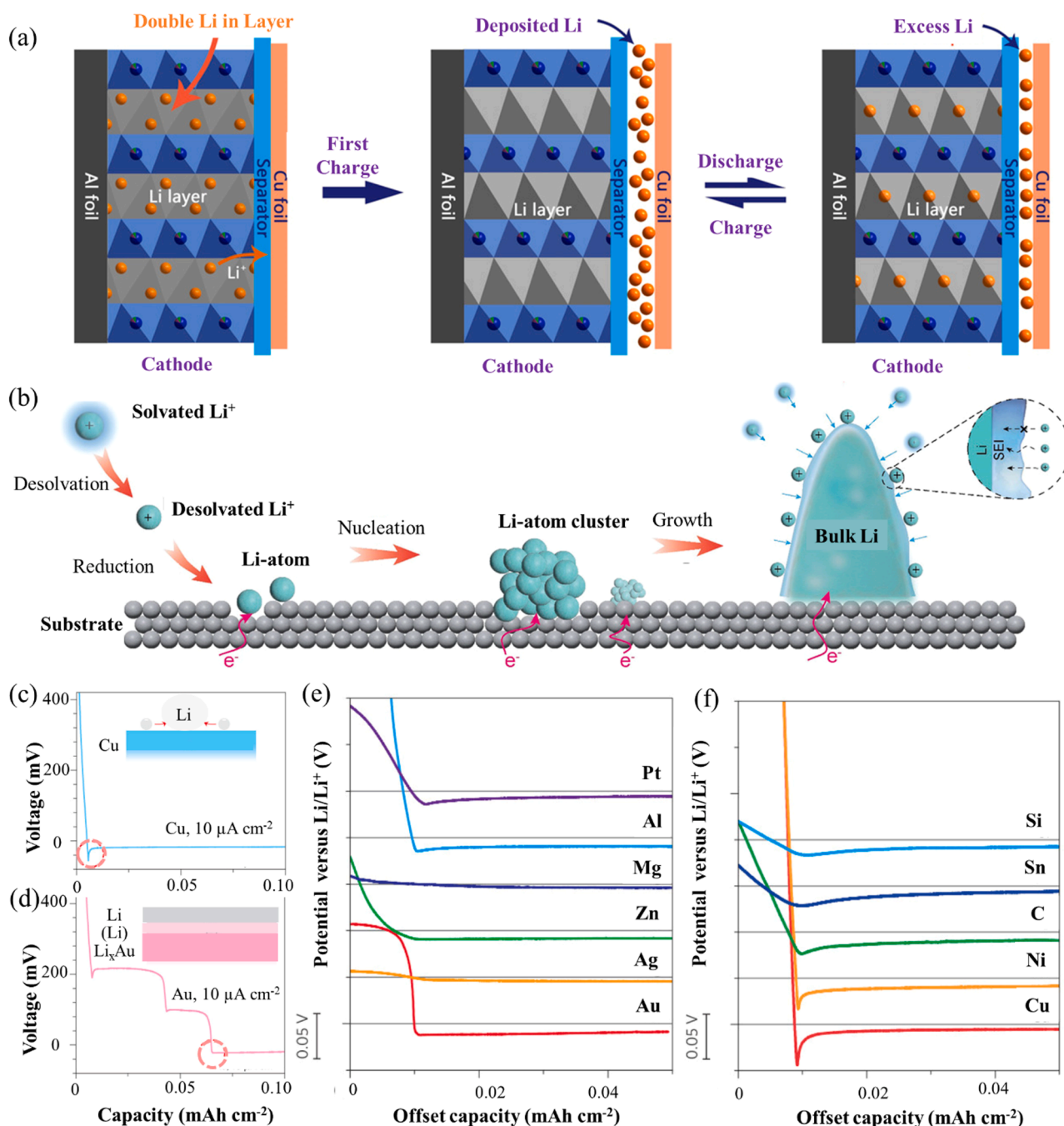
Fig. 3. (a) Scheme of extending the lifespan of AFLBs. Reproduced with permission [35]. Copyright 2021, Wiley-VCH.(b) Electrochemical processes in Li deposition. Reproduced with permission [36]. Copyright 2022, Wiley-VCH GmbH. (c) Voltage profile of galvanostatic Li-deposition on a copper substrate at 10 μA cm^{-2}. The inset shows a schematic mechanism of Li-nucleation, which explains the extra energy involved; (d) Voltage profile of galvanostatic Li-deposition on a gold substrate at 10 μA cm^{-2}. The inset shows a schematic of how a solid solution buffer layer of Au dissolved in Li-metal reduces the nucleation energy; (e) Voltage profiles of various materials with some solubility in Li-metal during Li-deposition at a current density of 10 μA cm^{-2}; (f) Shifted voltage profiles of various materials with negligible solubility in Li-metal during Li-deposition at a current density of 10 μA cm^{-2}. Reproduced with permission [37]. Copyright 2016, Springer Nature.

[37] also measured the Li-nucleation overpotential at other current collectors, including Au, Ag, Zn, Mg, Al, Pt, Si, Sn, Cu, and Ni. A lower overpotential was observed when Au, Ag, Zn, and Mg were used as current collectors (Fig. 3c-f). That can be explained by the solubility of these metals in lithium. Before the Li-metal phase starts to be formed, these metal substrates are alloyed with Li-metal to form a solid solution. Such a solution acts as a buffer layer that reduces the Li-nucleation barriers and improves the stability of the Li-metal anodes.

Pande *et al* [42] computationally screened various metal candidates as current collectors for AFLBs. The authors classified the selected

metals into two categories based on whether being alloyed with Li-metals: (1) Standard transition-metal current-collectors materials without showing apparent Li-alloy phases, such as Cu, Fe, Ti, Ni, Cr, V, Mo, W, Zr, Mn; (2) Li-alloys, including LiZn, Li$_9$Al$_4$, Li$_2$Ga, LiB, Li$_{22}$Si$_5$, Li$_{17}$Sn$_4$, Li$_{22}$Pb$_5$, Li$_3$Cd, and Li$_3$Ag. The authors found lower thermodynamic nucleation overpotentials and activation energies with Li-alloying materials. For that reason, metal-based substances that form alloys with Li-metal, *e.g.* Zn, Al, B, Cd, Ag, Si, Pb, Sn, and Mg, are more suitable as current collectors for AFLBs. They have better dendrite-control capability. There are three primary ways to optimize the current collectors:

(i) replacing copper with alternative metal, (ii) dopping copper with other metals, or (iii) coating copper with a thin layer of other metal (or alloyed) material.

After the Li-nucleation process, many Li-nuclei are distributed at the surface of the current collectors. Following nucleation, the growth process develops at the nuclei's surface. Subsequent Li-ions are preferentially deposited with the initial nucleus to grow into larger Li-metal [43]. The morphology of initially formed Li-nuclei evolves towards various types during the Li-growth process, such as balls, needles, columns, or a mixture of them, which depends on the type of electrolyte and the deposition conditions [13,44–46]. The formed SEI on the different types of deposited Li-morphology will be present in different mechanical stability. In the meantime, the morphological evolution of deposited Li-metal is governed by the SEI layer's real-time and local thermodynamic properties, the reaction front, and the kinetic barrier for electrochemical Li-deposition and dissolution during the growth process [47]. That could be rationalized because Li-ions have to migrate through the SEI layer and transfer charges to the substrate underneath to realize Li-reduction and growth of Li-deposition. Therefore, regulating the morphology of deposited Li-metal and SEI layers is essential for enhancing cell performance.

To further understand the relationship between Li-morphology and SEI, many elaborate theories have been proposed for understanding the Li-metal deposition process, such as [48–50]

1) The heterogeneous model describing initial nucleation and early growth behavior (Fig. 4a);
2) The surface diffusion model showing that Li-metal usually tends to 1D-deposition, owing to the high surface diffusion barrier (Fig. 4b);
3) The crystallographic model demonstrating the preferential single crystallographic orientation of Li-deposition;
4) The space-charge model illustrating that Li-ion distribution directly impacts the reaction activity of different sites;

5) The Li-SEI model revealing the unusual Li-nucleation and deposition below the SEI surface (Fig. 4c).

Despite all these models, a considerable difference in behavior is found after the initial nucleation on metallic current collectors in various AFLBs. This difference distinguishes results from the formation of by-products of the electrolyte decomposition during Li-metal deposition. Such a complex behavior is challenging to capture by a single model [53]. Therefore, the Li-SEI model was recently developed to simulate the Li-metal deposition and the electrolyte decomposition as a consequence of SEI fracture using a modified Palomar-Pardave model [54]. This model integrates two types of electrolyte decomposition mechanisms: instantaneous diffusion control and SEI fracturing. The Li-SEI model quantitatively describes the Li-nucleation and growth mechanism, coupling SEI fracturing [55]. It was found that SEI fractures originate from electrolyte decomposition and accelerate with time due to the continuous SEI fracturing during Li-deposition. Furthermore, SEI fracturing increases with overpotential. However, it declines in electrolytes containing fluoroethylene carbonate (FEC) as an additive. Thus, the Li-SEI model provides a novel route for a quantitative understanding of Li-nucleation and growth mechanism and electrolyte degradation on various substrates. It is also instructive for improving the energy density and stability of AFLBs by using suitable electrolyte additives, which effectively reduce SEI fracturing.

2.2. The nature of solid-electrolyte interphase

Almost all liquid electrolytes can be readily reduced and decomposed when coupled with Li-metal anodes during the cycling process, causing SEI formation. Such behavior is usually attributed to Li-metal's low potential and highly reactive nature. The nature of the SEI significantly influences the power and lifetime of Li-metal batteries [56]. Accurately elucidating the formation mechanism of SEI layers is essential for LIBs investigations. In 1979, Peled first reported that Li-metal spontaneously
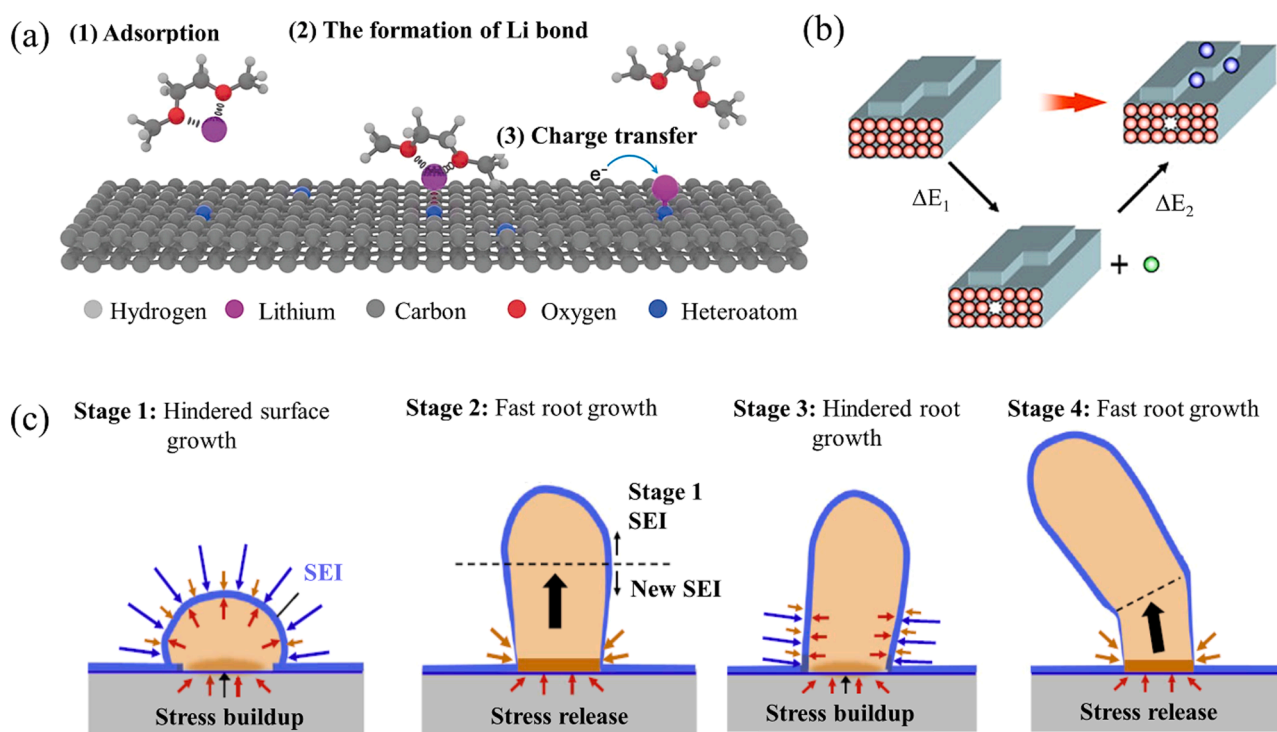
Fig. 4. (a) Scheme of a heterogeneous deposition model illustrating the Li-nucleation processes on conductive frameworks, including absorption, forming Li-bonds, and charge transfer. Reproduced with permission [18]. Copyright 2019, American Association for the Advancement of Science. (b) Scheme of movement of one atom from the bulk phase to the surface on Li-metal. Reproduced with permission [51]. Copyright 2012, Elsevier. (c) Schematic illustration of the mechanism of Li-whisker growth on Li-metal below the SEI. Reproduced with permission [52]. Copyright 2017, Elsevier.

reacted with conventional organic liquid electrolytes and proposed to denote these reaction products as SEI [57]. The SEI layer was discovered to be ionically conductive but electronically insulating [58]. Goodenough et al. [59] unravel the SEI formation process using the relationship between the lowest unoccupied molecular orbital (LUMO) and highest occupied molecular orbital (HOMO) of electrolytes. When the chemical potential of anodes (μ_A) is outside the electrochemical stability window of the applied electrolytes, electrons escape from the anode to reduce the solvent molecules in the electrolyte. This process results in forming an SEI passivation layer at the anode surface. On the other hand, the passivation layers may form at the cathode surface, with electrolyte oxidation and forming a so-called cathode electrolyte interface (CEI).

SEI/CEI layers can continuously grow throughout the battery cycling when the electrode potentials are outside the electrolyte stability voltage window. In this regard, choosing proper electrode materials that match the electrochemical stability windows is imperative to avoid thick SEI layers. However, the chemical potential of Li-metal is located well above the LUMO of most applied organic electrolyte solvent molecules, at least at commonly used Li-salt concentrations such as 1 M. That applies to ethylene carbonate (EC), propylene carbonate (PC), diethyl carbonate (DEC), dimethyl carbonate (DMC), and anions, such as PF_6. Therefore, the SEI formation layers at Li-metal surfaces are thermodynamically impossible to avoid. However, modulating the morphology of the deposited Li-metals to form a continuous and homogeneous SEI
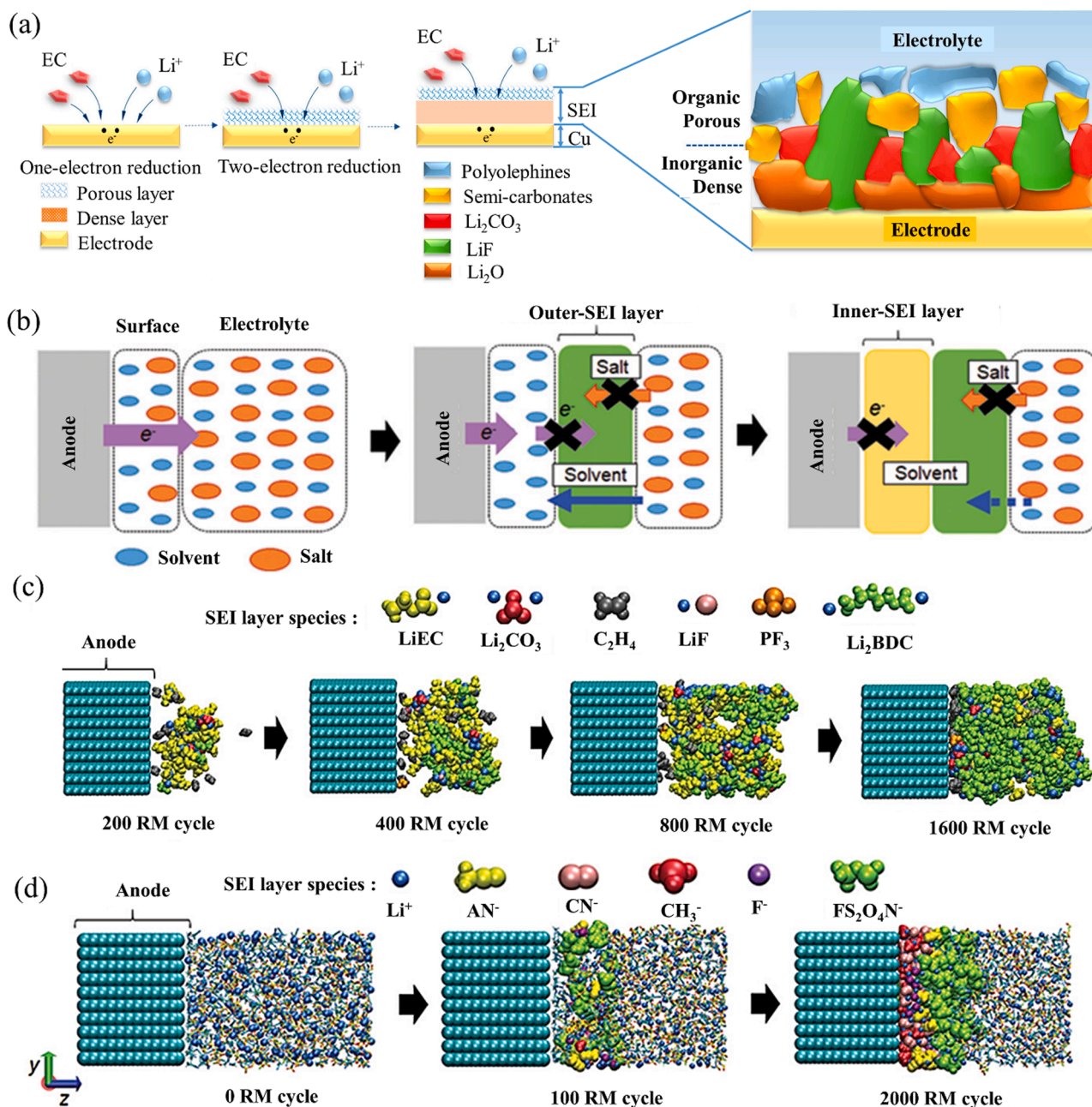
Fig. 5. (a) Schematic of complete SEI formation mechanism combining the two-layer structure chemistry and "bottom-up" growth dynamics. Reproduced with permission [63]. Copyright 2021, American Chemical Society. (b) Schematic of "bottom-up growth mechanism" of SEI layer in the electrolyte interpreted by the RM simulation. (c) Simulated SEI layer formation process at a graphite anode in 1.1 M $LiPF_6$/EC electrolyte (bulk electrolyte not shown). (d) Simulated SEI layer formation process at a carbon anode in a 5 M LiFSA/AN electrolyte (cyan: carbon, red: oxygen, white: hydrogen, yellow: sulfur, green: fluorine, blue: Li-ion). Reproduced with permission [61]. Copyright 2021, Wiley-VCH.

layer, which facilitates better protection of the Li-anode. In addition, optimizing the physical and electrochemical SEI properties and inducing stable and highly ionic-conductive SEI formation could potentially improve the performance of AFLBs.

Many theoretical and experimental approaches have been developed to understand SEI in more detail. The Red Moon (RM) method, [60] combining the Monte Carlo (MC) with Molecular Dynamics (MD) methods, has been successfully applied to demonstrate the morphological growth process at an atomic level in several battery systems [61]. The initial SEI formation process follows a bottom-up growth mechanism illustrated by Fig. 5a-b. Three main stages can be seen in Fig. 5b. (i) Initially, the salt anions are predominantly reduced at the anode surface to form an organic-based outer SEI layer. (ii) Secondly, the reduction products, such as F^- and CO_3^{2-}, begin to leave the anode surface to form aggregates in the electrolyte. (iii) Finally, the solvent molecules between the anode surface and the outer-SEI layer are reduced to form inorganic-based inner-SEI components [62]. Consequently, the thickness of the SEI layer continues to grow. The SEI formation continues until the formed Li-metal surface is entirely covered with SEI, inhibiting further reactions between Li-metal and the electrolyte. The experiments, such as isotope-assisted Time-of-Flight Secondary Ion Mass Spectrometry (TOF-SIMS)[63] and Atomic Force Microscopy (AFM), [64] also confirm the bottom-up growth model. Principally, the SEI formation process consumes both the Li-metal anode and the organic electrolyte, which will have a detrimental effect on the reversible storage capacity of AFLBs [65].

The chemical composition of SEI is primarily governed by electrolyte components, including Li-salts, solvents, and additives [66–69] Generally, SEI is composed of a mixture of inorganic and organic Li-salts (Fig. 5a). Inorganic Li-salts mainly include Li_2O, LiF, Li_2CO_3, and potentially Li_2S or Li_3N, depending on the types of solute and solvent in the electrolytes. The organic species include alkoxides in electrolytes with ethers and alkyl carbonates with carbonate esters, oligomers, and polymers. LiF is widely considered an essential component in SEI layers, beneficial for stabilizing Li-metal anodes [70]. Many investigations have been performed to improve the Li-metal stability by manipulating the LiF-formation in SEI layers [71]. For example, Tan *et al* [72] applied a hieratically porous LiF nano-box additive in LiF-solvated-based electrolytes. The authors demonstrated that a highly fluorinated SEI enables stable cycling of Li-metal anodes. The composition of SEI has been investigated by X-ray photoelectron spectroscopy (XPS), [73,74]. Fourier-transformed infrared spectroscopy (FTIR), [75] nuclear magnetic resonance (NMR), [76] SIMS, [77] and other techniques.

The structure of SEI layers has been extensively resolved by applying a combination of characterization techniques and simulation methods. The relationship between the structure and cell performance has been revealed [78,79]. The formed SEI layers were found to have heterogeneous multilayer structures in various electrolytes, with a high amount of inorganic salts at the electrode side and more organic salts at the electrolyte side (Fig. 5c). However, when different electrolytes are utilized, the morphology of the SEI layer might change [80,81]. For example, it was found that the morphology of SEI layers in PC-based electrolytes is more unstable than that formed in EC-based electrolytes, which shows that organic solvents affect the SEI layer morphology [82]. The Li-salt concentration in liquid electrolytes is also a crucial factor influencing the SEI morphology. More concentrated electrolytes induce more stable SEI layers, which is attributed to the fact that fewer free-solvent molecules can solvate the SEI layer components (Fig. 5d) [61]. Therefore, selecting appropriate organic solvents and using high-concentration electrolytes could lead to a more stable SEI morphology and improve the stability of AFLBs.

The mechanical, [83] kinetics, [84] and chemical properties [85] of SEI can significantly influence the deposition behavior and cycling performance of Li-metal anodes. The Young modulus of the SEI is typically in the range of hundreds of MPa to several GPa, which depends highly on the electrolyte composition. The kinetic properties of SEI

analyzed by electrochemical impedance spectroscopy (EIS) [86] and cyclic voltammetry (CV) [87] confirmed that the charge-transfer resistance ranges from tens to several hundred ohms·cm². Chemical properties, such as chemical and thermal SEI stability, have also been evaluated by theoretical calculations [58] and experimental characterizations [88]. Li_2O crystals in the SEI were demonstrated to function as a nucleophilic agent in the decomposition of ester solvents in electrolytes, leading to the mosaic structure [89]. Chen *et al* [90] revealed that the average Li-ion mobility of the outer-SEI layer is ~1.5 times higher than that of the inner-SEI layer. That is explained by the higher Li-ion conductivity of Li_2CO_3 and $ROCO_2Li$ (main components of the outer SEI) than LiF (the main component of the inner SEI). However, Han *et al.* [91] confirmed that the $ROCO_2Li$ would decompose into Li_2CO_3, damaging the chemical stability of SEI.

Specific SEI requirements should be evaluated from both kinetic and thermodynamic perspectives to design high-quality SEI layers for high-performance AFLBs [36]. Regarding kinetics, an ideal SEI should be highly Li-ion conductive to facilitate rapid Li-ion transportation and fast redox reactions (Li-metal plating and stripping). The Li-ion conductivity within SEI should be homogeneous, which enables the uniform potential distribution of the current distribution and Li-metal deposition. That, in turn, promotes spherical or columnar Li-metal growth with minimal stress in the SEI layers, minimizing SEI breakage and the formation of "dead" Li-metal. Consequently, the CE of Li-metal plating and stripping will be improved. From a thermodynamic point of view, the SEI should be thermodynamically stable during charging and discharging. It must be highly resistant to long-term electrolyte decomposition, particularly at high temperatures (*e.g.*, 60 °C). Moreover, the highly thermodynamically stable SEI layer will effectively prevent direct contact of Li-metal with the electrolytes. That will reduce active Li-metal losses and maintain the battery capacity during long-term cycling.

Conclusively, this section described the Li-metal nucleation and growth processes at the current-collectors surface. The formation of the SEI layer and its composition, structure, and properties were also discussed. Designing an ideal SEI layer has been marked as the most promising route to improving the performance of AFLBs. A highly stable and compact SEI layer is favorable for reducing the Li-nucleation overpotential at the current-collectors surface. In addition, the composition and SEI structure have been controlled by optimizing the electrolyte composition or additives, thereby significantly improving the Li-metal anode cycling stability.
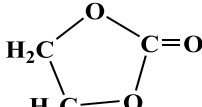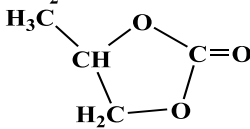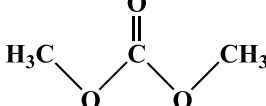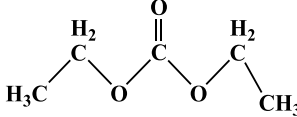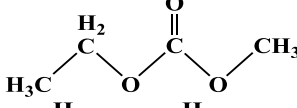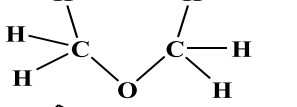
3. Electrolyte engineering

Electrolyte engineering is essential for developing high-performance AFLBs. As stated in Section 2, the cycling stability of Li-metal anodes in AFLBs is primarily determined by the SEI properties, which are, in return, controlled by electrolyte compositions. In general, designing appropriate electrolytes can determine the morphology of deposited Li-metals and limit the parasitic reactions that continuously consume active Li-metal and electrolytes, extending the cycle life performance of AFLBs. Electrolyte engineering strategies are elaborated to achieve stable cycling of AFLBs with high energy density. Examples are manipulating the electrolyte composition, including organic solvents, salt chemistries, concentrations, additives, or even using solid electrolytes.

3.1. Solvent design

Traditional liquid electrolytes can be classified into two groups based on the solvent chemistries: 1) carbonate-based solvents, such as ethylene carbonate (EC), propylene carbonate (PC), diethyl carbonate (DEC) and dimethyl carbonate (DMC), and 2) ether-based electrolytes, such as dimethyl ether (DME), 1,3-dioxolane (DOL). The applications of these two kinds of electrolytes vary substantially because of their naturally different properties (Table 1) [92]. Carbonate-based electrolytes are commonly used in commercial LIBs due to the wide electrochemical

Table 1
Properties of organic solvents used in LIBs electrolyte systems.

	Name	Structure	$T_{m,P}$, °C	$T_{b,P}$, °C	ε (25 °C)
Carbonate-based solvents	Ethylene carbonate (EC)		36.4	248	89.78
	Propylene carbonate (PC)		−48.8	242	64.92
	Dimethyl carbonate (DMC)		4.6	91	3.107
	Diethyl carbonate (DEC)		−74.3	126	2.805
	Ethylmethyl carbonate (EMC)		−53	110	2.958
Ether-based solvents	Methoxymethane (DME)		−138.5	−23	5
	1,3-Dioxolane (DOL)		−95	74	7.34

stability window (> 4.5 V *vs.* Li/Li$^+$) and low cost [56]. Ether-based electrolytes provide stable and better interfacial contact with Li-metal electrodes, which is beneficial for reversible Li-metal plating and stripping [93].

For AFLBs, electrolyte solvents significantly influence the morphology of deposited Li-metal and the formed SEI properties. For example, Woo et al. [94] assembled AFLBs with a LiNi$_{1/3}Mn_{1/3}Co_{1/3}O_2$ (NCM111) cathode and Cu foil as anode current collectors. The authors found that these batteries showed a poor reversible capacity (the initial CE of 23%) in conventional carbonate-based electrolytes (1 M LiPF$_6$-EC/DMC) (Fig. 6a). This observation can be explained by the fact that the formed SEI layers in carbonate electrolytes contain brittle ionic species, which can easily break during Li-metal plating [95]. In contrast, the SEI layer formed in ether-based electrolytes is more flexible. Such SEI can sustain the tensions caused by substantial volume changes during the Li-metal plating process. Assegie *et al.* [96] also confirmed that the AFLBs with LiFePO$_4$ as cathode and a bare Cu current collector for the anode retained about 46% of the initial capacity after 100 cycles in an ether-based electrolyte (1 M lithium bis(trifluoromethylsulfonyl) imide (LiTFSI)-DME/DOL, 2 wt.% LiNO$_3$) at a (dis)charging rate of 0.1 C (Fig. 6b). Most of the ether-based electrolytes employed DME and DOL as a solvent for AFLBs reported so far. These solvents are more compatible with Li-metal electrodes in AFLBs. Unfortunately, most ether-based solvents show poor oxidation stability *versus* high-voltage cathodes (*e.g.*, transition metal oxides). Thus, further studies are still needed to develop appropriate electrolyte solvents for higher energy density AFLBs.

The modified Li-SEI model in Section 2.1 shows that fluorinated electrolytes can suppress SEI fracture by forming a stable LiF-rich SEI layer. The LiF-rich SEI layer has a high Li$^+$ surface diffusion rate and superior mechanical strength, which can facilitate uniform Li-deposition

[98]. Fluorinated electrolytes also have a wide window of electrochemical stability. That reduces the risk of side reactions and extends the battery's cycle life. In addition, fluorinated electrolytes have low viscosity and high ionic conductivity, facilitating Li-ion transport and reducing cell resistance [99]. Thus, fluorinated solvents attract the attention of researchers as alternative solvents for developing high-performance AFLBs. For example, Yu *et al* [97] developed a solvent engineering strategy by incorporating −CF_2− units to construct a novel fluorinated 1,4-dimethoxybutane (FDMB) solvent (Fig. 6c). Further mixing FDMB with 1 M lithium bis(difluorosulfonyl)imide (LiFSI) contributes to a mono-salt-mono-solvent electrolyte with a unique Li-F bond and high anion content. 1 M LiFSI-FDMB offers a high first-cycle CE of 97.6% with a rapid increase to values larger than 99% within five cycles in Cu‖Li cells (Fig. 6d). With 1 M LiFSI/FDMB electrolyte, the LiNi$_{0.5}$Mn$_{0.3}$Co$_{0.2}$O$_2$ (NMC532)‖Cu, the LiNi$_{0.6}$Mn$_{0.2}$Co$_{0.2}$O$_2$ (NMC622)‖Cu, and LiNi$_{0.8}$Mn$_{0.1}$Co$_{0.1}$O$_2$ (NM811)‖Cu batteries could retain 80% of their initial storage capacity after 100, 80, and 70 cycles, respectively cycles (Fig. 6e). The results are also attributed to the specific solvation structure of the FDMB electrolyte. The solvation structures of lithiumtriflate cocrystallized with DME/DMB/FDMB were obtained by MD simulations (Fig. 6f). The DME molecule coordinates with the Li$^+$ ion like a 'clamp' with both its –O– groups. For DMB, most Li$^+$-solvent coordination structures are 'linear', where only one –O– group on DMB is bound with one Li$^+$ ion. Different from either DME or DMB, a five-member ring structure is observed in LiFSI/FDMB, where the Li$^+$ ion is bound simultaneously with O$_{FDMB}$ and F$_{FDMB}$ atoms. Because FSI$^-$ anions are tightly bound in such a solvation environment, 1 M LiFSI/FDMB mitigates harmful parasitic reactions on Li metal anodes. That suppresses SEI formation on the Li surface. Meanwhile, Al corrosion caused by FSI$^-$ can also be suppressed, thus showing higher oxidation stability.
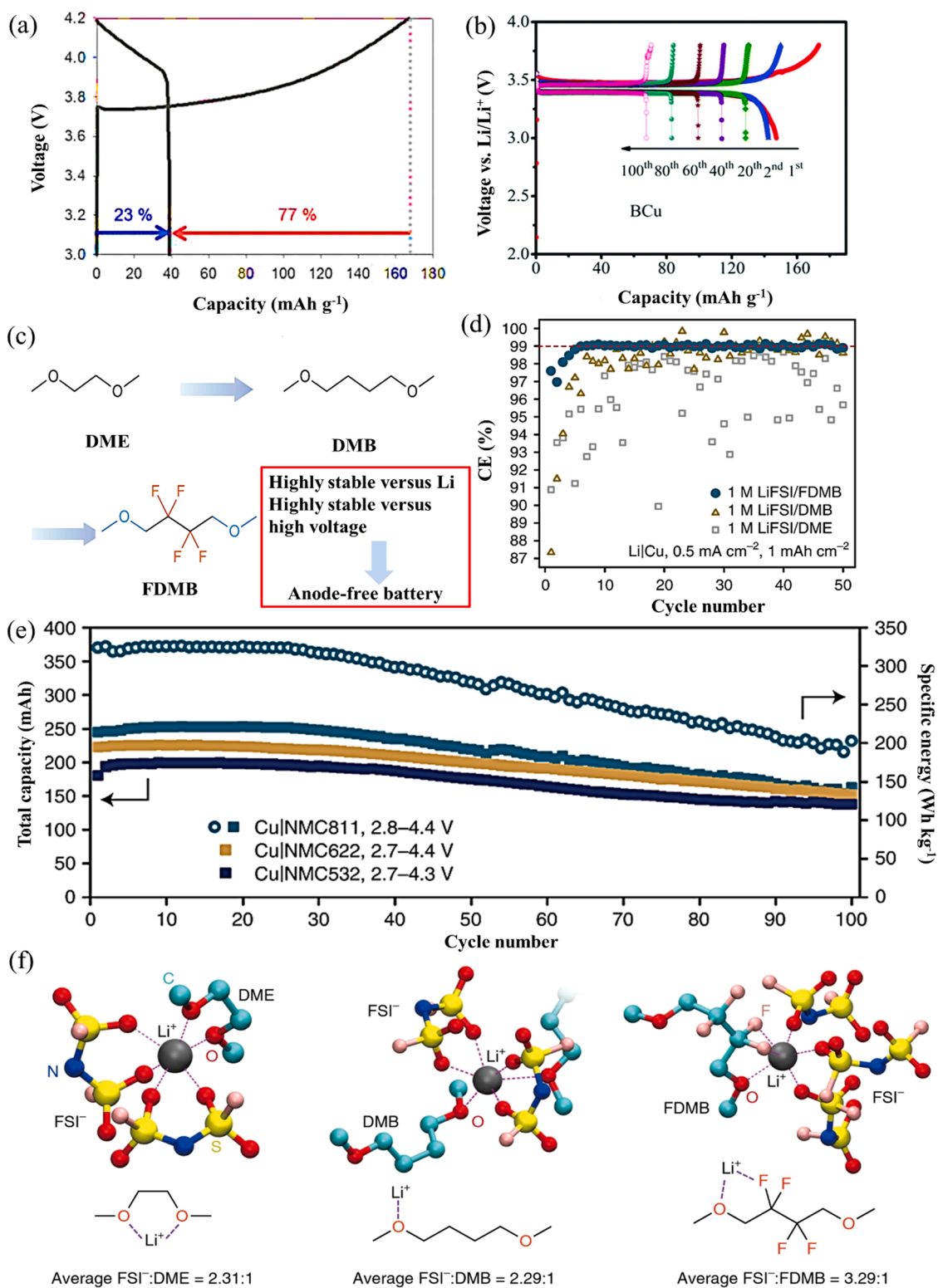
Fig. 6. (a) Voltage profile of a LiNi$_{1/3}$Mn$_{1/3}$Co$_{1/3}$O$_2$||Cu cell during the 1st cycle with 1.2 M LiPF$_6$ in EC/EMC (30:70 *wt*.%). Reproduced with permission [94]. Copyright 2014, IOP Publishing. (b)Voltage profiles of a bare Cu current collector with LiFePO$_4$ as a cathode in 1 M LiTFSI, DME/DOL, and 2 *wt*.% LiNO$_3$. Reproduced with permission [96]. Copyright 2019, Royal Society of Chemistry. (c) Molecular structures of DME, DMB, and FDMB; (d) Cycling performance of Li-metal CE in Cu||Li half cells using different electrolytes; (e) Cycling performance of anode-free NMC622||Cu pouch cells at 0.2C charging and 0.3C discharging. The specific energy was calculated on the basis of the real mass of the whole pouch cell; (f) Solvation structure of 1 M LiFSI/DME, LiFSI/DMB, and LiFSI/FDMB given by MD simulations and the corresponding average ratio of solvation bindings from FSI$^-$ anions to those from solvents in the solvation sheath. Reproduced with permission [97]. Copyright 2020, Springer Nature.

Fluorinated ether solvents have superior oxidation stability and low Li-ion solubility. That promotes the formation of more compact and thin SEI layers with reduced resistances [100,101]. Amanchukwu et al. [102] introduced a novel family of fluorinated ether electrolytes that combines the oxidative stability of hydrofluoroethers (HFEs) with the ionic conductivity of ethers. The synthesized HFEs-ether electrolyte has an anionic conductivity as high as 2.7×10^{-4} S cm^{-1} at 30 °C, and oxidative voltages up to 5.6 V. With the HFE-ether electrolyte, a Ni-rich layered cathode (NMC 811) can be cycled over 100 cycles at a C/5 rate. Although beneficial for improving the stability of AFLBs, fluorinated organic solvents are generally more expensive than carbonate-based and ether-based solvents. The reason is the cost-ineffective fluorination process. Thus, fluorinated organic solvents are not appealing for future large-scale production.

Recently, efforts have been devoted to designing co-solvents that combine fluorinated solvents with carbonate- or ether-based solvents. That represents a way to prepare cost-effective solvents for AFLBs. In 2020, Hagos *et al.* [103] produced a mixed-electrolyte solvent containing ethyl methyl carbonate (EMC), FEC, and 1, 1, 2, 2-tetrafluoroethyl-2, 2, 3, 3-tetrafluoropropyl ether (TTE). NMC111||Cu batteries with 1 M LiPF$_6$ in FEC/TTE/EMC (3:5:2 by vol.) electrolyte show appealing capacity retention of 40% and an average CE of 98.30% for 80 cycles at a current density of 0.2 mA cm^{-2} using a battery cutoff voltage of 4.5 V.

These novel fluorinated solvents can significantly improve the performance of AFLBs. However, the high production costs prevent them from being widely utilized. The combination of fluorinated organic solvents and carbonate-based electrolytes effectively prolonged the cycle life and retained a higher stable voltage range, favorable for producing high-energy-density AFLBs at low cost. However, the selection of the appropriate solvents combination, as well as the optimization of the composition ratio, becomes critical to develop high-performance electrolytes.

3.2. High-concentration electrolytes

It is well-known that SEI formation in AFLBs originates from the parasitic reaction of Li-metal and electrolytes. RM simulations [61] suggest that highly concentrated electrolytes form more stable SEI layers because less available free solvent molecules can solvate the SEI layer components. Concentrated liquid electrolytes will therefore lower the Li-ion consumption and, thus, improve the CE of AFLBs [24,104]. Additionally, with more Li-salt concentrated electrolytes, the formed SEI layers contain more inorganic components, increasing their mechanical strength. Furthermore, the SEI layers enriched with inorganic components reveal lower surface diffusion barriers, adequate surface energies, and multiple diffusion pathways, enabling smooth Li-metal deposition [42]. To date, various concentrated electrolytes have been proposed and tested for AFLBs.

In 2016, Qian et al. [24] first incorporated a high-concentration electrolyte (4 M LiFSI in DME) into an anode-free LiFePO$_4$||Cu cell. The assembled AFLBs exhibited excellent reversibility for the Li-metal plating/stripping process (CE > 99%). The CE of AFLBs can be further improved by adopting a slow charge/fast discharge protocol, which results in an extraordinarily high average CE of more than 99.8%. In concentrated electrolytes, the improved cell performance has been attributed to the different solvation structures. For the 1 M electrolyte, a large fraction of the solvent molecules and Li$^+$ are uncoordinated. However, only about 3% of the anions are uncoordinated, and the Li$^+$ cations are fully solvated in a 4 M electrolyte. Therefore, the electrolyte stability is improved due to the reduced availability of reactive solvent, and the increased Li$^+$ concentration enables high-rate Li plating/stripping. Rodriguez et al. [104] also demonstrated that concentrated 4 M LiFSI in DME-based electrolyte provides a superior cycling performance for an anode-free LiFePO$_4$||Cu cell compared with low-concentrated 1 M LiFSI, LiTFSI, or LiPF$_6$ electrolytes. These findings inspired a wave of efforts to study various electrolyte solvents for AFLBs [105,106].

Problems arising from the highly concentrated electrolytes are an increased viscosity, diminished ionic conductivity, and reduced ability to wet the separator [107]. In addition, highly concentrated Li-salts are not cost-effective and inappropriate for a wide range of battery applications. Fortunately, most of the challenges above may be resolved by diluting the concentrated electrolyte with inert co-solvents, also known as diluents. For example, Rodriguez et al. found that the AFLBs in 4 M LiFSI, DME concentrated electrolyte showed an enhanced capacity retention of 55% within 50 cycles, which is consistent with the pioneering work [24,104]. The authors also reported that the AFLBs using a dilute 1 M LiFSI, DME electrolyte (DME as the diluent) reached capacity retention 50% after 50 cycles. A diluted 1 M LiFSI, DME electrolyte showed a lower viscosity with higher ionic conductivity (16.9 mS cm^{-1} *versus* 5.7 mS cm^{-1} of 4 M electrolyte), facilitating Li-ion transportation during cycling [108]. Moreover, the DME solvent was less reactive with Li-metal. FEC is another commonly used solvent to dilute highly concentrated LiPF$_6$ electrolytes [106]. The anode-free NCM111||Cu cells with FEC diluted LiPF$_6$ electrolyte showed an average CE of 97.8% after 50 cycles with a capacity retention of 40%. Micro-structured analyses suggested a smooth and uniform Li-deposition.

Using concentrated electrolytes is a promising, facile, and effective strategy to meet most current requirements for developing high-energy-density AFLBs. Introducing an inert diluent to dilute concentrated electrolytes may resolve some remaining issues, such as high cost, high viscosity, and low ionic conductivity.

### 3.3. Dual-salt electrolytes

As stated in Section 3.2, using highly concentrated Li-salt electrolytes does not always positively affect the performance of AFLBs. Other efforts have been devoted to developing alternative promising electrolytes. Another-type of popular electrolyte for AFLBs is dual/multiple Li-salt electrolytes. In these dual-salt electrolytes, two different Li-salts could synergistically facilitate the formation of a thin protective SEI or CEI, improving the average CE and lifespan of AFLBs [25]. The commonly used Li-salts in liquid electrolytes can be divided into two families: (1) Inorganic Li-salts, like LiPF$_6$, LiBF$_4$, LiClO$_4$, and LiAsF$_6$. (2) Organic Li-salts, including lithium bis(oxalate)borate (LiBOB), lithium difluorooxalate borate (LiDFOB), lithium bis(difluorosulfonyl)imide (LiFSI), and lithium bis(trifluoromethylsulfonyl)imide (LiTFSI).

LiPF$_6$ is the most commonly used electrolyte Li-salt for commercial LIBs due to its high ionic conductivity (7.53 mS cm^{-1} in EC) and good electrochemical stability in non-protonic organic solvents. In addition, LiPF$_6$-based electrolytes help to build a protective film on the Al current collectors, thus weakening the corrosion of the electrolyte at Al. However, LiPF$_6$ has poor thermal stability and reacts readily with water traces to produce a highly reactive compound of PF$_5$. The PF$_5$ species readily react further with organic solvents in the electrolyte, causing battery performance degradation. In this regard, organic Li-salts show improved thermal and chemical stability. However, the organic-based Li-salts also reveal some disadvantages, such as low solubility, high viscosity, and high price (Table 2), [109] which seriously limits their practical applications. Dual-salt electrolytes can further improve the performance of electrolytes and reduce the production cost compared with highly concentrated electrolytes. Dual-salt electrolytes have become one of the most popular electrolytes for modern AFLBs.

Dahn et al. [73,111] reported long-life AFLBs that achieved 80% capacity for 90 cycles utilizing a double-salt carbonate-based liquid electrolyte with 0.6 M LiDFOB and 0.6 M LiBF$_4$ (Fig. 7a). The deposited Li-metal electrode exhibited a flat, mosaic-like morphology with compactly packed Li-metal columns. The column-like morphology, with diminished surface area, helps reduce the reaction rate between Li-metal and electrolytes (Fig. 7b and c). Further analyses demonstrated that the dual-salt electrolytes resulted in organic/inorganic fluorine-components-rich SEI formation with high strength and low porosity. That is essential for uniform Li-metal deposition. The

Table 2
Properties of commonly used Li-salts [110].

Salts	Properties of individual salts			Properties of electrolyte solutions (at 25°C)			Price (Sigma) €·g^{-1}
	$T_{m,P}$ °C	T_{decomp} °C	Stability against hydrolysis	σ_{ac} S·cm^{-1}	E_{ox} V	Passivation of Al	
LiClO$_4$	236	>236	Stable	~10^{-3}–10^{-2}	4.6	Yes	3.04
LiBF$_4$	293	~160	Unstable	~10^{-3}	5.2	Yes	18
LiPF$_6$	190	≥50	Unstable	~10^{-2}	4.2	Yes	10.04
LiB(C$_2$O$_4$)$_2$ (LiBOB)	350	290	Unstable	~10^{-3}	4.3	Yes	6.32
LiBF$_2$(C$_2$O$_4$) (LiDFOB)	272	200	Unstable	~10^{-3}	4.3	Yes	10.84
LiN(SO$_2$F)$_2$ (LIFSI)	132	>180	Stable	~10^{-2}	5.6	Yes	–
LiC$_2$NO$_4$F$_6$S$_2$ (LITFSI)	236	360	Stable	~10^{-3}–10^{-2}	5.3	No	5.31
LiAsF$_6$	340	240	Stable in nonaqueous solutions	~10^{-2}	5.1	Yes	8.76
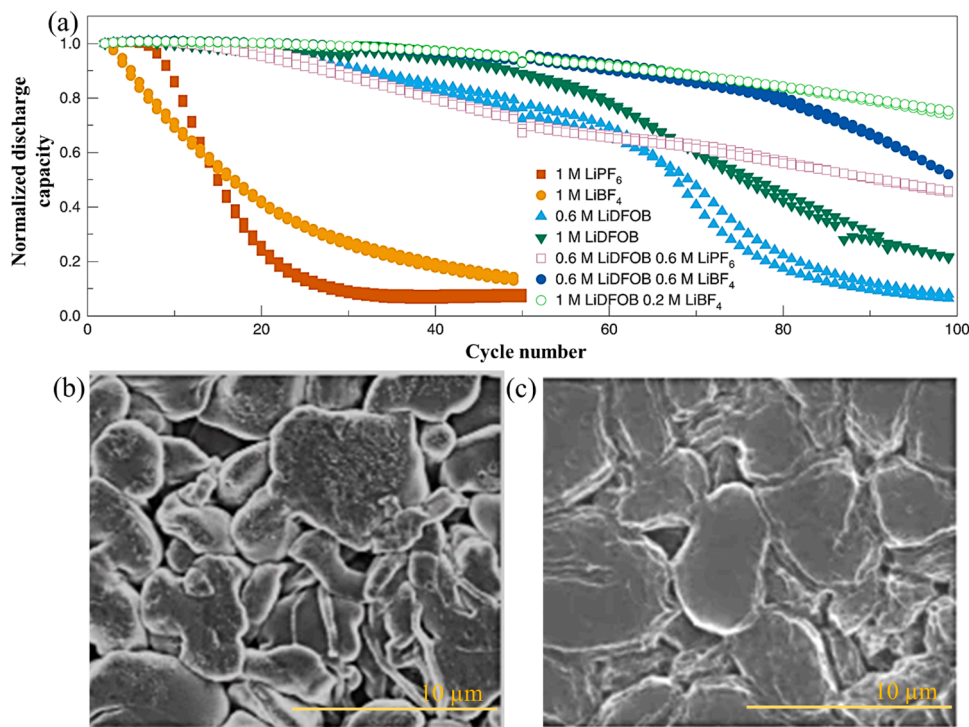
Fig. 7. (a) Capacity retention as a function of cycle number for anode-free pouch cells using electrolytes with different Li-salts; Scanning Electron Microscope (SEM) images of Li-morphology for two electrolytes with 1 M LiPF$_6$, (b) and 0.6 M LiDFOB and 0.6 M LiBF$_4$ (c). Reproduced with permission [73]. Copyright 2019, Springer Nature.

homogeneous SEI layer also effectively suppressed the side reactions between plated Li-metal and electrolytes. The assembled anode-free pouch cells with high areal capacity (2.4 mAh cm^{-2}) are one of the longest cycle-life AFLBs with 80% capacity retention after 90 cycles. Jahn also found that salt types and concentrations are important for cycling stability [73]. For example, replacing LiBF$_4$ with LiPF$_6$ caused the capacity retention to drop below 80%, even below 50 cycles. In terms of concentration ratios, the most optimal dual-salt mixture of 1 M LiDFOB and 0.2 M LiBF$_4$ resulted in a capacity of more than 80% after 90 cycles. It is, therefore, necessary to optimize these concentrations further and explore different salt combinations to achieve the best battery performance.

Similarly, increasing the salt concentration in dual-salt systems may also promote the stability of AFLBs. Beyene *et al.* [25] prepared a highly concentrated dual-salt electrolyte in a DME/DOL solvent consisting of 2 M LiFSI and 1 M LiTFSI in a DME/DOL solvent. Compared to the single-salt 3 M LiTFSI electrolyte, the LiFSI-LiTFSI dual-salt electrolytes facilitated lower voltage polarization in a Cu||Li half-cell. The FSI$^-$ anions were found to be less stable than TFSI$^-$ anions because FSI$^-$ can be more easily decomposed into inorganic SEI compounds (LiF, Li$_2$O, Li$_2$CO$_3$). Anode-free LiFePO$_4$||Cu cells with LiFSI-LiTFSI dual-salt

electrolyte revealed a higher CE of over 98.9% for 100 cycles than cells using 3 M LiTFSI single-salt electrolyte. Alvarado et al. [107] also developed a dual-salt electrolyte based on ether solvents (4.6 M LiFSI + 2.3 M LiTFSI in DME) for stabilizing Li-metal plating/stripping processes. The synergetic FSI$^-$ and TFSI$^-$ anions drew larger anion fragments into the SEI layer, promoting uniform and compact Li-metal deposition. With the LiFSI-LiTFSI electrolytes, the anode-free NMC622|| Cu cells have higher capacity retention (around 60%) than the cells equipped with the traditional 1 M LiPF$_6$ electrolyte (< 10%) within 50 cycles. The concentration ratios are also essential for highly concentrated dual-salt systems. Kim and coworkers examined the effectiveness of the LiPF$_6$+LiFSI dual-salt carbonate-based electrolyte system with various concentrations [112]. The authors demonstrated that a mixed salt ratio of LiPF$_6$/LiFSI > 1 resulted in limited capacity retention of the assembled AFLBs. In contrast, AFLBs containing electrolytes with a ratio of LiPF$_6$/LiFSI < 1 exhibited relatively stable cycling performance. It was revealed that a higher percentage of LiPF$_6$ could cause a significant resistance increase due to the increased viscosity. Note that when formulating highly concentrated dual-salt electrolytes, the viscosity, and wettability with respect to the separator or electrodes are also significant factors to be considered.

Despite these advances, the high price of highly concentrated dual-salt electrolytes remains a primary barrier to large-scale applications. Choosing the appropriate combination of efficient and low-cost salts and optimizing composition ratios become critical to furtherly improving the performance of AFLBs. Furthermore, optimizing additives can significantly increase the stability of low-concentration dual-salt electrolytes at a low cost. That makes dual-salt electrolytes more acceptable for practical applications.

3.4. Electrolyte additives

Effective electrolyte additives are chemicals usually used below 10%, either in weight or volume. The electrolyte additives can regulate the

chemical composition of the SEI layer to facilitate the Li-ion mobility and control the Li-metal plating/stripping behavior. Essentially there are two kinds of electrolyte additives, *i.e.* inorganic additives (LiNO$_3$, [96] LiAsF$_6$[113] and AlCl$_3$[114].) and organic additives (vinylene carbonate (VC), [12] and FEC) [115]. Many additives were introduced as sacrificial agents, which would be co-deposited and coordinated with Li-ions [116]. The additives have priority to be reduced by Li-metal anodes and may produce more stable SEI components. Nitrates (LiNO$_3$ or KNO$_3$) are the most commonly used inorganic additives due to their low cost and high efficiency in improving battery stability.

Sahalie et al. [117] investigated the effects of KNO$_3$ additive on the performance of AFLBs. They found that NO$_3^-$ anions can be reduced to form Li$_3$N-containing compact SEI. At the same time, K^+ cations can
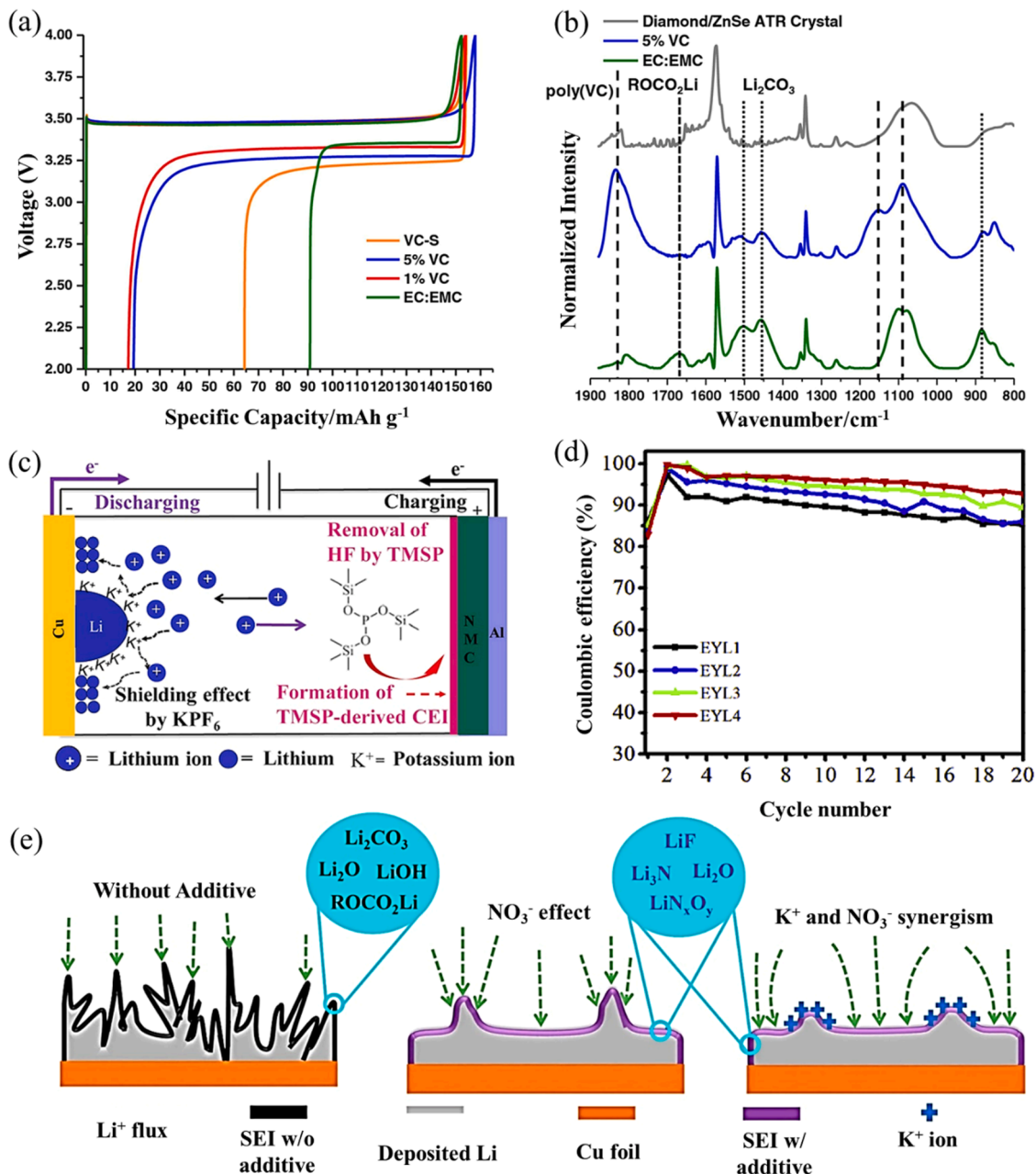
Fig. 8. (a) Voltage as a function of the specific capacity for the first Li-plating and stripping cycle in EC/EMC (green curve), 1% VC (red), 5% VC (blue), and VC-S (yellow) electrolyte; (b) Normalized ATR-FTIR spectra of Li-metal plated in EC/EMC and 5% VC electrolytes in the wavenumber range of 1900–800 cm^{-1}. A spectrum of the diamond/ZnSe ATR crystal is shown to emphasize overlapping regions. Reproduced with permission [12]. Copyright 2017, IOP Publishing. (c) Schematic illustration of the self-healing effect of KPF$_6$ and TMSP additives. (d) Coulombic efficiency of cells in various electrolytes as a function of cycle number (dis)charged at 0.2 mA cm^{-2}. I Schematic illustration of the self-healing electrostatic shielding mechanism [118]. Copyright 2019, Elsevier.

electrostatically shield the growth of Li-dendrite tips, leading to a smoother Li-metal deposition. Consequently, using a routine 1 M LiPF$_6$ electrolyte with a cost-effective KNO$_3$-additive, the 4.3 V AFLBs with NMC111 cathode resulted in 40% capacity retention after 50 cycles at 0.2 mA cm^{-2}. Considering organic electrolyte additives, VC was reported as an effective additive for a 1.2 M LiPF$_6$ liquid electrolyte in anode-free LiFePO$_4$||Cu cells. It improves the stability of Li-metal anodes (Fig. 8a) [12]. After the first charge to 4.0 V, the deposited Li-metal was analyzed by an attenuated total reflection-Fourier transform infrared spectrometry (ATR-FTIR). Strong absorption peaks were identified between 1850 and 1750 cm^{-1} and 1200–1050 cm^{-1} (Fig. 8b), indicating the presence of poly-VC, which was responsible for the improved Li-metal plating/stripping behavior in carbonate electrolytes.

As discussed in Section 2.1, introducing fluorine-containing additives facilitates the stability of AFLBs. FEC is one of the most celebrated electrolyte additives in Li-metal batteries. It forms a stable yet elastic LiF-rich SEI on Li-metal [119]. Inspired by this, many other fluorinated organic compounds have been explored as electrolyte additives to improve the performance of carbonate or ether-based electrolytes. For instance, a fluorinated ether additive (1,1,2,2 tetrafluoroethyl 2,2,3, 3-tetrafluoropropyl ether) has been reported to be a promising candidate additive in highly fluorinated and concentrated electrolytes. This was shown to result in LiF-enriched SEI and enhanced Li-metal plating/stripping reversibility [120,121].

Many new additives have been explored nowadays for both Li-metal batteries and AFLBs. Various additives involve many improvement mechanisms, including altering Li-ion solvation, optimizing SEI, and regulating Li-metal deposition morphology [113]. However, most additives are not compatible with either ether or ester solvents. Dual additives have therefore been developed to address this issue. Hagos et al. [118] reported a dual electrolyte additive of 2 wt.% potassium hexafluorophosphate (KPF$_6$) and 2 vol.% tris(trimethylsilyl) phosphite (TMSP) for anode-free NMC||Cu batteries (Fig. 8c). A high average CE of 95.21% upon 20 cycles was reached with a composite KPF$_6$-TMSP additive (Fig. 8d). The improved cycling performance was attributed to the self-healing effect of the KPF$_6$ additive and the removal of hydrofluoric acid by the reaction of PF$_5^-$ with water by TMSP. The same group also reported a bifunctional additive of KNO$_3$ and tris(trimethylsilyl)phosphite. These additives facilitated smooth Li-deposition (see Fig. 8e) [117]. Anode-free NMC||Cu cells with KNO$_3$ additives showed an average CE of 96.5% over 50 cycles. The much-improved Li-metal deposition behavior and cycle-life properties were due to new SEI components resulting from the decomposition of PF$_6^-$ and NO$_3^-$ as well as the electrostatic shielding of K^+ cations.

Electrolyte additives will not only reduce the electrolyte cost but can also improve the cycling stability of AFLBs. Developing low-cost, highly effective, and chemically stable additives is crucial for developing high-energy AFLBs. Eldesoky et al. [122] evaluated the impact of 65 additives or co-solvents on the performance of AFLBs, which covers most of the reported electrolyte additives. A composite containing 0.6 M each LiDFOB and LiBF$_4$ in FEC: DEC (1:2 v/v) was used as a base electrolyte, to which additives and co-solvents were added to investigate the cycle life. It was found that the addition of 5% propionitrile, 5% p-toluene sulfonyl isocyanate, 5% tris(2,2,2-trifluoroethyl) phosphate, 1% lithium perchlorate (LiClO$_4$), and 5% hexamethyl disiloxane could all lead to an improvement in energy retention. They also discovered that energy retention relates to the concentration of used additive or co-solvent. Further efforts are still needed to discover novel additives for AFLBs and optimize the concentration of the employed additives.

The application of additives is a simple, effective, and low-cost method. However, the mechanism of many additives in electrolytes remains unclear. Therefore, it is crucial to investigate how additives affect Li-growth and SEI formation processes in batteries. Developing high-performance and practical electrolytes and exploring efficient and low-cost additives will be continued.

3.5. Solid-state electrolytes

Solid-state electrolytes will improve battery safety by avoiding leakage and flammability issues caused by organic liquid electrolytes. Solid-state electrolytes maintain desirable mechanical stability, suppressing dendrite growth and ensuring stable interlayer formation for LIBs [123]. All-solid-state AFLBs can be constructed only with the help of solid-state electrolytes. Moreover, solid-state electrolytes offer AFLBs with high theoretical gravimetric and volumetric energy densities of 1514 Wh L^{-1} and 408 Wh kg^{-1}, respectively [9]. Many advanced electrolytes with high ionic conductivity and stability have been developed and made available for Li-metal batteries. Examples are the sulfide-type electrolytes and garnet-type oxide electrolyte Li$_7$La$_3$Zr$_2$O$_{12}$ (LLZO), NASION-based Li$_{1.4}$Al$_{0.4}$Ti$_{1.6}$(PO$_4$)$_3$ (LATP), and polymer-based electrolytes (PEO) [124]. However, the chemical stability window of many solid electrolytes is quite limited and may decompose to form the SEI upon direct contact with Li-metal. For example, Ti or Ge cations in NASICON-type solid electrolytes are being reduced by Li-metal [125]. The highly conductive solid electrolyte Li$_{10}$GeP$_2$S$_{12}$ (LGPS) [126] reacts with Li-metal to form Li$_2$S, Li$_3$P, and Ge/Ge$_4$Li$_{15}$ [127]. These reduction products on the Li-metal surface often convert to Li-alloys with high electronic conductivity, which cannot prevent the reduction reaction from continuing and eventually leading to battery deterioration [128]. Besides, other electrolytes behave differently in reduction reactions, such as LiPON, [26] oxide Garnet-type Li$_7$La$_3$Zr$_2$O$_{12}$ (LLZO) [129], and sulfide Argyrodite-type Li$_6$PS$_5$Cl (LPSCl) [130]. Their decomposition products have low electronic conductivity and can alleviate the interfacial degradation process. To date, several established solid-state electrolytes have been applied in AFLBs.

In 2000, Neudecker et al. [26] first reported a "Li-free" thin-film Li-metal battery based on a solid-state lithium-phosphorus-oxynitride (LiPON) electrolyte deposited by radio-frequency magnetron sputtering. The obtained LiCoO$_2$||LiPON||Cu AFLBs showed a capacity retention of 80% after 1000 cycles at a discharge current density of 1 mA cm^{-2}. The reported design was the most remarkable breakthrough in incorporating solid-state electrolytes into an anode-free configuration. However, the intrinsically high cost and limited areal capacity (100 μAh cm^{-2}) of the deposited thin-film AFLBs still restrict their application in portable devices and electric vehicles.

Recently, scientific attention has been attracted to building bulk-type solid-state AFLBs, promising record energy content. Chen *et al.* [131] systematically investigated the influence of Li-metal excess on the cycling performance of Li-metal batteries in solid-state electrolytes (SSEs) and liquid electrolytes. A garnet-type solid-state electrolyte Li$_{6.4}$La$_3$Zr$_{1.4}$Ta$_{0.6}$O$_{12}$ (LLZTO) pellet was coated with a solid-state plastic crystal electrolyte (PCE) and Au thin film. This design was used to modify the LLZTO/cathode interface and the anode/LLZTO interface, respectively. Then the modified LLZTO pellet was combined with a LiFePO$_4$ (LFP) cathode and different quantities of excess Li-metal anode. Li-metal batteries with the LLZTO electrolyte arrangement provide an initial CE of 96.8%, which increases to 99.8% at higher cycle numbers. That is much higher than its liquid electrolyte counterpart (initial CE = 79.4% increasing to 90%), indicating that the SSE-based system possesses a more stable cycle-life performance. However, reducing the excess Li-metal also leads to a dramatic limitation of cycling stability. In an anode-free configuration, a low initial discharge capacity of 76 mAh g^{-1} is followed by a rapid capacity decay upon cycling. This behavior is due to the poor CE of the Li-plating/stripping process, necessitating a high Li-excess in the system. While the comprehensive study demonstrates the benefits of SSE over liquid electrolytes in Li-metal batteries, it also highlights the importance of solid-state electrolytes.

Wang et al. [132] developed several AFLBs by laminating a Cu current collector (10 μm thick) to polished LLZO pellets followed by pressure-assisted heat treatment and studied the Li-nucleation at the Cu/LLZO interface. Using a half-cell configuration, Cu||LLZO||Li, and large amounts of Li-metal (5 mAh cm^{-2}, corresponding to 25 μm cm^{-2}

compact Li-metal), the synthesized batteries can be cycled reversibly with high efficiency (CE > 99%). The improved bonding between Cu and LLZO by polishing the solid-electrolyte and pressure-assisted heat treatment leads to superior cycle-life performance [131]. In full-cell configurations, a state-of-the-art NCA cathode (3 mAh cm^{-2}) infiltrated by PEO-LiTFSI, 2.7 mAh cm^{-2}, was plated on the other side of the LLZO electrolyte. However, when cycling at 60 °C at a C/10 rate, the complete AFLBs only provide 0.75 mAh cm^{-2} with relatively stable capacity retention. The inaccessible capacity was attributed to the non-optimized PEO-composite cathode. That conclusion is supported by the facts that: (i) a significantly higher capacity (2.4 mAh cm^{-2}) is attained at 80 °C and (ii) the half-cell measurements show high CE and excellent cycling stability for practically relevant areal capacities of > 4 mAh cm^{-2}, accordingly. Although the performance of the reported full-cells is currently not good sufficient, the results are a milestone for AFLBs, in which tailoring the design at the Cu/SSE interface turned out to be crucial for reversible cycling.

Another task in implementing all-solid-state AFLBs in practice is transitioning from laboratory-scale cells to application-ready formats. The most important limitation for obtaining energy densities surpassing commercial LIBs is the fraction of inactive materials. That fraction must be significantly decreased for solid AFLBs, for example, by lowering the thickness of the solid-state electrolyte. For this purpose, Zegeye *et al.* [133] constructed AFLBs by using an ultra-thin polymer composite solid electrolyte. The composite polymer electrolyte (CPE) with a total thickness of 15 to 20 μm was prepared from PEO, LiTFSI salt, and

Li$_{6.75}$La$_3$Zr$_{1.75}$Ta$_{0.25}$O$_{12}$ (LLZTO) by spin-coating (Fig. 9a). The polarization of Cu||LLZTO/PEO—CPE||Li cells is lower, and the stability is higher (<15 mV, 98.7% after 100 cycles) than that of Cu||PEO—CPE||Li cells (>40 mV, failures after 60 cycles) at 0.2 mA cm^{-2}. The improved CE and cycling behavior are attributed to the LLZTO filler, which distributes Li-ions uniformly and reduces the potential for dendrite growth. Complete AFLBs made from LLZTO-based solid electrolyte and an NMC cathode delivered an average CE of 98.8% with an initial areal capacity of 2.15 mAh cm^{-2} (Fig. 9b). However, the capacity drops 41% after 65 cycles at 0.1C. Adopting the composite solid electrolyte offers a new avenue for developing all-solid-state AFLBs.

Besides composite solid-state electrolytes, garnet-type and sulfide-based solid-state electrolytes were also used to construct all-solid-state AFLBs [128]. Recently, a new sulfide-based solid-state argyrodite (Li$_6$PS$_5$Cl) was reported as SSE for AFLBs (Fig. 9c) [27]. Crystalline argyrodite exhibits a high Li-ion conductivity of 1.8 mS cm^{-1} at room-temperature, equivalent to traditional liquid electrolytes. Argyrodite (Li$_6$PS$_5$Cl) powder was mixed with xylene and isobutyl isobutyrate to form a slurry. The slurry was coated on a PET film using a Doctor-Blade method and subsequently connected to an NMC cathode simply by adding 50 MPa external pressure. A warm isostatic press (WIP) applied 490 MPa pressure during full-cell fabrication (see Fig. 9c) to improve the contact at the current collector/electrode and electrolyte/electrode interfaces. Such external pressure resulted in uniform interfaces and stable Li-deposition. Consequently, the anode-free NMC|| SSE||Ag-C complete cell showed outstanding cycling stability over 1000
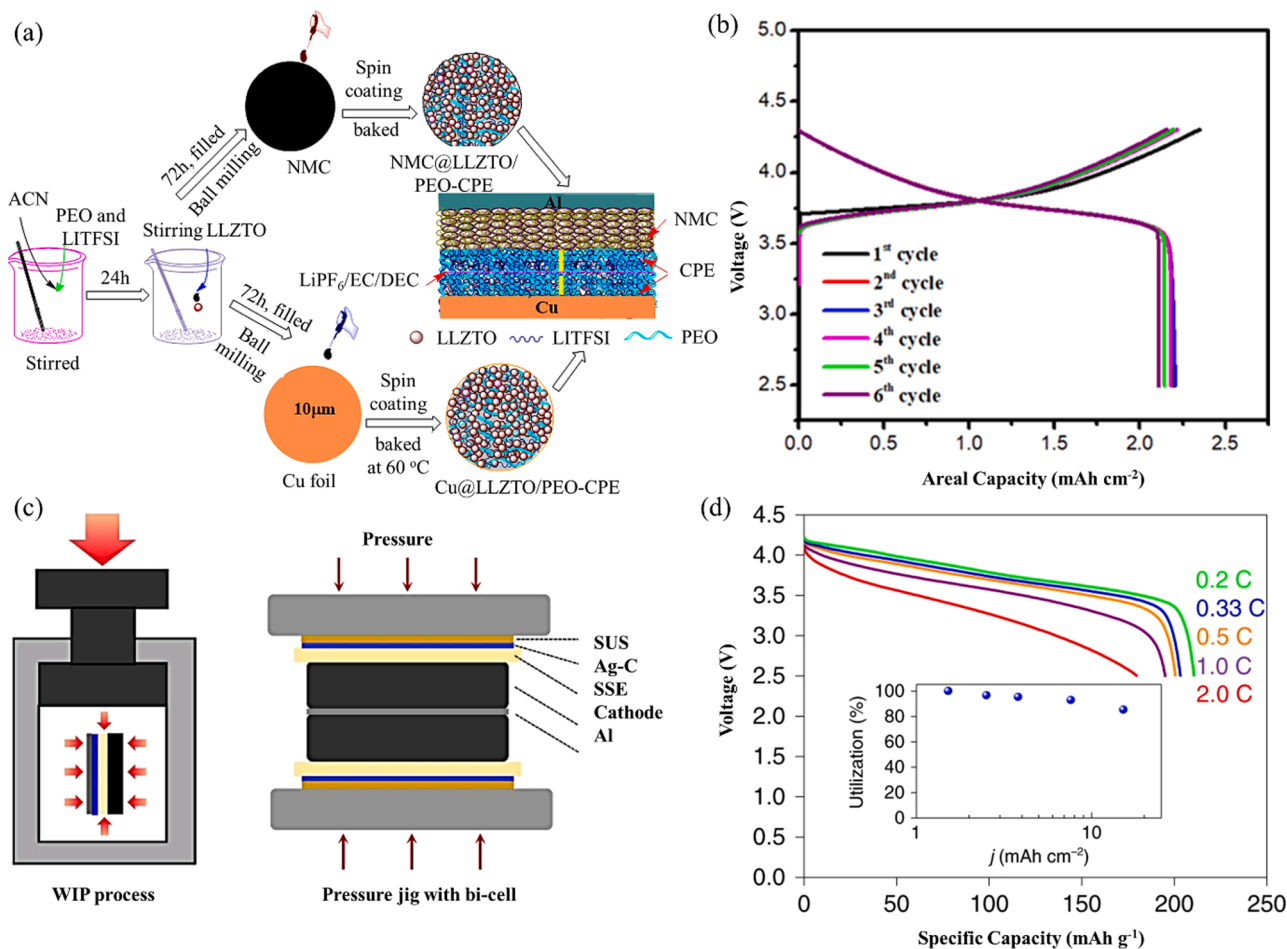
Fig. 9. (a) Schematic design of an ultrathin laminated solid-state LLZTO/PEO—CPE at both the anode and cathode. (b) Charge/discharge voltage profile of NCM|| LLZTO/PEO—CPE||Cu cells. Reproduced with permission [133]. Copyright 2020, American Chemical Society. (c) Schematic of pressurization process during the fabrication and operation of ASSB. After the cell assembly and stacking, pressurization was applied using the WIP. (d) Voltage profiles were plotted with cell capacity at different C-rates. Reproduced with permission [27]. Copyright 2020, Springer Nature.

cycles and a high energy density of over 900 Wh L^{-1}. In addition, the full-cells exhibit an excellent rate performance, which delivered a high specific capacity of 200 mAh/g at 1 C-rate (Fig. 9d). All-solid-state AFLBs can deliver higher energy density, improve safety and prolong the cycle life. However, many factors still hinder the practical application of all-solid-state AFLBs, such as the high impedance of electrolyte-electrodes interface, low ionic conductivity, and electrochemical stability window [128]. Similar to all-solid-sate Li-metal batteries, common interface engineering strategies can be applied to improve the interfacial properties of SSEs. That includes using an artificial layer, nanosized 3D scaffolds, and interfacial wetting for *in situ* reaction between the electrolytes and cathode [134,135]. To address these issues, solid-state electrolytes still require further exploration towards reducing the interfacial resistance, lowering manufacturing costs, and improving the mechanical flexibility of complete cells [136].

4. Engineering of current collectors

Plating the limited Li-source from the cathode onto the anode current collectors is the most critical step for AFLBs. During the Li-plating process, the main challenge currently arises from the high nucleation overpotential due to the poor binding between Li-metal and the anode current collectors. The Li-nucleation overpotential hinders the smooth deposition of Li-metal and induces an increased SEI formation. Reducing the nucleation potential is essential to promote more homogeneous deposition and eliminate parasitic reactions [13]. Constructing lithiophilic current-collectors surfaces by pretreatment methods was the most reliable method to reduce the nucleation overpotential and achieve more uniform Li-metal deposition. Artificial engineering of current collectors can be accomplished by regulating the ion and electron distribution to ensure a more uniform nucleation geometry and promote a more compact SEI [6,11,113,137]. Additionally, an artificial layer deposited on the current-collectors surface could directly isolate the formed Li-metals from electrolytes, suppressing side reactions and SEI formation. Besides, replacing a planar substrate with a three-dimensional one can increase the available surface area for Li-metal deposition. That is also favorable for a flatter Li-metal plating and homogeneous SEI generation. 3D structuring helps improve energy density and prolong the cycle life of AFLBs [138].

4.1. Surface modifications

4.1.1. Lithiophilic coatings

Replacing Cu with other metals, particularly transition metals, [42] will effectively reduce the Li-nucleation overpotential. That can be achieved in two ways. First is coating Cu with thin metal layers. The second is completely replacing the copper current collectors. Apart from transition metals, various Li-alloys, like Li-Mg, Li-Sn, Li-Pb, Li-Si, Li-Ag, Li-Cd, Li-B, Li-Al, and Li-Zn, were also employed as anode current collectors to reduce overpotentials and regulate the Li-deposition morphology [42]. For example, Wang *et al.* [139] constructed a Li-Sn alloy on Cu, which displays a stable Li-plating/stripping cycling performance with an average CE of 94.1% for 400 cycles at 1 mA cm^{-2} in a Cu‖Li-Sn cell, much better than bare Cu. In a full-cell configuration, AFLBs with a Li-rich Mn-based cathode (LRM)‖ Li-Sn showed a 16.7% increase in capacity and 14.1% increase in capacity retention after 20 cycles compared to LRM‖Li-Sn batteries. The Li-Sn alloy layer is capable to smooth the morphology and improve the connectivity of the deposited Li-metal. In addition, the Li-Sn surface has potential of strong bonding with Li-metal, allowing to deposit of thicker Li-metal layers with a firm connection to the substrate, in contrast to the peeling off of Li-metal at bare Cu [139].

However, like pure Li-metal, Li-alloys remain highly reactive, which may limit their practical application. Therefore, developing more stable lithiophilic current collectors is in urgent demand. Chen et al. [140] designed full-cell AFLBs with Li$_2$S as cathode and Au-modified Cu foil as anodic current collectors, which showed a high energy density of up to 626 Wh kg^{-1}. The Au-modification resulted in forming a Li$_x$Au alloy and corresponding solid solutions, which successfully lowered the nucleation barrier of Li-deposition and induced a dendrite-free morphology. Consequently, the anode-free Li$_2$S‖Au/Cu full-cell exhibits a high-capacity retention of 53% after 150 cycles. Although the Au layer showed excellent properties, the high cost prevents it from being commercially used. The cost-reduction efforts have been made to explore low-cost metal layers that can be alloyed with Li-metal. For example, Liu et al. [141] employed atomically distributed Zn on commercial Cu foils to form a Cu$_{99}$Zn layer by magnetic sputtering. The Cu$_{99}$Zn substrate exhibited superior wetting for molten Li-metal (Fig. 10a). During Li-metal deposition, Cu$_{99}$Zn alloys first with Li-metal to form a solid-solution, which highly reduces the deposition interface energy, before pure Li-metal is deposited. As illustrated in Fig. 10b, Cu$_{99}$Zn foil exhibited low nucleation overpotentials in the voltage curves during the plating process. It maintained a CE of over 98% (Fig. 10c).

Recently, multi-metal alloy layers combining several metals have been designed to improve anode-free batteries. Lin *et al.* [142] designed a multi-metal-layer coated on Cu current collectors composed of Ga, In, and Sn. Compared with the pristine Cu current collectors, the multi-metal-layered current collectors initiate Li-ion storage by an alloying reaction, forming an epitaxially-induced layer, as illustrated in Fig. 11. Moreover, benefiting from the lower LUMO energy of LiFSI than DME, the alloying process with an operating potential of around 0.75 V also promotes the formation of a LiF-rich SEI, which is favorable for the uniform plating of Li-metal [97]. The plating morphology of Li-metal on the multi-metal-layered current collectors is very compact and smooth (Fig. 11a) rather than the porous dendritic Li-metal shown in Fig. 11b-c. The capacity retention of anode-free multi-layer pouch cell NCM811‖ multi-metal-layered current collectors increased from 66 to 84% at 0.1 C with a remarkable energy density of 420 Wh kg^{-1} after replacing Cu with a multi-metal-layered current collector [142].

Apart from metal layers, various lithiophilic compounds and composites were also synthesized for AFLBs. Wondimkun et al. [143] prepared a lithiophilic hybrid current collector by using a two-step spin-coating technique. The hybrid current collectors significantly lowered the Li-nucleation barrier, achieving higher capacity retention of 55.7% after 60 cycles in carbonate-based electrolyte with FEC at 0.5 mA cm^{-2}. Using lithiophilic silver nanoparticles with polydopamine (Ag@PDA) as nucleation seeds was critical in facilitating homogeneous initial nucleation. That method produces an alloy LiAg phase, which maximizes exploiting the limited Li source for plating and stripping. Simultaneously, the outermost graphene oxide (GO) layer on top of Ag@PDA was used to buffer the Li-ion flux in AFLBs. The synergistic effect of Ag@PDA-GO composites enabled uniform Li-deposition and a dendrite-free morphology during repeated cycling.

Sahalie *et al.* [144] also synthesized an Al$_2$O$_3$/polyacrylonitrile (PAN) composite layer (AOP) coated on Cu to promote more compact and smoother Li-deposits in combination with an NMC111 cathode. The multifunctional AOP layer leads to SEI layers with moderate mechanical support and sufficient strength to suppress dendritic growth. The formation of Li-Al-O/Al$_2$O$_3$ species at the bottom part of the AOP layer reveals a good lithiophilicity. The effect of PAN is manifested by its flexible binding ability and high nitrogen content, which is highly lithiophilic. Consequently, NMC‖AOP@Cu cells operating at 0.2 mA cm^{-2} retain 30% of their storage capacity after 82 cycles. By then, NMC‖Cu cells retain about 30% of their original capacity after only 52 cycles.

Nowadays, numerous lithiophilic layers have been developed to coat Cu to improve the Li-metal plating/stripping stability. However, the profound lithiation or Li-alloying process may cause substantial volume expansion of the lithiophilic current collectors. These current collectors might then be separated from the Cu current collectors due to layer cracking and material losses. Thinning the lithiophilic layers could eliminate these lithiation-induced volume changes. Moreover, the thin-
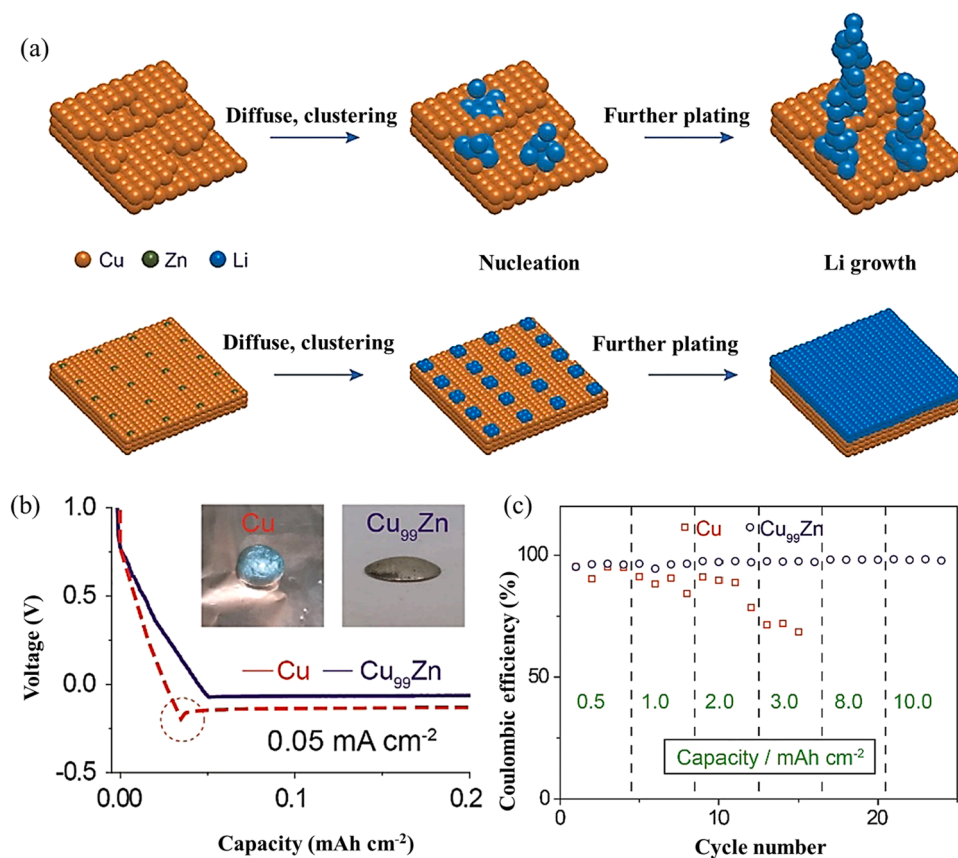
Fig. 10. (a) Schematic showing the Li-plating process at Cu and Cu$_{99}$Zn substrates. (b) Voltage profiles during initial Li-plating with 0.05 mA cm^{-2} at Cu and Cu$_{99}$Zn; the inset shows the wetting behavior of molten lithium on Cu and Cu$_{99}$Zn. Reproduced with permission [141]. Copyright 2018, Elsevier.

layer construction of the intermediate alloy layer should also be balanced with facile ionic pathways [6].

4.1.2. Artificial protective SEI layers

Although depositing lithiophilic layers onto current collectors reduces the Li-nucleation overpotential, the as-deposited Li-metal still has a high reactivity toward non-aqueous liquid electrolytes. That results in the formation of thick SEI layers, thereby consuming large amounts of Li-ions and causing limited CE and poor cycle life. In this regard, improving the electrochemical performance of AFLBs also requires effective management at the anode/electrolyte interface (or SEI layers) [11]. In general, naturally formed SEI layers on deposited Li-metal cannot sustain long-term cycling due to their poor mechanical properties and inability to accommodate volume changes upon cycling [145]. Furthermore, the inhomogeneous chemical composition and morphology within naturally formed SEI lead to non-uniform Li-ion transport and non-planar Li-deposition [146,147]. Intensive studies have been conducted toward introducing artificial SEI layers to establish chemically/mechanically stable and uniform Li-metal/electrolyte interfaces.

Inorganic-based materials are commonly employed as artificial SEI candidates for AFLBs due to their relatively high ionic conductivity and mechanical strength [148]. For example, Wondimkun et al. prepared binder-free graphene oxide (GO) films (around 1.15 μm) as artificial SEI for anode-free NMC||Cu cells. Combining FEC electrolyte additives, the spin-coated ultrathin GO offered numerous nano-channels for Li-ion transport and enabled homogeneous Li-plating [115]. The anode-free NMC||Cu-GO full-cells show a high average CE of 98% and capacity retention of 44% after 50 cycles. Similarly, an ultrathin layer of Al$_2$O$_3$ (15 nm) was deposited on Cu substrates as artificial SEI [149]. The pinhole-free Al$_2$O$_3$ coatings facilitate flat and compact Li-deposits. When

the artificial SEI (Al$_2$O$_3$) is used, the CE of the assembled anode-free cell can reach up to 98.9%. In contrast, the CE of a cell without artificial-SEI protection was only 91%. In addition to chemically regulating Li-ion transport, inorganic artificial SEI with a shear modulus twice that of Li-metal are expected to prevent non-planar Li-deposition or Li-dendrite growth [150]. For example, graphene possesses a high Young's modulus of 1 TPa, considerably larger than Li-metal (4.9 GPa) [151]. Therefore, graphene can mechanically suppress the growth of Li-dendrites. Due to its superior properties, multi-layered graphene was employed as an artificial SEI for anode-free LiFePO$_4$||Cu batteries [96]. These multi-layered graphene films substantially reduce the polarization and nucleation overpotential of Li-metal. Besides, delocalized π electrons in graphene can homogenize the Li-ion flux. Based on these advantages, the AFLBs equipped with multi-layered (285 nm) graphene-modified Cu substrates and LiFePO$_4$ cathodes achieved capacity retention of 61% after 100 cycles, 16% higher than those based on unmodified Cu substrates [96].

Polymer-based artificial SEI generally has higher flexibility but lower mechanical modulus than its inorganic-based counterparts. The multiple functional groups in polymers can assist in regulating Li-ion transport [148]. Assegie and co-authors used spin-coating to deposit polyethylene oxide (PEO) films on Cu substrates as an artificial SEI (Fig. 12a) [152]. The electrostatic interaction between Li-ions and polar oxygen atoms in PEO films promotes uniform and planar Li-deposition (Fig. 12b-c). In addition, the PEO film prevents excessive contact between Li-metal and liquid electrolytes, avoiding natural and non-uniform SEI formation. Anode-free LiFePO$_4$||Cu@PEO full-cells exhibited an average CE of 98.6% and capacity retention of 30% after 100 cycles (Fig. 12d). Notably, the thickness and uniformity of the PEO coatings were discovered to be essential in influencing the Li-deposition morphology and cycling performance.
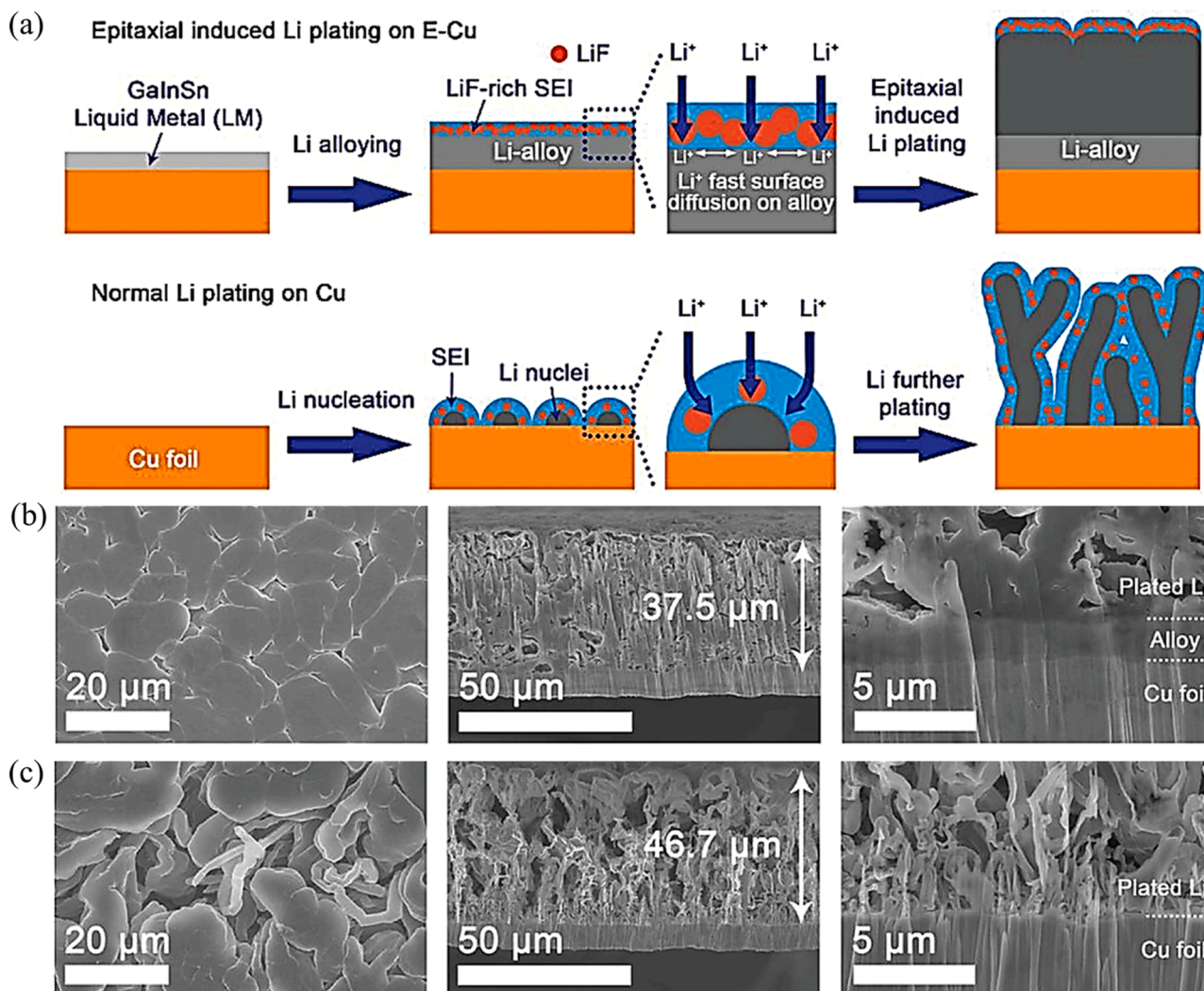
Fig. 11. (a) Schematic representation of Li-alloying and epitaxial-induced (E) plating on E-Cu and Cu. SEM image (left) and cross-sectional SEM images (middle and right) of E-Cu (b) and Cu (c) current collectors after 5 mAh cm^{-2} Li-plating with a current density of 0.5 mA cm^{-2}. [142]. Copyright 2021, Wiley-VCH.

Organic-inorganic composites are also promising candidates for artificial SEI, which combine the high mechanical strength and high ionic conductivity of inorganics with the high flexibility of organic materials [148]. For example, Abrha et al. [29] developed a thin inorganic-rich interfacial film composed of lithium perchlorate (LiClO$_4$), cubic garnet Li$_7$La$_{2.75}$Ca$_{0.25}$Zr$_{1.75}$Nb$_{0.25}$O$_{12}$ (LLCZN), and poly-vinylidene difluoride (PVDF) (Fig. 13a). The inclusion of LiClO$_4$ and LLCZN was employed to improve the Li-ion conductivity and strength of the composites. The PVDF polymer improves the mechanical flexibility of the films. The composite artificial SEI promoted uniform deposition of Li-metal and induced the formation of LiF/LiCl-rich SEI (Fig. 13b-c). As a result, the constructed anode-free NMC||Cu@LLCZN-PVDF full-cells showed capacity retention of 58.6% and an average CE of 97.6% after 30 cycles. However, Young's modulus (~10.6 MPa) of the LLCZN-PVDF composite film is lower than that of Li-metal. That may not be sufficient for mechanical inhibition of the growth of non-planar Li-metal. Further studies must be carried out toward manipulating the composition ratio and structure of the composite artificial SEI by considering the ionic conductivity, mechanical strength, chemical/structural uniformity, and fabrication cost. Furthermore, the artificial SEI is an inactive material unable to host Li-ions. Therefore, the thickness and volume of artificial SEI must be carefully chosen to preserve the volume and achieve high volumetric capacities of synthesized complete AFLBs [11].

4.2. 3D structural design

The morphology of deposited Li-metal and SEI layer in AFLBs is mainly governed by the structure of current collectors. Current collectors with specific micro- and/or nanostructures (also known as 3D electrode hosts) have been proven beneficial for uniform Li-metal deposition and prolonging the cycle life of AFLBs [153]. Li metal can be plated on and stripped from 3D-structured hosts without causing severe volume expansion [154]. In particular, the current collectors with 3D porous structures offered an increased surface area with increased nucleation sites. That reduces the local current density and arranges a redistribution of Li-ion flux, ultimately ensuring more uniform deposition without Li dendrites.

The most popular 3D-based host for Li-metal deposition is carbon-based materials [154]. Kwon et al. [155] manufactured a multivacancy-defect-enriched carbon surface as anode current collectors for AFLBs by electrochemical etching. In contrast to the formation of a non-uniform SEI and Li-dendrite growth at a graphite surface, [156] the multivacancy-defect structures address the critical issues of a Li-metal surface by constructing a thin and uniform SEI. Such an SEI reduces electrolyte decomposition and enables even distribution of Li-nuclei that laterally grow on the current-collectors surface (Fig. 14a). This behavior is attributed to the fact that the multivacancy-defect carbon can lower the Fermi energy level of current collectors. It is
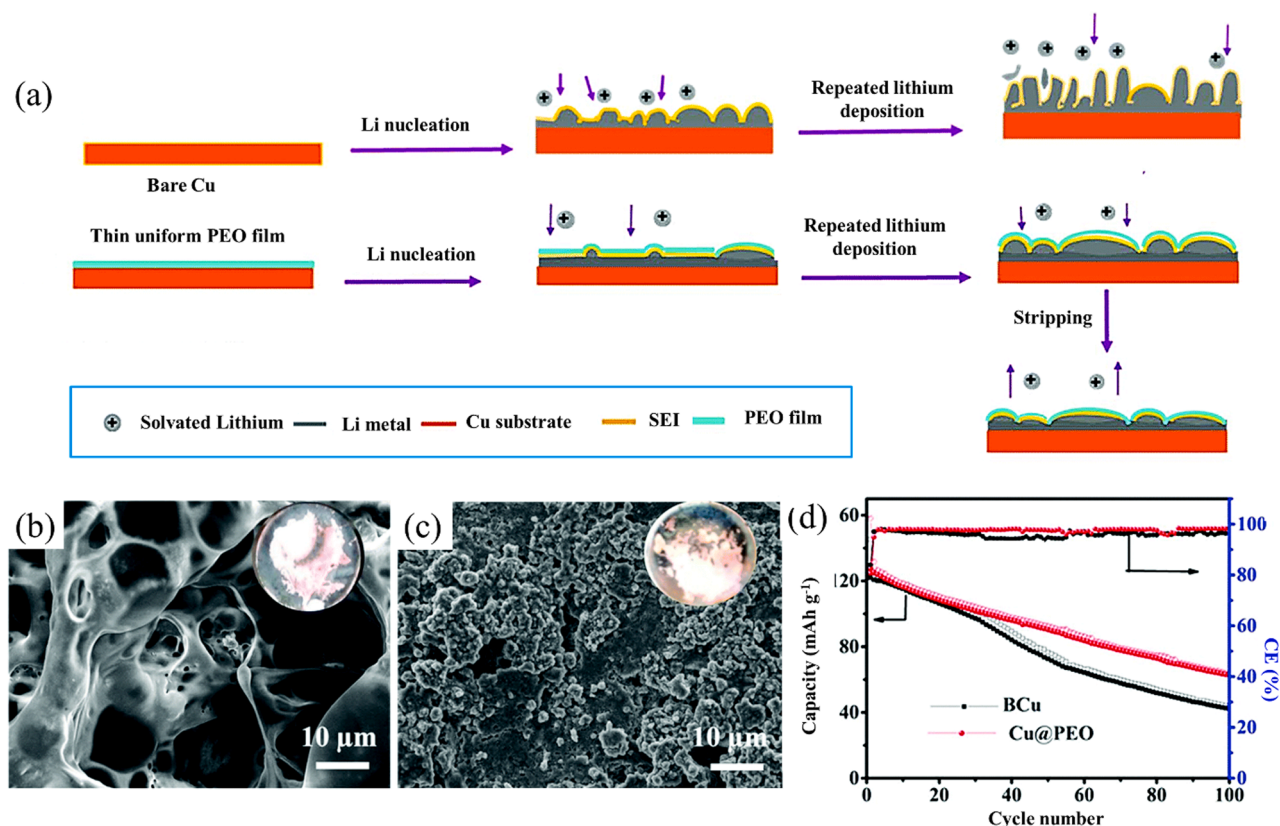
Fig. 12. (a) Schematic diagrams of Li-plating and stripping on bare Cu electrode, thick and thin PEO film coating. Morphology of deposited Li-metal in full-cell anodes Cu@PEO (b) and BCu (c) after 100 cycles in 1 M LiPF$_6$ and EC/DEC. (d) Cycling performance of bare copper electrode (BCu/LFP) and modified electrode (Cu@PEO/LFP). Reproduced with permission [152]. Copyright 2018, Royal Society of Chemistry.
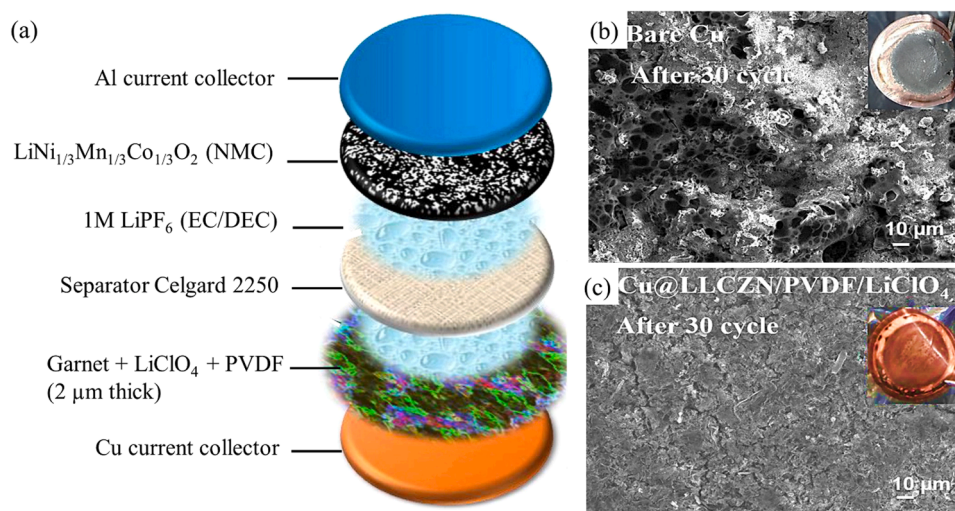
Fig. 13. (a) Schematic configuration of a tested anode-free battery with artificial SEI layer of garnet composite. SEM images of Li-plating NMC||Cu (b) and NMC|| Cu@(LLCZN/PVDF (84:16) /LiClO$_4$) after 30 cycles (c) [29]. Copyright 2019, Elsevier.

beneficial to suppress electron transfer to the LUMO of the electrolyte, offering a strong binding of Li-ions via orbital hybridization (electron transfer). The multivacancy-defective carbon was applied as current collectors in NCM-based AFLBs, showing capacity retention of 90% after 50 cycles at a current density of 2.0 mA cm^{-2} (Fig. 14b).

Apart from carbon-based 3D current collectors, 3D porous Cu foams have also been widely applied as current collectors for AFLBs. Cheng et al. [157] found that substituting 2D-Cu with 3D Cu foam could lower the Li-nucleation overpotential and facilitate homogenous Li-deposition.

To further reduce the Li-nucleation overpotential, Ag layers were deposited on 3D-Cu. That effectively stabilized the Li-deposition behavior. Li$_2$S||Ag@3D-Cu AFLBs showed excellent electrochemical properties with an initial area capacity of up to 7.4 mAh cm^{-2} and a high capacity retention of 64.9% after 40 cycles. Lithiophilic zinc oxide was also loaded onto a Cu foam and nickel-cobalt alloy as a 3D-based current collector for AFLBs [28]. With its lithiophilic properties, zinc oxide reduces the Li-nucleation overpotential, forming an even and compact Li-metal layer (Fig. 15a). Additionally, the lithiophilic zinc oxide
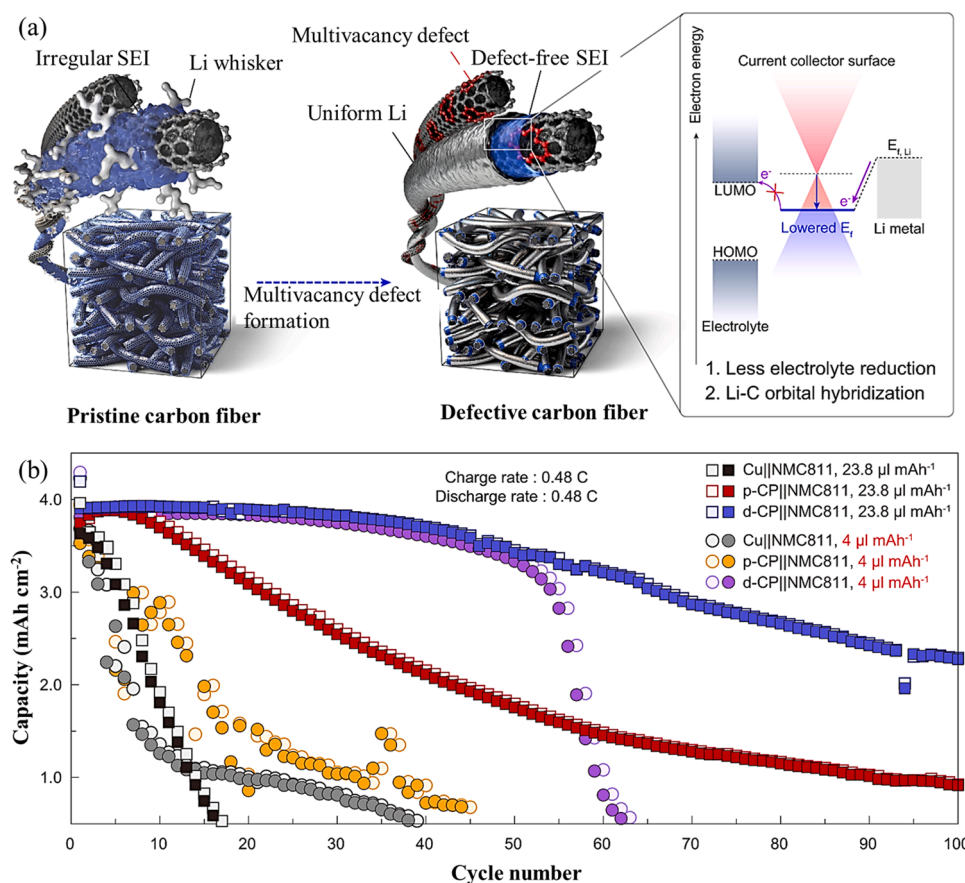
Fig. 14. (a) Schematic of the dual functionality of an electron-deficient carbon surface. (b) Plots of charge and discharge capacity as a function of cycle number for anode-free NCM811 full-cells with 1 M LiPF$_6$ EC/DEC+10% FEC+1% VC. Reproduced with permission [155]. Copyright 2020, Springer Nature.

successfully increases the level of thickness Li-deposition (from 300 μm of copper foam to 1000 μm), resulting in effective CE improvements. Under a total capacity of 1 mAh cm^{-2} at a current density of 1 mA cm^{-2}, the CE of the assembled AFLBs remains above 95% after 590 cycles (Fig. 15b). Remarkably, the symmetric cells were cycled for more than 560 h at 2 mA cm^{-2} with a capacity of 1 mAh cm^{-2} (Fig. 15c).

With the ability to overcome lithiation-induced volume expansion and uneven Li-deposition, 3D structured current collectors have considerably improved the cycling performance and energy density in AFLBs. However, the fabrication costs should be considerably lowered while keeping the desired morphology and porosity [113]. Fortunately, the continuously progressing etching and 3D printing technologies, which can facilitate the high-accuracy synthesis of various 3D structures, will promote the development of 3D current collectors for AFLBs soon.

5. Test condition optimization

External factors such as working temperature and stacking pressure influence the morphological evolution of Li-deposition significantly. It was confirmed that the stacking pressure influences the Li-plating and tripping processes as well as the SEI properties in different ways in both liquid- and solid-electrolyte-based batteries [158]. The applied charging and discharging strategies, *i.e.* current densities and cut-off voltages, also affect the cycling performance of AFLBs. Therefore, optimizing these test conditions is also important to improve the stability of deposited Li-metals and formed SEI. Various testing protocols have been designed to test AFLBs correctly.

5.1. Current densities

Cycling current densities strongly influence the morphology of deposited Li-metal and the SEI in AFLBs, affecting the overall battery performance. Jiao et al. [159] discovered that when the used current density was increased, the thickness of the degradation layer at the Li-metal anode increased. Such behavior resulted in a reduction in the thickness of the remaining bulk Li-metal layer. The number and size of degradation-layer fractures also increased so that the amount of the deposited Li-metal declined. In addition, at the lower current densities, more inorganic and less conductive species, such as LiF and Li$_2$CO$_3$, are formed in SEI, resulting in a higher impedance. Consequently, higher current densities result in a more rapid capacity decay and a shorter cycle life. Therefore, optimizing the current densities of the (dis) charging processes is an effective method for controlling the thickness, forming more stable SEI layers.

To explore the effect of current densities on cycling performance, Louli et al. [7] investigated the effect of (dis)charging current density on the performance of AFLBs utilizing three different cycling conditions for NMC532||Cu batteries: symmetric charging and discharging, asymmetric faster charging, and asymmetric slower charging. The authors discovered that the relative rate of charging *vs.* discharging is more important than the absolute current densities. Moreover, cycling with an asymmetric slower charging protocol is optimal, consistent with previous research on cells with Li-metal anodes [160]. It was found that the symmetric cycling resulted in cells retaining 80% of their original capacity after 50 cycles (Fig. 16a). On the other hand, the AFLBs tested with asymmetric faster charging protocols degrade to 80% of the original capacity within only 40 cycles. The fast charging protocol reduced the cycle life since efficient Li-plating deteriorates at higher charging
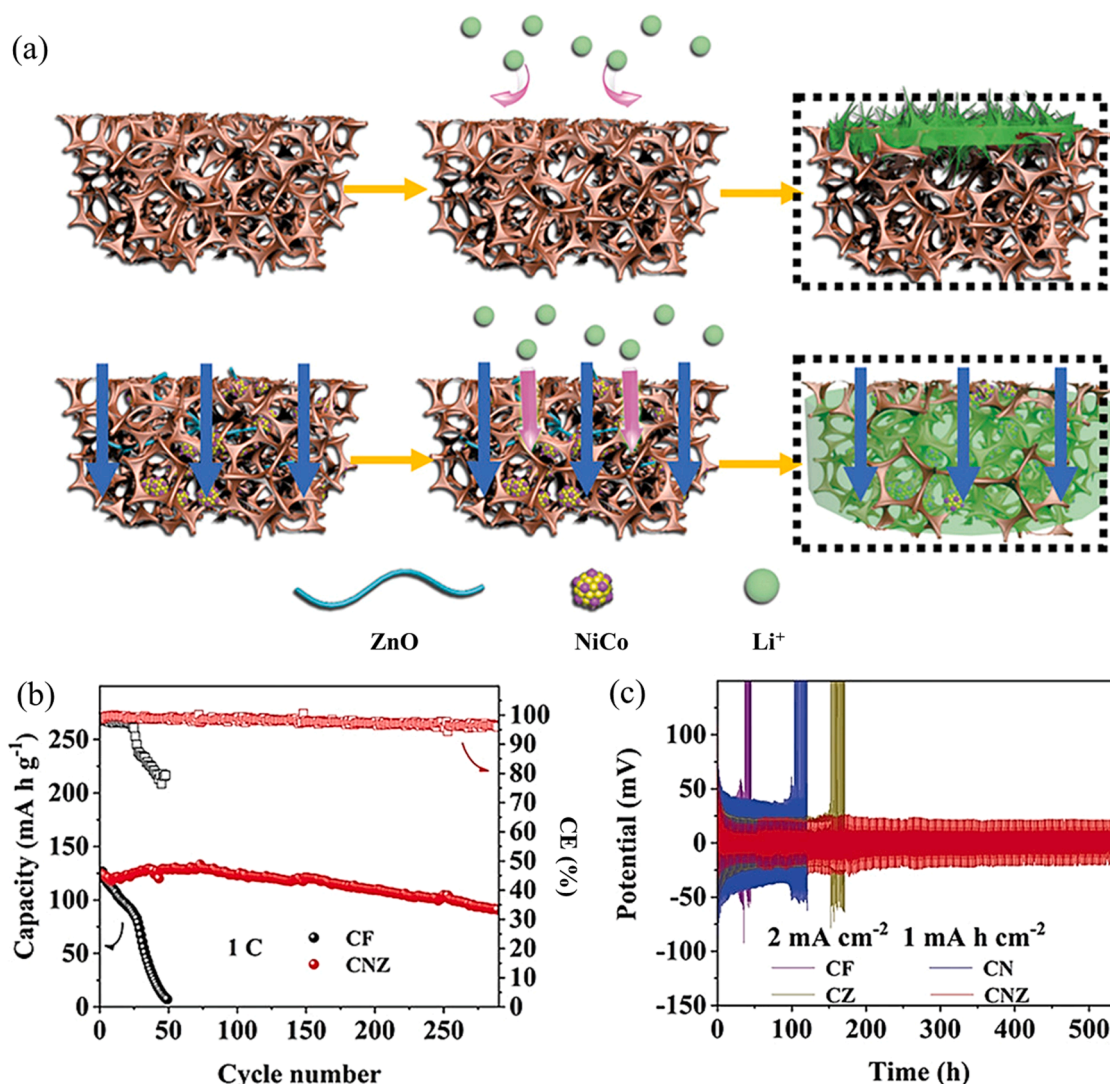
Fig. 15. (a) Schematic diagrams for comparing Li-deposition on Cu foam and Ni/Co-ZnO—Cu foam. (b) Discharge capacity and CE of full cells at a current density of 1 C. (c)The cycle performance of the four current collectors for Li-free anodes with a fixed capacity of 1 mAh cm^{-2} at 2 mA cm^{-2}. Reproduced with permission [28]. Copyright 2022, Wiley-VCH.

rates [159]. Finally, NMC532‖Cu batteries cycled with the asymmetric slow charging procedures (C/10 D/4) showed the best performance, retaining 80% of their capacity after 80 cycles (Fig. 16a). That was better than the other two test conditions. Notably, the authors demonstrated that under asymmetric slow-discharge test conditions, the battery's cycle life depends more on the relative ratio of the charging and discharging rates rather than the absolute current densities. The absolute current densities determine the operational duration of batteries (Fig. 16b).

The primary reason for the differences in cell properties is the different Li-morphology when utilizing these charging and discharging protocols. Using the symmetric (C/5 D/5) protocol (Fig. 16c), medium-sized 10–15 μm Li-nodules are formed. The area of the porous Li-metal deposited is determined by the space between the nodules. Since the ideal Li-morphology should possess a lower surface area, these medium-sized nodules result in a moderate cycle life of 50 cycles. The Li-morphology in cells cycled with an asymmetric faster-charging protocol is shown in Fig. 16c. The protocol results in forming smaller Li-grains of 5–10 μm. The faster (C/2 D/5) protocol exhibits loose grains with interspersed porous Li-deposition.

In contrast, the slower (C/4-D/10) protocol clearly exhibits a more compact morphology. Smaller Li-particles with an increased surface area result in a lower lifetime [162] It is consistent with the worse (~40 cycles) lifetime for cells cycled with the asymmetric faster-charging protocol. The Li-morphology for cells cycled with the superior asymmetric slower charging protocol is shown in Fig. 16c. With the protocol, large 15–25 μm Li-grains are formed. Porous deposited Li-metal are observed between these large grains at (C/2.5 D/1) and, to a lesser extent, at (C/5 D/2). At (C/10 D/4), the large Li-grains are tightly packed, resulting in a flat mosaic Li-metal. The ideal Li-morphology results in the lowest Li-metal inventory loss, consistent with a cycle life of about 80 cycles using the protocol. Therefore, the size of the formed Li-metal particles can be effectively controlled by optimizing the charging and discharging rates. This optimization reduces the formation of SEI layers and improves the cycle life of AFLBs.

5.2. Cut-off voltage

The cut-off voltage is another crucial parameter affecting the stability of the battery during cycling. At first, higher cut-off voltages can occasionally result in a worse cycling performance due to the reaction of Li-salts and organic solvents, as well as the degradation of cathode materials. However, employing a low cut-off voltage will decrease the battery energy density. Consequently, establishing an appropriate cut-
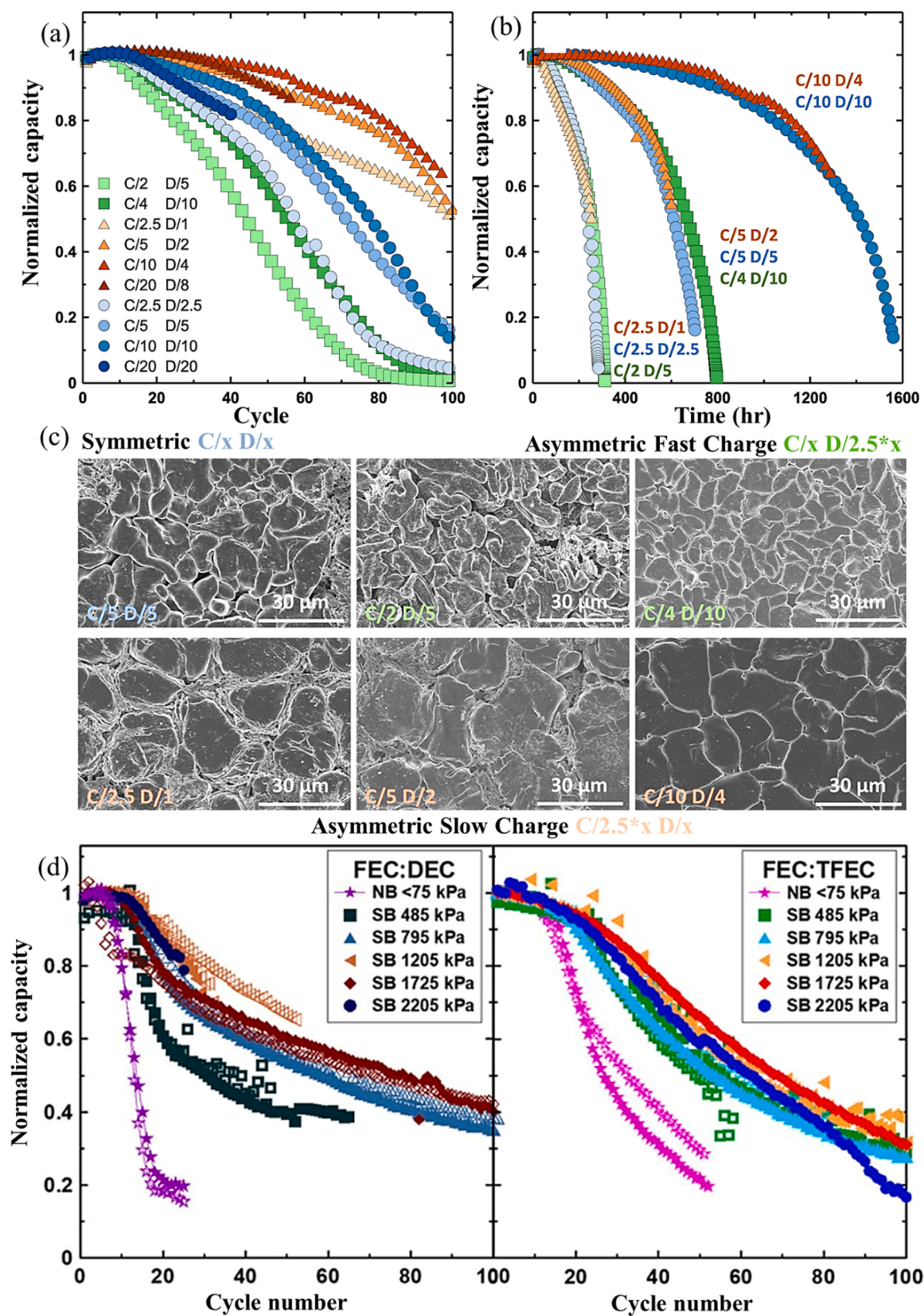
Fig. 16. (a) Normalized capacity as a function of cycle number for all charge-discharge rate tests; cells tested with a symmetric charge-discharge protocol (blue), an asymmetric protocol with faster charging (green), and an asymmetric protocol with slower charging (orange). (b) Normalized capacity *vs.* time for all charge-discharge rate tests. (c) Li-morphology generated in a cell cycled with symmetric charging and discharging, asymmetric faster charging, and asymmetric slower charging. Reproduced with permission [7]. Copyright 2021, IOP Publishing. (d) Cycling data for cells containing 1 M LiPF$_6$ in FEC/DEC (1:2 v:v) (left) and 1 M LiPF$_6$ FEC/TFEC (1:2 v:v) (right) electrolyte constrained under different pressures between 75 and 2205 kPa. Reproduced with permission [161]. Copyright 2019, IOP Publishing.

off voltage is required to achieve cells with excellent capacity stability and high energy density.

Louli *et al.* [7] applied an upper cut-off voltage of 4.5 V with different lower cut-off voltages of 3.0, 3.6, 3.8, and 4.05 V for NCM532||Cu cells, corresponding to a depth of discharge of 90, 80, 45 and 23%, respectively. It was discovered that the lower cut-off voltage of 3.0 V results in a capacity loss of 40% in 100 cycles. The same capacity loss occurs after over 160 cycles at 80% (3.6 V) and over 630 cycles at 45% (3.8 V). The lower cut-off voltage of 4.05 V causes only a 10% capacity loss during 1000 cycles, attributed to a larger Li-reservoir to replenish lost Li-metal by enlarging the lower cut-off voltage. However, a lower depth of discharge would sacrifice part of the area capacity to improve the cycling life.

Furthermore, multiple cut-off voltages were used throughout the initial and subsequent charging and discharging processes. For example, Chen *et al.* [140] designed Li_2S||Cu/Au full-cells, which were initially charged and discharged with 0.05 C between 1.7 and 3.8 V and cycled between 1.7 and 2.8 V *vs.* Li/Li^+. In the initial cycle, more Li^- ions were stripped from the Li_2S cathode and plated onto the vacant anodic current collectors to contribute to higher capacities. Then, reducing the upper cut-off voltage improves the cycling stability by reducing the side reactions. Therefore, combining different cut-off voltages for charging and discharging is a promising approach for balancing the energy density and stability of anode-free cells.

5.3. Mechanical pressure

External pressures should also be considered in the practical application of AFLBs [163,164]. Force-displacement measurements performed at increasing pressures up to 200 PSI (~1400 kPa) revealed that the electrode stack thickness of Li-metal batteries increased with cycling, along with capacity loss. That may be attributed to porous dendritic Li-growth, accumulation of dead Li-metal, and SEI growth [165]. The mechanical pressure could physically suppress the dendrite growth and maintain a more planar, lower-surface-area morphology [166]. Louli et al. [161] demonstrated that high pressure improves the cycling stability and plating/stripping efficiency of AFLBs. The authors reported that 4.5 V anode-free pouch cells exhibited stable capacity retention of over 50% within 50 cycles at a moderate pressure of 485 kPa (Fig. 16d). Applying excessive pressure to the cell might cause the current collectors to fracture and the positive electrode to delaminate. Furthermore, the polymer separators are deformed at high pressures, which may also hinder Li-ion transport through separators. Therefore, the optimization of pressure is also necessary to improve the cycling stability of AFLBs. Generally, the commonly accepted stack pressure in the range of 100–1000 kPa is used to construct commercial pouch cells. However, in the cases of coin cells using the springs, the maximum applied pressure can be as high as about 1378.95 kPa [166]. Furthermore, the volume expansion of AFLBs during the Li-plating process would increase the pressure applied to the battery components, which also deserves further investigation.

Thus, test conditions are essential for the morphology of the formed Li-metal and SEI layers in AFLBs. The morphology influences the cycle life. Consequently, optimizing the test conditions will significantly increase the cycle life of anode-free cells. The majority operate at low current densities and voltages now. However, it is necessary to investigate the ability to operate at high current densities and voltages to enable larger energy density output. That will broaden the practical application of anode-free cells.

6. Advanced characterization technology

In AFLBs, Li growth and the SEI formation process are two major factors affecting cell stability. In the previous sections, we have described many ways to improve the performance of anode-free batteries. However, many of their underlying mechanisms are not understood

in detail. Fortunately, many advanced characterization methods have been developed in recent years, especially in-situ and in-operando analytical techniques. These techniques have successfully revealed the 3D structural evolution of Li-deposition in real-time and at various length scales. In particular, the chemistry and structure of SEI on the nanoscale were partially resolved. That helps to understand Li plating/stripping, SEI formation mechanism, and its physicochemical properties [36,135].

There are various methods to classify the characterization techniques used to investigate the Li-growth and SEI formation process of Li-metal anodes [36,135]. This section focuses on advanced in-situ and operando technologies applied for AFLBs. The detection techniques are classified into imaging-based and spectroscopic-based. For the former, the Li-growth and SEI formation process can be observed directly, *e.g.* by optical images, SEM, or transmission X-ray microscopy (TXM). Spectroscopic-type technologies such as XPS and NMR record a characteristic spectrum of Li-containing, SEI species or observe changes in the cell's electrochemical, mechanical, or chemical signals to infer the presence of Li and Li-containing species [167]. Both imaging and spectroscopic type techniques can be applied to characterize the Li-dendrites, dead-Li, and SEI formation, for understanding the mechanisms of capacity decay in AFLBs.

6.1. Imaging-based methods

Imaging methods directly visualize the growth process of Li-containing species or SEI layers in the cells. Local imaging is a commonly used method for observing Li growth during the charging and discharging process and detecting the formation of Li dendrites, dead Li, and SEI layers [167].

Recently, some in-situ and operando imaging techniques methods, [168] like SEM, [169] transmission electron microscopy (TEM), [52] and optical microscopy (OM), [44] have been devoted to dynamically visualizing the evolution of Li plating and/or stripping at nanometer- or micrometer-scale, unveiling dynamic information about initial Li nucleation, the subsequent growth, and dissolution. Huang et al. observed the Li deposition/dissolution upon cycling by in-situ OM observation [170]. They found that Li dendrites were formed due to the inhomogeneous plating of Li grown on different spots of Cu foil (Fig. 17a). In addition, a non-uniform dissolution of Li and the formation of a rough surface at the deposited Li were observed. That phenomenon resulted from the locally heterogeneous current distribution, further accelerating the formation of dendritic Li on the Cu electrode. During the stripping process, the deposited Li was dissolved. However, the dissolution was inhomogeneous. That is attributed to the higher charge-transfer resistance. As a result, a large amount of dead Li was left on the Cu surface at the end of the stripping process. These observations visually explain the process of Li-dendrite and dead-Li formation, which leads to poor cycling performance of AFLBs.

In-situ transmission X-ray microscopy (TXM) imaging technique can also visualize the dendritic or mossy lithium (Fig. 17c) [171]. Hwang and co-workers also developed a versatile thin-plastic cell, which offers a good contrast between Li and electrolytes so that the Li growth and stripping can be clearly observed. Real-time observation reveals that the Li growth and stripping rate in the vertical direction are faster than in the lateral direction. That indicates faster growth from the base and faster stripping from the tip-top.

Pei et al. studied Li nucleation and growth on Cu by a galvanostatic method combined with SEM using Li||Cu cell [13]. They found that the overpotential and Li nuclei sizes are inversely proportional. It was attributed that nuclei seeds and smaller Li morphologies can cause increased electrolyte consumption and SEI formation due to the increased surface area. Based upon this understanding, the instantaneous nucleation of Li during galvanostatic electrodeposition was utilized to improve the uniformity and particle density of deposited Li metal, which enhances electrode performance and safety. Fuchs et al.
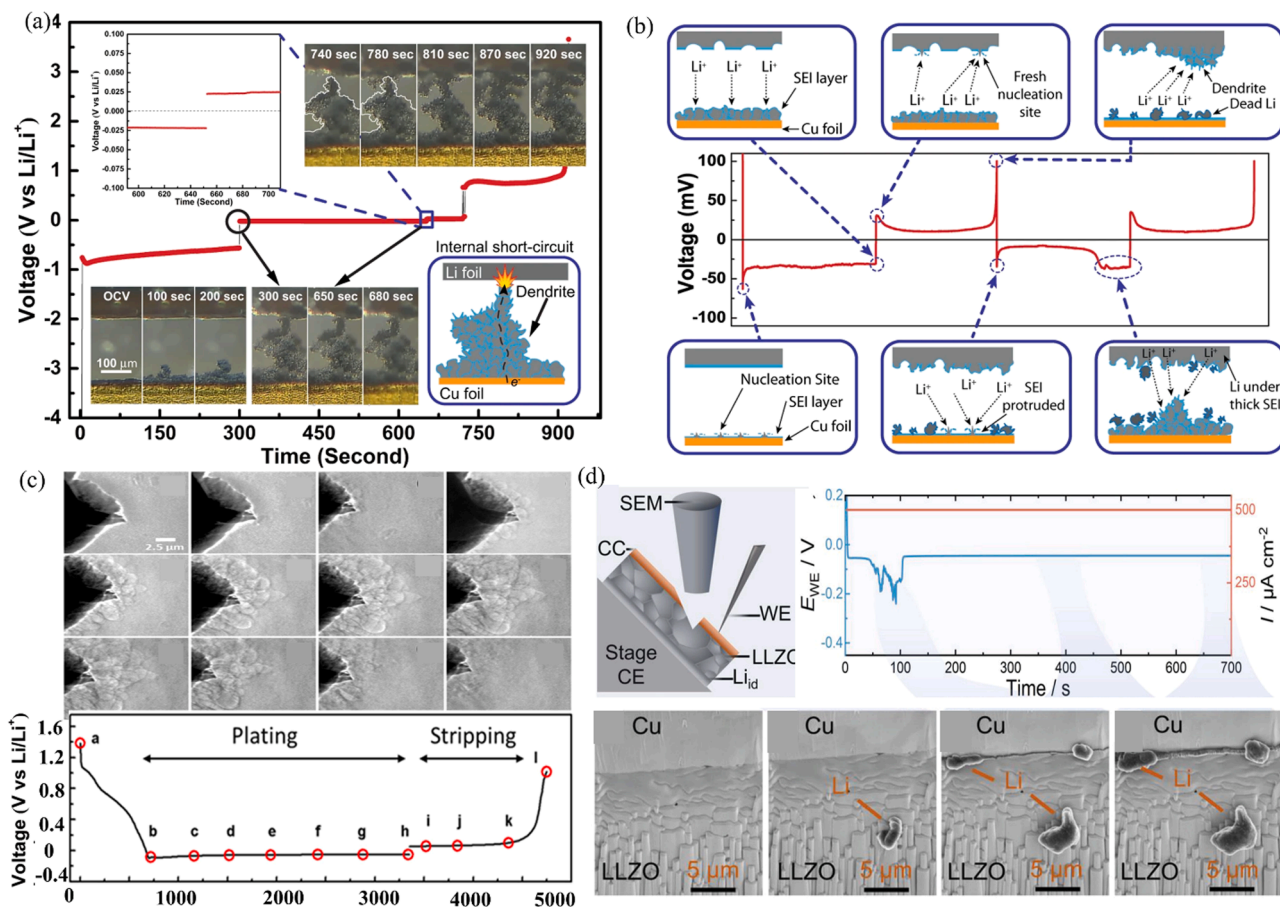
Fig. 17. (a) In situ OM measurement of Li deposition/dissolution on Cu electrode under an ultrahigh current density of 500 mA cm^{-2} for demonstration of short-circuiting. It should be noted that the observed short circuit region is different from the initial observation region for the Li-plating process; (b) Scheme of Li deposition/dissolution on Cu foil during cycling of Li/Cu cell under a current density of 0.2 mA cm^{-2} Reproduced with permission [170]. Copyright 2021, Springer nature. (c) In operando TXM images of lithium plating and stripping and the bottom is the cycling curve of the *in situ* cell at the current density of 1 mA cm^{-2}. Reproduced with permission [171]. 2017 American Chemical Society. (d) The schematic setup was used to observe lithium plating with 100 μA cm^{-2} at the interface at Cu$_{foil}$|LLZO, and voltage profile during plating with 500 μA cm^{-2} and screenshots of a video recorded during the plating and lithium growth process. Reproduced with permission [13]. Copyright 2023, Wiley-VCH GmbH.

used operando SEM to examine the cross-section during lithium plating at solid Cu||LLZO interfaces (Fig. 17d) [172]. They found three different lithium growth modes: (i) vertical whisker growth, (ii) film growth, and (iii) dendritic growth. It was discovered that Li microstructures evolved from whisker growth to film or dendritic growth with increasing current densities during plating. It was confirmed that using thick current collectors to suppress Li whiskers penetration. Optimizing the current density and plating protocol is also of importance for depositing homogeneous Li-metal electrodes.

The imaging-based methods also can detect the SEI layers, such as *in situ* TEM and AFM. However, these advanced *in situ* techniques have not yet been developed for AFLBs. It is worth mentioning that Huang et al. combined *in situ* OM with the charge and discharge curves to explore the mechanisms of SEI formation successfully (Fig. 17b) [170]. At the beginning, the initial energy barrier of Li-nucleation on the clean Cu surface needs to be overcome, which causes the higher overpotential seen from the curve. Then, Li underneath the thick SEI layer on Li foil starts to dissolve and deposit onto the nucleation sites on the Cu surface, accompanied by the decrease of overpotential. Next, in the Li-stripping process from the Cu surface, the overpotential is induced by the resistance of the SEI layer protruding and fresh Li growth on the Li surface. At the end of the Li-stripping process from the Cu surface, the cell voltage suddenly lifted due to the total consumption of active Li, leaving some dead Li at the Cu surface. In the following cycles, the deposition/dissolution of Li is similar to the first cycle in general, including SEI

fracture, fresh Li nucleation, dendrite growth, and dead Li formation at both sides. Until dendrites grow from the electrode surface and penetrate the SEI layer, leading to short circuits in the battery. Therefore, managing the growth of dendrites and the stability of SEI is an ongoing challenge in developing high-performance and safe AFLBs.

The imaging-based methods offer lively insight into the mechanisms of lithium metal growth and the origin of capacity degradation. Nevertheless, it should be noted that the Li-nucleation is challenging to be captured due to the very fast process nature. Moreover, the small size of Li-nuclei makes Li-nuclei difficult to be tested. In addition, the small thickness of SEI layers also makes it difficult to measure their physico-chemical properties accurately. Therefore, there is still an urgent need to develop or apply advanced technologies to explore the Li-nucleation process in detail in AFLBs.

6.2. Spectroscopic detection

The imaging-based Li detection techniques are often needed to operate under high-vacuum or cryo-operation conditions. Meanwhile, electron beam damage in SEM or TEM makes in-situ observation of the Li metal deposition difficult [36]. To overcome these drawbacks, some spectroscopic non-destructive methods, such as NMR, XPS, or electron paramagnetic resonance EPR, have been developed to observe changes in the electrochemical, mechanical, or chemical signals [36,135].

Menkin et al. employed in-situ solid-state NMR on Cu||LFP cells to

study the plating and stripping of Li (Fig. 18a) [173]. Upon plating, a new signal at ~260 ppm emerges, corresponding to the Li-metal deposits. The shift to higher frequencies is a result of the Knight shift. It was shown that the Li-metal signal during electrodeposition on Cu grows in intensity during the plating and decreases upon stripping. However, the Li-metal peak still remains at the end of discharge, indicating the presence of dead Li.

Accordingly, Geng et al. used in-situ electron paramagnetic resonance (EPR) to monitor variation during Li deposition [174]. They applied the in-situ EPR technique to monitor the variation during Li deposition (Fig. 18b). The EPR method can detect the semiquantitative distribution of the Li deposits by the 2D spatial-spatial imaging, to visualize the Li-nucleation and the growth. The red color indicates the local excessive deposits (LEDs) attributed to the growth of mossy or dendritic Li (Fig. 18c). The homogeneous deposits in the first cycle generate a compact SEI coating on the electrode, leading to worse nucleation kinetics in these areas. As a result, the second Li nucleation mainly occurs on the borders and the sites of dead Li where the SEI may be thin. The distribution of Li plating densities is quite different between the first and the second plating. The LEDs grow primarily during the second plating, which indicates that the current flows are mainly concentrated in these sites. Geng et al. also found that the LEDs' sizes are reduced after cycling. The homogeneity of the Li microstructures also becomes worse.

In situ spectroscopic techniques are also often used to probe the SEI and characterize the SEI evolution mechanisms. That is essential for understanding the operation of AFLBs. The good examples of this group technique are sputter-etched XPS, [178]. ToF-SIMS, [179] laser ablation inductively coupled plasma mass spectrometry (LA–ICP–MS), [180] and laser-induced breakdown spectroscopy [181]. Most of these techniques are based on sputter etching with ions or pulsed laser to the sample surface, which is challenging to characterize the SEI formation during cycling. Therefore, developing *in situ* technologies is still important to detect the interphase in AFLBs. Davis et al. investigate the role of sulfide SE stability during Li plating on LPSCl (electrically insulating SEI) and LGPS (electrically conducting SEI) electrolytes in anode-free cells using operando video microscopy and operando XPS (Fig. 18d) [175]. Operando XPS analysis of SEI components demonstrate the dynamic evolution of SEI formation in the LPSCl SEs (Fig. 18e). In particular, the low Faradaic efficiency in the LGPS samples corresponds to continuous SEI formation throughout the experiment. In contrast, in the LPSCl samples, the interface stabilizes following initial SEI formation, after which Li metal plates at the anode-free surface. It is attributed to the electrically insulating nature of the SEI components in LPSCl. Electronic transport across SEI/SE interface is blocked when the SEI becomes sufficiently compact and thick. Therefore, LPSCl exhibits significantly higher Faradaic efficiency and correspondingly minimal Li loss in AFLBs during the SEI formation process.

Furthermore, spectroscopic detection can be applied to explore the mechanism of side reactions in batteries, for example, by detecting the by-products of SEI formation reactions. The online gas evolution analysis was performed by assembling the anode-free cell with electrolytes (Fig. 18f) [176]. Since the Li anode is highly reactive toward the electrolyte, at the open-circuit voltage (OCV) stage, the SEI is formed chemically. When using an anode-free cell, the interfacial reaction happens at both the anode and cathode. Then CO_2, CO, and C_2H_4 gasses are found and evolved at the beginning of the first charge due to the electrolyte decomposition at the in-situ formed Li. However, above 4.38 V in the first, second, and third cycles, the evolution of CO and CO_2 together with O_2 release is due to both electrochemical and/or chemical interfacial reactions on the surface of the cathode.

In AFLBs, the capacity fade mainly results from forming SEI species and dead Li. That also leads to irreversible volume changes. Li et al. developed an in-situ optical-fiber-sensor-derived monitoring technique to detect strain evolution (Fig. 18g) [177]. The authors fixed the fiber Bragg grating (FBG) sensors on the surface of the battery. The stretch

and contract of cell skin caused by the periodic change and irreversible change in volume can be recorded and quantized throughout the lifetime (Fig. 18h). It was found that the surface strain reaches the maximum in the middle of the first charging, and the peak value is much higher than those of other cycles. That is attributed to intensive gas generation and SEI formation in the first cycle. The accumulation of gas leads to an increase in strain. Once the SEI is formed, gas production decreases significantly. Meanwhile, part of the gas is expelled into the prepared gas bag. As a result, gas accumulation reaches the maximum in the middle of the first charging process. Therefore, the strain increases sharply at first and decreases dramatically due to less gas accumulation. Furthermore, the surface strain decreases with cycling, corresponding to a lower charge/discharge capacity, which is related to the battery's capacity fade.

Some advanced spectroscopic detection techniques have been developed to detect interphase formation in conventional Li-metal batteries, such as *in situ* X-ray and neutron-based techniques, introduced in detail in our former review. [135]. However, many in-situ techniques have not yet been applied to the AFLBs system. It can be expected that with efforts continuously being devoted, more and more of these versatile techniques will be applied to develop high-performance AFLBs.

7. Summary and perspectives

Anode-free Li-metal batteries (AFLBs) are promising battery systems with higher energy density and excellent safety. However, most of the reported AFLBs were based on intercalation cathodes. The research on anode-free topologies is still in its early stage. AFLB systems based on liquid electrolytes still face a significant challenge in practical use due to their short cycle life. For the formation and evolution mechanism of SEI layers, the origin of the substantial capacity loss and low CE of AFLBs was clarified in this review.

The progress in developing AFLBs via tuning Li-growth and engineering SEI was summarized. Despite the advances in developing excellent electrolytes (Table 3) and current collectors (Table 4), further work is still needed to maximize cell CE and cycle life to achieve the benchmark for AFLBs commercialization. Thus, the following aspects should be considered in future AFLBs research:

(i) Controlling homogenous and compact deposited Li-metal and SEI layers are essential for improving the cycle stability of AFLBs. The SEI morphology is influenced mainly by the deposition of Li-metal. The interactions between Li-metal and electrolytes influence SEI properties. The design of current collectors and electrolytes should be studied more systematically to successfully manage the Li-nucleation and growth process by lowering the nucleation overpotential. Designing high-surface-area or 3D current collectors is a viable technique to boost the energy density of AFLBs. Furthermore, 3D provides a larger area for Li-metal deposition, minimizing the non-coplanar Li-metal growth and resulting in more homogeneous SEI layers. Rapid advances in novel etching technologies, such as photolithography and 3D printing, would pave the way for more efficient design and manufacturing of novel 3D-structured current collectors.

(ii) Improving the mechanical properties of SEI layers can effectively protect the deposited Li-metal and reduce Li-ion consumption during cycling. Li-metal anodes undergo significant volume changes during cycling. Therefore, mechanically stable SEI layers can accommodate volume-change-induced stress with fewer cracks. Using fluorine-based organic solvents or adding fluorine-containing additives helps to form a compact and LiF-riched SEI layer with appropriate mechanical properties. That improves the cycling stability of AFLBs. Furthermore, designing an artificial SEI with good mechanical properties and high Li-ion conductivity can protect the Li-metal from electrolyte corrosion. That reduces side reactions and improves battery capacity stability. The
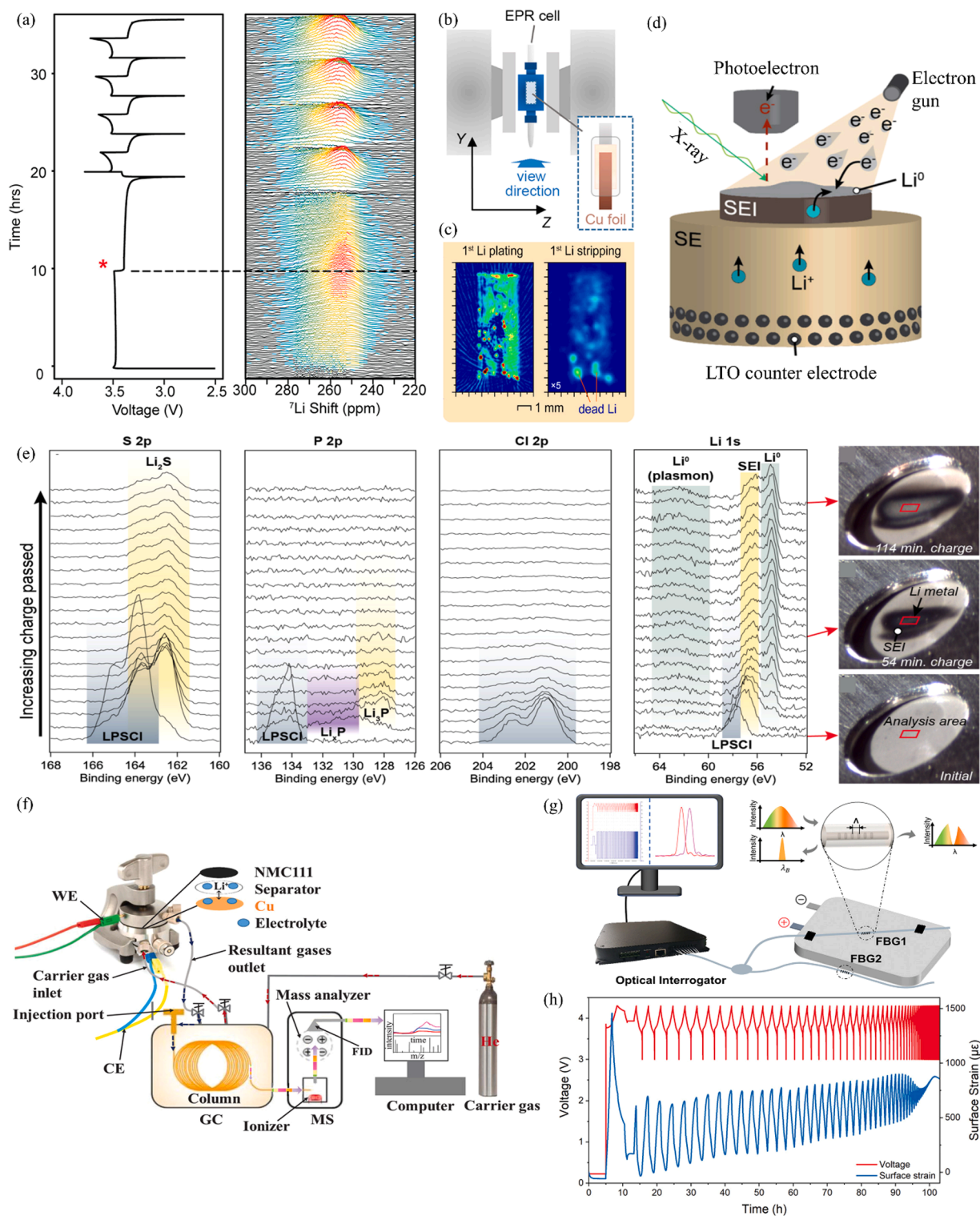
Fig. 18. (a) Galvanostatic cycling of *in situ* Cu-LFP cells where a current of 0.1 mA cm^{-2} was used for the first cycle and 0.5 mA cm^{-2} for subsequent cycles; plating and stripping were performed for a constant capacity of 1 mAh cm^{-2} and In situ ^{7}Li NMR spectra. Reproduced with permission [173]. Copyright 2021, American Chemical Society. (b) Schematic for the EPR coordinate frame and the EPR cell orientation. The inset shows the view direction of the 2D spatial–spatial images; (c) In situ spatial–spatial EPR for the first cycle. Reproduced with permission [174]. Copyright 2021, American Chemical Society. (d) Operando XPS cell using an electron gun as a virtual electrode; (e) Operando XPS core scans and corresponding optical microscopy for the LPSCl sample, with each scan corresponding to an additional 6 min of charging. Reproduced with permission [175]. Copyright 2021, IOP publication. (f) Schematic illustration of the EL-CELL connecting with GC–MS designed for online gas formation analysis in the AFLBs. Reproduced with permission [176]. Copyright 2020, Wiley-VCH GmbH. (g) The schematic diagram of the experimental setup for strain monitoring; (h) The galvanostatic curves and strain signal of the lifetime of the pouch cell. Reproduced with permission [177]. Copyright 2022, Wiley-VCH GmbH.

Table 3

Summary of electrolyte optimization for AFLBs.

Category	Anode	Cathode	Electrolyte	Cut-off Voltage (V)	Current density	Discharge Capacity	Capacity retention (%-cycles)	Average CE	Ref
Co-solvents	Cu	NMC532	1M LiPF$_6$ in FEC/TFEC	1.25–4.5	0.5C	170 mAh/g	55%−60	99%	[182]
	Cu	NMCAM	LiFSI in DME/LHCE	3.5–4.4	1/3 C	200 mAh/g	40%−80	99.3%	[23]
	Cu	NMC 622	Triethylmethylphosphonium bis (fluorosulfonyl)imide/LiFSI=1:1	4.5–1.5	0.5C	4.6 mAh/cm^2	53%−100	99.4%	[183]
High concentration electrolytes	Cu	LFP	4M LiFSI in DME	3.0–3.8	1C	148 mAh/g	54%−100	99.8%	[24]
	Cu	LFP	3M LiFSI in DOL/DME	3.0–3.8	1/3 C	1.5 mAh/cm^2	40%−100	98.78%	[105]
	Cu	NCM811	6M LiFSI in DME	2.2–4.3	0.2C	203 mAh/cm^2	84 %−100	94.92%	[35]
	Cu	NCM811	6M LiFSI in DME	2.2–4.3	0.2C	12 mAh/cm^2	96%−100	–	[184]
Dual-salt electrolytes	Cu	LFP	2M LiFSI+1M LiTFSI in DOL/DME	3.0–3.8	1/3C	1.5 mAh/cm^2	32%−100	98.9%	[25]
	Cu	LFP	1M LiNO$_3$+1M LiFSI in DME	3.0–3.8	0.1C	–	66%−50	99.17%	[185]
	Cu	NMC622	4.6M LiFSI+2.3M LiTFSI in DME	2.7–4.4	1/3C	1.44 mAh/cm^2	55%−54	98.37%	[107]
	Cu	NMC532	1M LiDFOB+0.2M LiBF$_4$ in FEC/DEC	3.6–4.5	0.5C	2.4 mAh/cm^2	80%−90	99.75%	[73]
Additives	Cu	NMC111	2M LiPF$_6$ in EC/DEC+50% FEC	2.5–4.3	0.1C	2 mAh/cm^2	40%−50	97.8%	[106]
	Cu	NMC111	1M LiPF$_6$ in EC: DEC+0.5M KNO$_3$	2.5–4.3	0.1C	156.2 mAh/g	40%−50	95.21%	[117]
	Cu	NMC111	1M LiPF$_6$ in EC/ DEC+2% KPF$_6$-TMSP	2.5–4.3	0.1C	2.03 mAh/cm^2	48%−20	95.21%	[118]
	Ni	Li$_2$S	1M LiTFSI in DOL/DME + 2wt% LiNO$_3$	1.8–2.8	0.1C	969 mAh/g	84%−100	–	[186]
	Cu	LFP	2M LiFSI + 0.1M LiNO$_3$ in DME/TFTE (1:1 in v/v)	2.5–4	1/3 C	150 mAh/g	64.5%−50	99.3%	[187]
	Cu	NCM811	1M LiFSI into DME/HFE = 1/2vol.%+ 0.02M LiDFOB	2.7–4.3	0.3C	3.0 mAh/cm^2	95%−50	99.4%	[188]
	Cu	LFP	2M LiFSI in DME + 5mM CsI$_3$	2.5–3.8	0.5C	170 mAh/g	80%−110	85%	[189]
	Cu	NCM811	4M LiTFSI in FEC + succinonitrile	3–4.3	0.1C	190.1 mAh/g	60.9%−50	99%	[190]
	Cu	NCA	1M LiPF$_6$ in EC/DEC + LiNO$_3$-G2	3–4.3	1C	2 mAh/cm^2	73%−50	98.58%	[191]
	Ni	Li$_2$S	1.0M LiTFSI + 0.5M LiNO$_3$ in DOL/DME+SnI$_4$	1.7–2.8	0.1C	–	80%−95	99%	[192]
Solid-state electrolyte	Cu	LCO	LiPON electrolyte	3.0–4.2	–	–	80%−1000	99.98%	[193]
	Cu	LFP	Ternary-salt GPE	2.5–4.0	0.2C	1.73 mAh/cm^2	62.2%−100	99.5%	[194]
	Cu	Li$_2$S	CGPE-LiTFSI-Ti$_3$C$_2$T$_x$ MXene	1.7–2.8	0.25C	819 mAh/g	80%−300	99.2%	[195]

artificial interface layer can be prepared either by the spin coating technology, physical/chemical vapor deposition, and self-assembly on the substrate or by forming the coordinate bond directly on the substrate. With novel deposition techniques, such as ALD and PLD, versatile compounds with high ionic conductivity and electrochemical compatibility can be deposited onto the current collectors of AFLBs. Additionally, more complex nanocomposites and polymers can be applied as artificial layers by spin-coating, which is easy and cheap. Furthermore, the in-situ coating is a novel method to create stable SEI layers. The conversion compounds, such as Cu$_3$N, can be deposited on the current collector. They make Li-ions flux more uniform, suppressing Li dendrites growth and reacting with Li ions to form stable SEI layers.

(iii) More Li could be placed into the batteries to compensate for the Li loss. That can be an effective way to extend cycle life. Prelithiation of the current collectors, particularly lithiophilic ones, could indeed reduce the surface potential and promotes the Li nucleation and Li growth processes. In addition, it can also achieve a higher cycling capacity. Enlarging Li-content can compensate for the Li loss at the cathode side. An example of such a technique is coating a Li-containing multifunctional sacrificial agent on the cathode surface, including Li$_2$O, LiF, or Li$_2$CO$_3$.

(iv) Test conditions influence the cycling performance and energy density of AFLBs, including working current density, temperature, and stacking pressure. Most AFLBs are cycled with lower current densities to ensure a higher capacity and cycling stability. However, using lower current densities requires significant operation time, limiting the practical applicability. Fortunately, recent studies revealed that cycling with a lower charging current and a higher discharging current improved the battery cycling stability. Furthermore, the relative rate of charge *vs.* discharge has a more noticeable impact on the cycle life than the absolute current densities. As a result, optimizing the relative charging and discharging rates will further promote the potential applications of AFLBs. Furthermore, widening the operating temperature range will facilitate the extension of its practical applications.

(v) While a low cut-off voltage helps to improve cycle stability, it reduces the energy density of AFLBs. Exploring how to increase the cycling stability at high cut-off voltages would open the path for AFLBs to deliver higher energy densities. Feasible approaches include high-energy cathode materials, such as high-capacity materials (LCO, NCM811, and Li$_2$S), and high-voltage materials (LiNi$_{0.5}$Mn$_{1.5}$O$_4$ and LiCoPO$_4$) in AFLBs. However, it is worth noting that the stable voltage range of electrolytes must be coupled with the operating cut-off voltages of the applied cathode materials.

(vi) All-solid-state AFLBs exhibit higher energy density and safety. However, improving the compatibility between the solid-electrolyte and the Li-metal anode is the main challenge. In addition to using a combination of existing materials, all-solid-state AFLBs require fundamental material innovations such as solid-electrolyte with higher ionic conductivity and wider electrochemical stable windows, and current collectors with low nucleation, low diffusion energy barriers, and large specific surface areas. Besides, it is essential to further reduce interfacial

Table 4
Summary of current-collectors engineering methods for AFLBs.

Anode	Cathode	Electrolyte	Cut-off Voltage (V)	Current density	Discharge Capacity	Capacity retention (%-cycles)	Average CE	Ref.
Au/PI	LFP	1M LiTFSI in DOL/DME + 2% LiNO$_3$	3.0–3.8	1/3C	1.5 mAh/cm^2	20% −340	98.7%	[196]
Ag@Cu foam	Li$_2$S	1M LiTFSI in DOL/DME +1 wt% LiNO$_3$	1.7–2.8	0.1C	697.5 mAh/g	56%–180	97%	[157]
Stainless steel /Si	LFP	4M LiFSI in DME	3.0–3.8	0.1C	154 mAh/g	47%–100	–	[197]
Cu/Sn	NCA	1M LiPF$_6$ in FEC/EMC	3.0–4.2	0.5C	155 mAh/g	12%–80	97.3%	[198]
Cu/C-Sn	LRM	1M LiPF$_6$ in FEC/FEMC/ HFE	2.0–4.8	0.1C	200 mAh/g	83.3%–20	99.4%	[139]
Cu$_{99}$Zn	TiS$_2$	1M LiTFSI in DOL/DME	1.6–2.6	0.1C	200 mAh/g	55%–120	99.5%	[141]
Cu/Cu$_3$N	LFP	1M LiTFSI in DOL/DME+ 0.4M LiNO$_3$	3.0–3.8	0.5C	0.4 mAh/cm^2	30%–50	97.6%	[199]
Cu/GO	NMC111	1M LiPF$_6$ in EC: DEC+5% FEC	2.5–4.5	0.1C	1.76 mAh/cm^2	44%–50	98%	[115]
Cu/MLG	LFP	1M LiTFSI in DOL/DME+2% LiNO$_3$	3.0–3.8	0.1C	151 mAh/g	61%–100	99.51%	[96]
Cu/SiO$_x$	LFP	4M LiFSI in DME	3.0–3.8	0.5C	120 mAh/g	53%–100	99.3%	[200]
Cu/PEO	LFP	1M LiTFSI in DOL/DME +2wt% LiNO$_3$	3.0–3.8	0.2 C	127 mAh/g	30%–200	98.6%	[152]
Cu/CPE	NMC111	1M LiPF$_6$ in EC/DEC	2.5–4.3	0.1C	2 mAh/cm^2	59%–30	97.6%	[29]
Cu/Benzotriazole	LFP	1M LiNO$_3$+ 1M LiFSI in DME	2.4–4.2	1C	130 mAh/g	73%–5	99.38%	[201]
Cu/PdTe$_2$	LFP	1M LiTFSI in DOL/DME+ 2wt% LiNO$_3$	3.0–3.8	0.2C	107 mAh/g	62%–100	99.5%	[202]
Cu/Ag-PDA-GO	NCM111	1M LiPF$_6$ in EC/DEC + 5% FEC	2.5- 4.5	0.2C	2.25 mAh/cm^2	71% −40	98.6%	[143]
Cu/C-PVDF-LiN	LFP	1M LiPF$_6$ + 0.02M LiNO$_3$ in EC/ DMC+5 wt% VC	2.0 −4.0	1/3C	125 mAh/g	49%–100	99.3%	[203]
Cu/Li$_2$Te	NCM	argyrodite LPSCl	2.5–4.3	0.2 C	165 mAh/g	80%–50	99%	[204]
Cu/SrF$_2$	NCM111	1M LiPF6 in EC/DEC(1:1 v/v) +5% FEC	2.5–4.3	0.2C	2.62 mAh/cm^2	51.01%–60	98.62%	[205]
Cu/Ag-P doped polymer	LFP	3M LiTFSI in DME/DOL(1:1, v/v)	2.5–4.2	1C	3 mAh/cm^2	72%–200	99.8%	[206]
Cu/ silicon–polyacrylonitrile	LNMO	4.5 LiFSI in Py$_{13}$FSI +1wt% LiTFSI	3–4.7	1/3C	120 mAh/g	80%–120	99%	[207]
Cu/BPEI-Ag-LiNO$_3$	NCM811	1.3m LiPF$_6$ in EC/DEC (3/7, v/v) +10 wt.% FEC	3–4.2	0.5C	4.2 mAh/cm^2	61.6%–50	99%	[208]
Cu/Ga-In-Sn	NCM111	1M LiPF6 in FEC/DMC (1:1 v/v)	2.7–4.3	1/3C	150 mAh/g	58%–25	97%	[209]
Cu-CuCl	LFP	1M LiTFSI +1 wt% LiNO$_3$ in DOL/DME (1:1 v/v)	2–4.2	0.1C	125 mAh/g	78.4%–50	99.5%	[210]
Cu-Li$_{4.4}$Sn	NCM811	6M LiFSI in DME	3.0–4.3	0.3C	4 mAh/cm^2	85.5%–50	99%	[211]

defects during the manufacturing process, for example, by improving contact through *in situ* coating or deposition.

(vii) Finally, by integrating theoretical modeling with advanced cryo-electron microscopy and *in-situ* observation techniques, a deeper understanding of the Li-metal deposition/stripping behavior, the SEI formation, and degradation processes become possible. Although the anode-free batteries have been integrated with *in situ* techniques to observe the Li-growth and SEI formation process, such as Raman spectroscopy, SEM, TEM, and OM, many more advanced and accurate analytical techniques such as neutron scattering and X-ray diffraction or scattering, should be developed to connect multidisciplinary domains and substantial open breakthroughs. Furthermore, other abundant alkali metal batteries, such as Na, Mg, and Al, are also considered promising candidates for next-generation anode-free batteries.

Declaration of Competing Interest

The authors declare that they have no known competing financial interests or personal relationships that could have appeared to influence the work reported in this paper.

Data availability

No data was used for the research described in the article.

Acknowledgement

References

[1] R.V. Noorden, The rechargeable revolution: a better battery, Nature 507 (7490) (2014) 26–28.

[2] J. Liu, Z. Bao, Y. Cui, E.J. Dufek, J.B. Goodenough, P. Khalifah, Q. Li, B.Y. Liaw, P. Liu, A. Manthiram, Pathways for practical high-energy long-cycling lithium metal batteries, Nat. Energy 4 (3) (2019) 180–186.

[3] L. Chen, X. Fan, X. Ji, J. Chen, S. Hou, C. Wang, High-energy Li metal battery with lithiated host, Joule 3 (3) (2019) 732–744.

[4] T. Krauskopf, F.H. Richter, W.G. Zeier, J. Janek, Physicochemical concepts of the lithium metal anode in solid-state batteries, Chem. Rev. 120 (15) (2020) 7745–7794.

[5] X.-B. Cheng, R. Zhang, C.-Z. Zhao, Q. Zhang, Toward safe lithium metal anode in rechargeable batteries: a review, Chem. Rev. 117 (15) (2017) 10403–10473.

[6] A. Shao, X. Tang, M. Zhang, M. Bai, Y. Ma, Challenges, strategies, and prospects of the anode- free lithium metal batteries, Adv. Energy Sustain. Res. 3 (4) (2022), 2100197.

[7] A.J. Louli, M. Coon, M. Genovese, J. deGooyer, A. Eldesoky, J.R. Dahn, Optimizing cycling conditions for anode-free lithium metal cells, J. Electrochem. Soc. 168 (2) (2021), 020515.

[8] S. Nanda, A. Gupta, A. Manthiram, Anode- free full cells: a pathway to high-energy density lithium- metal batteries, Adv. Energy Mater. 11 (2) (2020), 2000804.

[9] C. Heubner, S. Maletti, H. Auer, J. Hüttl, K. Voigt, O. Lohrberg, K. Nikolowski, M. Partsch, A. Michaelis, From lithium-metal toward anode-free solid-state batteries: current developments, issues, and challenges, Adv. Funct. Mater. 31 (51) (2021), 2106608.

[10] A.J. Louli, A. Eldesoky, J. deGooyer, M. Coon, C.P. Aiken, Z. Simunovic, M. Metzger, J.R. Dahn, Different positive electrodes for anode-free lithium metal cells, J. Electrochem. Soc. 169 (4) (2022), 040517.

[11] W. Yao, P. Zou, M. Wang, H. Zhan, F. Kang, C. Yang, Design principle, optimization strategies, and future perspectives of anode-free configurations for high-energy rechargeable metal batteries, Electrochem. Energ. Rev. 4 (3) (2021) 601–631.

[12] Z.L. Brown, S. Jurng, B.L. Lucht, Investigation of the lithium solid electrolyte interphase in vinylene carbonate electrolytes using Cu||LiFePO$_4$ cells, J. Electrochem. Soc. 164 (9) (2017) A2186–A2189.

[13] A. Pei, G. Zheng, F. Shi, Y. Li, Y. Cui, Nanoscale nucleation and growth of electrodeposited lithium metal, Nano Lett. 17 (2) (2017) 1132–1139.

[14] B. Horstmann, J. Shi, R. Amine, M. Werres, X. He, H. Jia, F. Hausen, I. Cekic-Laskovic, S. Wiemers-Meyer, J. Lopez, Strategies towards enabling lithium metal in batteries: interphases and electrodes, Energy Environ. Sci. 14 (10) (2021) 5289–5314.

[15] H. Wu, H. Jia, C. Wang, J. Zhang, W. Xu, Recent progress in understanding solid electrolyte interphase on lithium metal anodes, Adv. Energy Mater. 11 (2020), 2003092.

[16] Z. Shadike, S. Tan, R. Lin, X. Cao, E. Hu, X.Q. Yang, Engineering and characterization of interphases for lithium metal anodes, Chem. Sci. 13 (2022) 1547–1568.

[17] J.-G. Zhang, W. Xu, J. Xiao, X. Cao, J. Liu, Lithium metal anodes with nonaqueous electrolytes, Chem. Rev. 120 (24) (2020) 13312–13348.

[18] X. Chen, X.-R. Chen, T.-Z. Hou, B.-Q. Li, X.-B. Cheng, R. Zhang, Q. Zhang, Lithiophilicity chemistry of heteroatom-doped carbon to guide uniform lithium nucleation in lithium metal anodes, Sci. Adv. 5 (2) (2019) eaau7728.

[19] L. Sun, G. Yuan, L. Gao, J. Yang, M. Chhowalla, M.H. Gharahcheshmeh, K. K. Gleason, Y.S. Choi, B.H. Hong, Z. Liu, Chemical vapour deposition, Nat. Rev. Methods Primers 1 (1) (2021) 5.

[20] E. Cha, J.H. Yun, R. Ponraj, D.K. Kim, A mechanistic review of lithiophilic materials: resolving lithium dendrites and advancing lithium metal-based batteries, Mater. Chem. Front. 5 (17) (2021) 6294–6314.

[21] D. Kang, M. Xiao, J.P. Lemmon, Artificial solid-electrolyte interphase for lithium metal batteries, Batteries Supercaps 4 (3) (2021) 445–455.

[22] Z. Tong, B. Bazri, S.-F. Hu, R.-S. Liu, Interfacial chemistry in anode-free batteries: challenges and strategies, J. Mater. Chem. A 9 (12) (2021) 7396–7406.

[23] L. Su, H. Charalambous, Z. Cui, A. Manthiram, High-efficiency, anode-free lithium–metal batteries with a close-packed homogeneous lithium morphology, Energy Environ. Sci. 15 (2) (2022) 843–854.

[24] J. Qian, B.D. Adams, J. Zheng, W. Xu, W.A. Henderson, J. Wang, M.E. Bowden, S. Xu, J. Hu, J.-G. Zhang, Anode-free rechargeable lithium metal batteries, Adv. Funct. Mater. 26 (39) (2016) 7094–7102.

[25] T.T. Beyene, H.K. Bezabh, M.A. Weret, T.M. Hagos, C.J. Huang, C.H. Wang, W. N. Su, H. Dai, B.J. Hwang, Concentrated dual-salt electrolyte to stabilize li metal and increase cycle life of anode free Li-metal batteries, J. Electrochem. Soc. 166 (8) (2019) A1501–A1509.

[26] B.J. Neudecker, N.J. Dudney, J.B. Bates, ''Lithium-free'' thin-film battery with in situ plated Li anode, J. Electrochem. Soc. 147 (2) (2000) 517–523.

[27] Y.-G. Lee, S. Fujiki, C. Jung, N. Suzuki, N. Yashiro, R. Omoda, D.-S. Ko, T. Shiratsuchi, T. Sugimoto, S. Ryu, J.H. Ku, T. Watanabe, Y. Park, Y. Aihara, D. Im, I.T. Han, High-energy long-cycling all-solid-state lithium metal batteries enabled by silver–carbon composite anodes, Nat. Energy 5 (4) (2020) 299–308.

[28] J. Zhang, H. Chen, M. Wen, K. Shen, Q. Chen, G. Hou, Y. Tang, Lithiophilic 3D copper-based magnetic current collector for lithium-free anode to realize deep lithium deposition, Adv. Funct. Mater. 32 (13) (2022) 2110110.

[29] L.H. Abrha, T.A. Zegeye, T.T. Hagos, H. Sutiono, T.M. Hagos, G.B. Berhe, C.-J. Huang, S.-K. Jiang, W.-N. Su, Y.-W. Yang, B.-J. Hwang, Li₇La₂.₇₅Ca₀.₂₅Zr₁.₇₅Nb₀.₂₅O₁₂@LiClO₄ composite film derived solid electrolyte interphase for anode-free lithium metal battery, Electrochim. Acta 325 (2019), 134825.

[30] N. Von Aspern, G.-V. Röschenthaler, M. Winter, I. Cekic-Laskovic, Fluorine and lithium: ideal partners for high-performance rechargeable battery electrolytes, Angew. Chem. Int. Ed. 58 (45) (2019) 15978–16000.

[31] L. Suo, Y.-S. Hu, H. Li, M. Armand, L. Chen, A new class of Solvent-in-Salt electrolyte for high-energy rechargeable metallic lithium batteries, Nat. Commun. 4 (1) (2013) 1481.

[32] H. Chen, A. Pei, D. Lin, J. Xie, A. Yang, J. Xu, K. Lin, J. Wang, H. Wang, F. Shi, D. Boyle, Y. Cui, Uniform high ionic conducting lithium sulfide protection layer for stable lithium metal anode, Adv. Energy Mater. 9 (22) (2019), 1900858.

[33] X. Zhang, A. Wang, X. Liu, J. Luo, Dendrites in lithium metal anodes: suppression, regulation, and elimination, Acc. Chem. Res. 52 (11) (2019) 3223–3232.

[34] X. Shen, Y. Li, T. Qian, J. Liu, J. Zhou, C. Yan, J.B. Goodenough, Lithium anode stable in air for low-cost fabrication of a dendrite-free lithium battery, Nat. Commun. 10 (1) (2019) 900.

[35] L. Lin, K. Qin, Q. Zhang, L. Gu, L. Suo, Y.S. Hu, H. Li, X. Huang, L. Chen, Li-Rich Li₂[Ni₀.₈Co₀.₁Mn₀.₁]O₂ for anode-free lithium metal batteries, Angew. Chem. Int. Ed. 60 (15) (2021) 8289–8296.

[36] Y. Xu, K. Dong, Y. Jie, P. Adelhelm, Y. Lu, Promoting mechanistic understanding of lithium deposition and solid-lectrolyte interphase (SEI) formation using advanced characterization and simulation methods: recent progress, limitations, and future perspectives, Adv. Energy Mater. 12 (2022) 2200398.

[37] K. Yan, Z. Lu, H.-W. Lee, F. Xiong, P.-C. Hsu, Y. Li, J. Zhao, S. Chu, Y. Cui, Selective deposition and stable encapsulation of lithium through heterogeneous seeded growth, Nat. Energy 1 (3) (2016) 16010.

[38] A.B. Gunnarsdóttir, C.V. Amanchukwu, S. Menkin, C.P. Grey, Noninvasive in situ NMR study of "dead lithium" formation and lithium corrosion in full-cell lithium metal batteries, J. Am. Chem. Soc. 142 (49) (2020) 20814–20827.

[39] W. He, W. Guo, H. Wu, L. Lin, Q. Liu, X. Han, Q. Xie, P. Liu, H. Zheng, L. Wang, X. Yu, D.-L. Peng, Challenges and recent advances in high capacity Li-rich cathode materials for high energy density lithium-ion batteries, Adv. Mater. 33 (50) (2021) 2005937.

[40] L. Zhou, D.L. Danilov, R.-A. Eichel, P.H.L. Notten, Host materials anchoring polysulfides in Li–S batteries reviewed, Adv. Energy Mater. 11 (15) (2021), 2001304.

[41] W. Plieth, 10 - Corrosion and corrosion protection, in: W. Plieth (Ed.), Electrochemistry For Materials Science, Elsevier, Amsterdam, 2008, pp. 291–321.

[42] V. Pande, V. Viswanathan, Computational screening of current collectors for enabling anode-free lithium metal batteries, ACS Energy Lett. 4 (12) (2019) 2952–2959.

[43] X.-R. Chen, B.-C. Zhao, C. Yan, Q. Zhang, Review on Li deposition in working batteries: from nucleation to early growth, Adv. Mater. 33 (8) (2021) 2004128.

[44] P. Bai, J. Li, F.R. Brushett, M.Z. Bazant, Transition of lithium growth mechanisms in liquid electrolytes, Energy Environ. Sci. 9 (10) (2016) 3221–3229.

[45] Y. Xu, A.S. Menon, P.P.R.M.L. Harks, D.C. Hermes, L.A. Haverkate, S. Unnikrishnan, F.M. Mulder, Honeycomb-like porous 3D nickel electrodeposition for stable Li and Na metal anodes, Energy Storage Mater. 12 (2018) 69–78.

[46] K. Dong, Y. Xu, J. Tan, M. Osenberg, F. Sun, Z. Kochovski, D.T. Pham, S. Mei, A. Hilger, E. Ryan, Y. Lu, J. Banhart, I. Manke, Unravelling the mechanism of lithium nucleation and growth and the interaction with the solid electrolyte interface, ACS Energy Lett. 6 (5) (2021) 1719–1728.

[47] X. Gao, Y.-N. Zhou, D. Han, J. Zhou, D. Zhou, W. Tang, J.B. Goodenough, Thermodynamic understanding of Li-dendrite formation, Joule 4 (9) (2020) 1864–1879.

[48] A. Jana, R.E. García, Lithium dendrite growth mechanisms in liquid electrolytes, Nano Energy 41 (2017) 552–565.

[49] P. Barai, K. Higa, V. Srinivasan, Lithium dendrite growth mechanisms in polymer electrolytes and prevention strategies, Phys. Chem. Chem. Phys. 19 (2017) 20493–20505.

[50] H. Liu, X.-B. Cheng, Z. Jin, R. Zhang, G. Wang, L.-Q. Chen, Q.-B. Liu, J.-Q. Huang, Q. Zhang, Recent advances in understanding dendrite growth on alkali metal anodes, EnergyChem 1 (1) (2019), 100003.

[51] C. Ling, D. Banerjee, M. Matsui, Study of the electrochemical deposition of Mg in the atomic level: why it prefers the non-dendritic morphology, Electrochim. Acta 76 (2012) 270–274.

[52] A. Kushima, K.P. So, C. Su, P. Bai, N. Kuriyama, T. Maebashi, Y. Fujiwara, M. Z. Bazant, J. Li, Liquid cell transmission electron microscopy observation of lithium metal growth and dissolution: root growth, dead lithium and lithium flotsams, Nano Energy 32 (2017) 271–279.

[53] T.M. Hagos, H.K. Bezabh, C.J. Huang, S.K. Jiang, W.N. Su, B.J. Hwang, A powerful protocol based on anode-free cells combined with various analytical techniques, Acc. Chem. Res. 54 (24) (2021) 4474–4485.

[54] M. Palomar-Pardavé, B.R. Scharifker, E.M. Arce, M. Romero-Romo, Nucleation and diffusion-controlled growth of electroactive centers: reduction of protons during cobalt electrodeposition, Electrochim. Acta 50 (24) (2005) 4736–4745.

[55] B. Thirumalraj, T.T. Hagos, C.-J. Huang, M.A. Teshager, J.-H. Cheng, W.-N. Su, B.-J. Hwang, Nucleation and growth mechanism of lithium metal electroplating, J. Am. Chem. Soc. 141 (46) (2019) 18612–18623.

[56] S. Li, M. Jiang, Y. Xie, H. Xu, J. Jia, J. Li, Developing high-performance lithium metal anode in liquid electrolytes: challenges and progress, Adv. Mater. 30 (17) (2018), 1706375.

[57] A.N. Dey, B.P. Sullivan, The electrochemical decomposition of propylene carbonate on graphite, J. Electrochem. Soc. 117 (2) (1970) 222.

[58] A. Wang, S. Kadam, H. Li, S. Shi, Y. Qi, Review on modeling of the anode solid electrolyte interphase (SEI) for lithium-ion batteries, NPJ Comput. Mater. 4 (1) (2018) 15.

[59] J.B. Goodenough, Y. Kim, Challenges for rechargeable Li batteries, Chem. Mater. 22 (3) (2010) 587–603.

[60] M. Nagaoka, Y. Suzuki, T. Okamoto, N. Takenaka, A hybrid MC/MD reaction method with rare event-driving mechanism: atomistic realization of 2-chlorobutane racemization process in DMF solution, Chem. Phys. Lett. 583 (2013) 80–86.

[61] N. Takenaka, A. Bouibes, Y. Yamada, M. Nagaoka, A. Yamada, Frontiers in theoretical analysis of solid electrolyte interphase formation mechanism, Adv. Mater. 33 (37) (2021) 2100574.

[62] D. Li, D. Danilov, Z. Zhang, H. Chen, Y. Yang, P.H.L. Notten, Modeling the SEI-formation on graphite electrodes in LiFePO₄ batteries, J. Electrochem. Soc. 162 (6) (2015) A858–A869.

[63] Z. Liu, P. Lu, Q. Zhang, X. Xiao, Y. Qi, L.-Q. Chen, A bottom-up formation mechanism of solid electrolyte interphase revealed by isotope-assisted time-of-flight secondary ion mass spectrometry, J. Phys. Chem. Lett. 9 (18) (2018) 5508–5514.

[64] A. Tokranov, B.W. Sheldon, C. Li, S. Minne, X. Xiao, In situ atomic force microscopy study of initial solid electrolyte interphase formation on silicon electrodes for Li-ion batteries, ACS Appl. Mater. Interfaces 6 (9) (2014) 6672–6686.

[65] S.A. Han, H. Qutaish, M.-S. Park, J. Moon, J.H. Kim, Strategic approaches to the dendritic growth and interfacial reaction of lithium metal anode, Chem. Asian J. 16 (24) (2021) 4010–4017.

[66] S. Jiao, X. Ren, R. Cao, M.H. Engelhard, Y. Liu, D. Hu, D. Mei, J. Zheng, W. Zhao, Q. Li, N. Liu, B.D. Adams, C. Ma, J. Liu, J.-G. Zhang, W. Xu, Stable cycling of high-voltage lithium metal batteries in ether electrolytes, Nat. Energy 3 (9) (2018) 739–746.

[67] G.G. Eshetu, X. Judez, C. Li, M. Martinez-Ibañez, I. Gracia, O. Bondarchuk, J. Carrasco, L.M. Rodriguez-Martinez, H. Zhang, M. Armand, Ultrahigh performance all solid-state lithium sulfur batteries: salt anion's chemistry-induced anomalous synergistic effect, J. Am. Chem. Soc. 140 (31) (2018) 9921–9933.

[68] Y. Jie, X. Ren, R. Cao, W. Cai, S. Jiao, Advanced liquid electrolytes for rechargeable Li metal batteries, Adv. Funct. Mater. 30 (25) (2020), 1910777.

[69] Q. Wang, Z. Yao, C. Zhao, T. Verhallen, D.P. Tabor, M. Liu, F. Ooms, F. Kang, A. Aspuru-Guzik, Y.-S. Hu, M. Wagemaker, B. Li, Interface chemistry of an amide

electrolyte for highly reversible lithium metal batteries, Nat. Commun. 11 (1) (2020) 4188.

[70] Z. Shadike, H. Lee, O. Borodin, X. Cao, X. Fan, X. Wang, R. Lin, S.-M. Bak, S. Ghose, K. Xu, C. Wang, J. Liu, J. Xiao, X.-Q. Yang, E. Hu, Identification of LiH and nanocrystalline LiF in the solid–electrolyte interphase of lithium metal anodes, Nat. Nanotechnol. 16 (5) (2021) 549–554.

[71] Y. Lu, Z. Tu, L.A. Archer, Stable lithium electrodeposition in liquid and nanoporous solid electrolytes, Nat. Mater. 13 (10) (2014) 961–969.

[72] Y.-H. Tan, G.-X. Lu, J.-H. Zheng, F. Zhou, M. Chen, T. Ma, L.-.L. Lu, Y.-H. Song, Y. Guan, J. Wang, Z. Liang, W.-S. Xu, Y. Zhang, X. Tao, H.-B. Yao, Lithium fluoride in electrolyte for stable and safe lithium-metal batteries, Adv. Mater. 33 (42) (2021), 2102134.

[73] R. Weber, M. Genovese, A.J. Louli, S. Hames, C. Martin, I.G. Hill, J.R. Dahn, Long cycle life and dendrite-free lithium morphology in anode-free lithium pouch cells enabled by a dual-salt liquid electrolyte, Nat. Energy 4 (8) (2019) 683–689.

[74] D. Lin, Y. Liu, Y. Li, Y. Li, A. Pei, J. Xie, W. Huang, Y. Cui, Fast galvanic lithium corrosion involving a Kirkendall-type mechanism, Nat. Chem. 11 (4) (2019) 382–389.

[75] E. Markevich, G. Salitra, F. Chesneau, M. Schmidt, D. Aurbach, Very stable lithium metal stripping–plating at a high rate and high areal capacity in fluoroethylene carbonate-based organic electrolyte solution, ACS Energy Lett. 2 (6) (2017) 1321–1326.

[76] M.A. Hope, B.L.D. Rinkel, A.B. Gunnarsdóttir, K. Märker, S. Menkin, S. Paul, I. V. Sergeyev, C.P. Grey, Selective NMR observation of the SEI–metal interface by dynamic nuclear polarisation from lithium metal, Nat. Commun. 11 (1) (2020) 2224.

[77] S. Menkin, C.A. O`Keefe, A.B. Gunnarsdottir, S. Dey, F.M. Pesci, Z. Shen, A. Aguadero, C.P. Grey, Toward an understanding of SEI formation and lithium plating on copper in anode-free batteries, J. Phys. Chem. C 125 (30) (2021) 16719–16732.

[78] W. Zhang, Z. Shen, S. Li, L. Fan, X. Wang, F. Chen, X. Zang, T. Wu, F. Ma, Y. Lu, Engineering wavy-nanostructured anode interphases with fast ion transfer kinetics: toward practical Li-metal full batteries, Adv. Funct. Mater. 30 (39) (2020), 2003800.

[79] J. Chen, T. Liu, L. Gao, Y. Qian, Y. Liu, X. Kong, Tuning the solution structure of electrolyte for optimal solid-electrolyte-interphase formation in high-voltage lithium metal batteries, J. Energy Chem. 60 (2021) 178–185.

[80] Y. Li, W. Huang, Y. Li, A. Pei, D.T. Boyle, Y. Cui, Correlating structure and function of battery interphases at atomic resolution using cryoelectron microscopy, Joule 2 (10) (2018) 2167–2177.

[81] J. Wang, W. Huang, A. Pei, Y. Li, F. Shi, X. Yu, Y. Cui, Improving cyclability of Li metal batteries at elevated temperatures and its origin revealed by cryo-electron microscopy, Nat. Energy 4 (8) (2019) 664–670.

[82] S.J. An, J. Li, C. Daniel, D. Mohanty, S. Nagpure, D.L. Wood, The state of understanding of the lithium-ion-battery graphite solid electrolyte interphase (SEI) and its relationship to formation cycling, Carbon N Y 105 (2016) 52–76.

[83] Y. Han, Y. Jie, F. Huang, Y. Chen, Z. Lei, G. Zhang, X. Ren, L. Qin, R. Cao, S. Jiao, Enabling stable lithium metal anode through electrochemical kinetics manipulation, Adv. Funct. Mater. 29 (46) (2019), 1904629.

[84] G.M. Hobold, J. Lopez, R. Guo, N. Minafra, A. Banerjee, Y. Shirley Meng, Y. Shao-Horn, B.M. Gallant, Moving beyond 99.9% Coulombic efficiency for lithium anodes in liquid electrolytes, Nat. Energy 6 (10) (2021) 951–960.

[85] F.-N. Jiang, S.-J. Yang, H. Liu, X.-B. Cheng, L. Liu, R. Xiang, Q. Zhang, S. Kaskel, J.-Q. Huang, Mechanism understanding for stripping electrochemistry of Li metal anode, SusMat 1 (4) (2021) 506–536.

[86] G. Zardalidis, D. Chatzogiannakis, E. Glynos, F. Farmakis, Electrochemical impedance spectroscopy study of surface film formation on lithium anodes and the role of chain termination on poly(ethylene oxide) electrolytes, ACS Appl. Energy Mater. 4 (7) (2021) 6815–6823.

[87] Y. Liu, X. Xu, M. Sadd, O.O. Kapitanova, V.A. Krivchenko, J. Ban, J. Wang, X. Jiao, Z. Song, J. Song, S. Xiong, A. Matic, Insight into the critical role of exchange current density on electrodeposition behavior of lithium metal, Adv. Sci. 8 (5) (2021) 2003301.

[88] J. Wu, M. Ihsan-Ul-Haq, Y. Chen, J.-K. Kim, Understanding solid electrolyte interphases: advanced characterization techniques and theoretical simulations, Nano Energy 89 (2021), 106489.

[89] R. Guo, B.M. Gallant, Li2O Solid electrolyte interphase: probing transport properties at the chemical potential of lithium, Chem. Mater. 32 (13) (2020) 5525–5533.

[90] C. Chen, T. Zhou, D.L. Danilov, L. Gao, S. Benning, N. Schön, S. Tardif, H. Simons, F. Hausen, T.U. Schülli, R.A. Eichel, P.H.L. Notten, Impact of dual-layer solid-electrolyte interphase inhomogeneities on early-stage defect formation in Si electrodes, Nat. Commun. 11 (1) (2020) 3283.

[91] B. Han, Z. Zhang, Y. Zou, K. Xu, G. Xu, H. Wang, H. Meng, Y. Deng, J. Li, M. Gu, Poor stability of Li2CO3 in the solid electrolyte interphase of a lithium-metal anode revealed by cryo-electron microscopy, Adv. Mater. 33 (22) (2021), 2100404.

[92] D. Aurbach, Review of selected electrode–solution interactions which determine the performance of Li and Li ion batteries, J. Power Sources 89 (2) (2000) 206–218.

[93] S. Chen, Z. Yu, M.L. Gordin, R. Yi, J. Song, D. Wang, A fluorinated ether electrolyte enabled high performance prelithiated graphite/sulfur batteries, ACS Appl. Mater. Interfaces 9 (8) (2017) 6959–6966.

[94] J.J. Woo, V.A. Maroni, G. Liu, Symmetrical impedance study on inactivation induced degradation of lithium electrodes for batteries beyond lithium-ion, J. Electrochem. Soc. 161 (2014) A827.

[95] F.A. Soto, Y. Ma, J.M. Martinez de la Hoz, J.M. Seminario, P.B. Balbuena, Formation and growth mechanisms of solid-electrolyte interphase layers in rechargeable batteries, Chem. Mater. 27 (23) (2015) 7990–8000.

[96] A.A. Assegie, C.-C. Chung, M.-C. Tsai, W.-N. Su, C.-W. Chen, B.-J. Hwang, Multilayer-graphene-stabilized lithium deposition for anode-Free lithium-metal batteries, Nanoscale 11 (6) (2019) 2710–2720.

[97] Z. Yu, H. Wang, X. Kong, W. Huang, Y. Tsao, D.G. Mackanic, K. Wang, X. Wang, W. Huang, S. Choudhury, Y. Zheng, C.V. Amanchukwu, S.T. Hung, Y. Ma, E. G. Lomeli, J. Qin, Y. Cui, Z. Bao, Molecular design for electrolyte solvents enabling energy-dense and long-cycling lithium metal batteries, Nat. Energy 5 (7) (2020) 526–533.

[98] X. Ren, Y. Zhang, M.H. Engelhard, Q. Li, J.-G. Zhang, W. Xu, Guided lithium metal deposition and improved lithium Coulombic efficiency through synergistic effects of LiAsF6 and cyclic carbonate additives, ACS Energy Lett. 3 (1) (2018) 14–19.

[99] B.A. Jote, T.T. Beyene, N.A. Sahalie, M.A. Weret, B.W. Olbassa, Z.T. Wondimkun, G.B. Berhe, C.-J. Huang, W.-N. Su, B.J. Hwang, Effect of diethyl carbonate solvent with fluorinated solvents as electrolyte system for anode free battery, J. Power Sources 461 (2020), 228102.

[100] R. Narayan, R. Dominko, Fluorinated solvents for better batteries, Nat. Rev. Chem. 6 (2022) 449–450.

[101] S. Drvarič Talian, S. Jeschke, A. Vizintin, K. Pirnat, I. Arčon, G. Aquilanti, P. Johansson, R. Dominko, Fluorinated ether based electrolyte for high-energy lithium–sulfur batteries: Li+ solvation role behind reduced polysulfide solubility, Chem. Mater. 29 (23) (2017) 10037–10044.

[102] C.V. Amanchukwu, Z. Yu, X. Kong, J. Qin, Y. Cui, Z. Bao, A new class of ionically conducting fluorinated ether electrolytes with high electrochemical stability, J. Am. Chem. Soc. 142 (16) (2020) 7393–7403.

[103] T.M. Hagos, T.T. Hagos, H.K. Bezabh, G.B. Berhe, L.H. Abrha, S.-F. Chiu, C.-J. Huang, W.-N. Su, H. Dai, B.J. Hwang, Resolving the phase instability of a fluorinated ether, carbonate-based electrolyte for the safe operation of an anode-free lithium metal battery, ACS Appl. Energy Mater. 3 (11) (2020) 10722–10733.

[104] R. Rodriguez, K.E. Loeffler, R.A. Edison, R.M. Stephens, A. Dolocan, A. Heller, C. B. Mullins, Effect of the electrolyte on the cycling efficiency of lithium-limited cells and their morphology studied through in situ optical imaging, ACS Appl. Energy Mater. 1 (11) (2018) 5830–5835.

[105] T.T. Beyene, B.A. Jote, Z.T. Wondimkun, B.W. Olbassa, C.-J. Huang, B. Thirumalraj, C.-H. Wang, W.-N. Su, H. Dai, B.-J. Hwang, Effects of concentrated salt and resting protocol on solid electrolyte interface formation for improved cycle stability of anode-free lithium metal batteries, ACS Appl. Mater. Interfaces 11 (35) (2019) 31962–31971.

[106] T.T. Hagos, B. Thirumalraj, C.-J. Huang, L.H. Abrha, T.M. Hagos, G.B. Berhe, H. K. Bezabh, J. Cherng, S.-F. Chiu, W.-N. Su, B.-J. Hwang, Locally concentrated lipf6 in a carbonate-based electrolyte with fluoroethylene carbonate as a diluent for anode-free lithium metal batteries, ACS Appl. Mater. Interfaces 11 (10) (2019) 9955–9963.

[107] J. Alvarado, M.A. Schroeder, T.P. Pollard, X. Wang, J.Z. Lee, M. Zhang, T. Wynn, M. Ding, O. Borodin, S.M. Ying, Bisalt ether electrolytes: a pathway towards lithium metal batteries with Ni-rich cathodes, Energy Environ. Sci. 12 (2019).

[108] J. Qian, W.A. Henderson, W. Xu, P. Bhattacharya, M. Engelhard, O. Borodin, J.-G. Zhang, High rate and stable cycling of lithium metal anode, Nat. Commun. 6 (1) (2015) 6362.

[109] J. Kalhoff, G.G. Eshetu, D. Bresser, S. Passerini, Safer electrolytes for lithium-ion batteries: state of the art and perspectives, ChemSusChem 8 (13) (2015) 2154–2175.

[110] O.V. Bushkova, T.V. Yaroslavtseva, Y.A. Dobrovolsky, New lithium salts in electrolytes for lithium-ion batteries (Review), Russ. J. Electrochem. 53 (7) (2017) 677–699.

[111] A.J. Louli, A. Eldesoky, R. Weber, M. Genovese, M. Coon, J. deGooyer, Z. Deng, R. T. White, J. Lee, T. Rodgers, R. Petibon, S. Hy, S.J.H. Cheng, J.R. Dahn, Diagnosing and correcting anode-free cell failure via electrolyte and morphological analysis, Nat. Energy 5 (9) (2020) 693–702.

[112] H. Choi, Y. Bae, S.-M. Lee, Y.-C. Ha, H.-C. Shin, B.G. Kim, A LiPF6-LiFSI blended-salt electrolyte system for improved electrochemical performance of anode-free batteries, J. Electrochem. Sci. Technol. 13 (1) (2022) 78–89.

[113] S. Li, Z. Luo, L. Li, J. Hu, G. Zou, H. Hou, X. Ji, Recent progress on electrolyte additives for stable lithium metal anode, Energy Storage Mater. 32 (2020) 306–319.

[114] H. Ye, Y.X. Yin, S.F. Zhang, Y. Shi, L. Liu, X.X. Zeng, R. Wen, Y.G. Guo, L.J. Wan, Synergism of Al-containing solid electrolyte interphase layer and Al-based colloidal particles for stable lithium anode, Nano Energy (2017) 411–417.

[115] Z.T. Wondimkun, T.T. Beyene, M.A. Weret, N.A. Sahalie, C.-J. Huang, B. Thirumalraj, B.A. Jote, D. Wang, W.-N. Su, C.-H. Wang, G. Brunklaus, M. Winter, B.-J. Hwang, Binder-free ultra-thin graphene oxide as an artificial solid electrolyte interphase for anode-free rechargeable lithium metal batteries, J. Power Sources 450 (2020), 227589.

[116] X. Wang, W. Mai, X. Guan, Q. Liu, W. Tu, W. Li, F. Kang, B. Li, Recent advances of electroplating additives enabling lithium metal anodes to applicable battery techniques, Energy Environ. Mater. 4 (3) (2021) 284–292.

[117] N.A. Sahalie, A.A. Assegie, W.-N. Su, Z.T. Wondimkun, B.A. Jote, B. Thirumalraj, C.-J. Huang, Y.-W. Yang, B.-J. Hwang, Effect of bifunctional additive potassium nitrate on performance of anode free lithium metal battery in carbonate electrolyte, J. Power Sources 437 (2019), 226912.

[118] T.M. Hagos, G.B. Berhe, T.T. Hagos, H.K. Bezabh, L.H. Abrha, T.T. Beyene, C.-J. Huang, Y.-W. Yang, W.-N. Su, H. Dai, B.-J. Hwang, Dual electrolyte additives of

potassium hexafluorophosphate and tris (trimethylsilyl) phosphite for anode-free lithium metal batteries, Electrochim. Acta 316 (2019) 52–59.

[119] T. Li, X.-Q. Zhang, P. Shi, Q. Zhang, Fluorinated solid-electrolyte interphase in high-voltage lithium metal batteries, Joule 3 (11) (2019) 2647–2661.

[120] X. Fan, X. Ji, L. Chen, J. Chen, T. Deng, F. Han, J. Yue, N. Piao, R. Wang, X. Zhou, X. Xiao, L. Chen, C. Wang, All-temperature batteries enabled by fluorinated electrolytes with non-polar solvents, Nat. Energy 4 (10) (2019) 882–890.

[121] Y. Qiao, H. Yang, Z. Chang, H. Deng, X. Li, H. Zhou, A high-energy-density and long-life initial-anode-free lithium battery enabled by a Li2O sacrificial agent, Nat. Energy 6 (6) (2021) 653–662.

[122] A. Eldesoky, A.J. Louli, A. Benson, J.R. Dahn, Cycling performance of NMC811 anode-free pouch cells with 65 different electrolyte formulations, J. Electrochem. Soc. 168 (12) (2021), 120508.

[123] S. Nanda, A. Gupta, A. Manthiram, Anode-free full cells: a pathway to high-energy density lithium-metal batteries, Adv. Energy Mater. 11 (2) (2021), 2000804.

[124] M. Balaish, J.C. Gonzalez-Rosillo, K.J. Kim, Y. Zhu, Z.D. Hood, J.L.M. Rupp, Processing thin but robust electrolytes for solid-state batteries, Nat. Energy 6 (3) (2021) 227–239.

[125] P. Hartmann, T. Leichtweiss, M.R. Busche, M. Schneider, M. Reich, J. Sann, P. Adelhelm, J. Janek, Degradation of NASICON-type materials in contact with lithium metal: formation of mixed conducting interphases (MCI) on solid electrolytes, J. Phys. Chem. C 117 (41) (2013) 21064–21074.

[126] N. Kamaya, K. Homma, Y. Yamakawa, M. Hirayama, R. Kanno, M. Yonemura, T. Kamiyama, Y. Kato, S. Hama, K. Kawamoto, A. Mitsui, A lithium superionic conductor, Nat. Mater. 10 (9) (2011) 682–686.

[127] S. Wenzel, S. Randau, T. Leichtweiß, D.A. Weber, J. Sann, W.G. Zeier, J. Janek, Direct observation of the interfacial instability of the fast ionic conductor Li10GeP2S12 at the lithium metal anode, Chem. Mater. 28 (7) (2016) 2400–2407.

[128] W.-Z. Huang, C.-Z. Zhao, P. Wu, H. Yuan, W.-E. Feng, Z.-Y. Liu, Y. Lu, S. Sun, Z.-H. Fu, J.-K. Hu, S.-J. Yang, J.-Q. Huang, Q. Zhang, Anode-free solid-state lithium batteries: a review, Adv. Energy Mater. 12 (26) (2022), 2201044.

[129] R. Murugan, V. Thangadurai, W. Weppner, Fast lithium ion conduction in garnet-type Li7La3Zr2O12, Angew. Chem. Int. Edit. 46 (41) (2007) 7778–7781.

[130] H.-J. Deiseroth, S.-T. Kong, H. Eckert, J. Vannahme, C. Reiner, T. Zaiß, M. Schlosser, Li6PS5X: a class of crystalline Li-rich solids with an unusually high Li + mobility, Angew. Chem. Int. Edit. 47 (4) (2008) 755–758.

[131] S. Chen, J. Zhang, L. Nie, X. Hu, Y. Huang, Y. Yu, W. Liu, All-solid-state batteries with a limited lithium metal anode at room temperature using a garnet-based electrolyte, Adv. Mater. 33 (1) (2021), 2002325.

[132] M.J. Wang, E. Carmona, A. Gupta, P. Albertus, J. Sakamoto, Enabling "lithium-free" manufacturing of pure lithium metal solid-state batteries through *in situ* plating, Nat. Commun. 11 (1) (2020) 5201.

[133] T.A. Zegeye, W.-N. Su, F.W. Fenta, T.S. Zeleke, S.-.K. Jiang, B.J. Hwang, Ultrathin Li6.75La3Zr1.75Ta0.25O12-based composite solid electrolytes laminated on anode and cathode surfaces for anode-free lithium metal batteries, ACS Appl. Energy Mater. 3 (12) (2020) 11713–11723.

[134] Q. Zhao, S. Stalin, C.-Z. Zhao, L.A. Archer, Designing solid-state electrolytes for safe, energy-dense batteries, Nat. Rev. Chem. 5 (3) (2020) 229–252.

[135] C. Chen, M. Jiang, T. Zhou, L. Raijmakers, E. Vezhlev, B. Wu, T.U. Schülli, D. L. Danilov, Y. Wei, R.-A. Eichel, P.H.L. Notten, Interface aspects in all-solid-State Li-based batteries reviewed, Adv. Energy Mater. 11 (13) (2021), 2003939.

[136] T. Ye, L. Li, Y. Zhang, Recent progress in solid electrolytes for energy storage devices, Adv. Funct. Mater. 30 (29) (2020), 2000077.

[137] P. Li, H. Kim, J. Ming, H.-G. Jung, I. Belharouak, Y.-K. Sun, Quasi-compensatory effect in emerging anode-free lithium batteries, eScience 1 (1) (2021) 3–12.

[138] Y. Tian, Y. An, C. Wei, H. Jiang, S. Xiong, J. Feng, Y. Qian, Recently advances and perspectives of anode-free rechargeable batteries, Nano Energy 78 (2020), 105344.

[139] X. Wang, Y. He, S. Tu, L. Fu, Z. Chen, S. Liu, Z. Cai, L. Wang, X. He, Y. Sun, Li plating on alloy with superior electro-mechanical stability for high energy density anode-free batteries, Energy Storage Mater. 49 (2022) 135–143.

[140] J. Chen, J. Xiang, X. Chen, L. Yuan, Z. Li, Y. Huang, Li2S-based anode-free full batteries with modified Cu current collector, Energy Storage Mater. 30 (2020) 179–186.

[141] S. Liu, X. Zhang, R. Li, L. Gao, J. Luo, Dendrite-free Li metal anode by lowering deposition interface energy with Cu99Zn alloy coating, Energy Storage Mater. 14 (2018) 143–148.

[142] L. Lin, L. Suo, Y.-S. Hu, H. Li, X. Huang, L. Chen, Epitaxial induced plating current-collector lasting lifespan of anode-free lithium metal battery, Adv. Energy Mater. 11 (9) (2021), 2003709.

[143] Z.T. Wondimkun, W.A. Tegegne, J. Shi-Kai, C.-J. Huang, N.A. Sahalie, M. A. Weret, J.-Y. Hsu, P.-L. Hsieh, Y.-S. Huang, S.-H. Wu, W.-N. Su, B.J. Hwang, Highly-lithiophilic Ag@PDA-GO film to suppress dendrite formation on Cu substrate in anode-free lithium metal batteries, Energy Storage Mater. 35 (2021) 334–344.

[144] N.A. Sahalie, Z.T. Wondimkun, W.-N. Su, M.A. Weret, F.W. Fenta, G.B. Berhe, C.-J. Huang, Y.-C. Huang, B.J. Hwang, Multifunctional properties of Al2O3/polyacrylonitrile composite coating on Cu to suppress dendritic growth in anode-free Li-metal battery, ACS Appl. Energy Mater. 3 (8) (2020) 7666–7679.

[145] H. Xiang, P. Shi, P. Bhattacharya, X. Chen, D. Mei, M.E. Bowden, J. Zheng, J.-G. Zhang, W. Xu, Enhanced charging capability of lithium metal batteries based on lithium bis(trifluoromethanesulfonyl)imide-lithium bis(oxalato)borate dual-salt electrolytes, J. Power Sources 318 (2016) 170–177.

[146] Y. Li, Y. Li, A. Pei, K. Yan, Y. Sun, C.-L. Wu, L.-M. Joubert, R. Chin, A.L. Koh, Y. Yu, J. Perrino, B. Butz, S. Chu, Y. Cui, Atomic structure of sensitive battery materials and interfaces revealed by cryo-electron microscopy, Science 358 (6362) (2017) 506–510.

[147] D. Aurbach, A. Zaban, Y. Gofer, Y.E. Ely, I. Weissman, O. Chusid, O. Abramson, Recent studies of the lithium-liquid electrolyte interface Electrochemical, morphological and spectral studies of a few important systems, J. Power Sources 54 (1) (1995) 76–84.

[148] R. Xu, X.-B. Cheng, C. Yan, X.-Q. Zhang, Y. Xiao, C.-Z. Zhao, J.-Q. Huang, Q. Zhang, Artificial interphases for highly stable lithium metal anode, Matter 1 (2) (2019) 317–344.

[149] Z. Tu, M.J. Zachman, S. Choudhury, K.A. Khan, Q. Zhao, L.F. Kourkoutis, L. A. Archer, Stabilizing protic and aprotic liquid electrolytes at high-bandgap oxide interphases, Chem. Mater. 30 (16) (2018) 5655–5662.

[150] A. Ferrese, J. Newman, Mechanical deformation of a lithium-metal anode due to a very stiff separator, J. Electrochem. Soc. 161 (9) (2014) A1350–A1359.

[151] C. Lee, X. Wei, J.W. Kysar, J. Hone, Measurement of the elastic properties and intrinsic strength of monolayer graphene, Science 321 (5887) (2008) 385–388.

[152] A.A. Assegie, J.-H. Cheng, L.-M. Kuo, W.-N. Su, B.-J. Hwang, Polyethylene oxide film coating enhances lithium cycling efficiency of an anode-free lithium-metal battery, Nanoscale 10 (13) (2018) 6125–6138.

[153] H. Zhao, D. Lei, Y.-B. He, Y. Yuan, Q. Yun, B. Ni, W. Lv, B. Li, Q.-H. Yang, F. Kang, J. Lu, Compact 3D copper with uniform porous structure derived by electrochemical dealloying as dendrite-free lithium metal anode current collector, Adv. Energy Mater. 8 (19) (2018), 1800266.

[154] Q. Yun, Y.-B. He, W. Lv, Y. Zhao, B. Li, F. Kang, Q.-H. Yang, Chemical dealloying derived 3D porous current collector for Li metal anodes, Adv. Mater. 28 (32) (2016) 6932–6939.

[155] H. Kwon, J.-H. Lee, Y. Roh, J. Baek, D.J. Shin, J.K. Yoon, H.J. Ha, J.Y. Kim, H.-T. Kim, An electron-deficient carbon current collector for anode-free Li-metal batteries, Nat. Commun. 12 (1) (2021) 5537.

[156] B. Han, Y. Zou, G. Xu, S. Hu, Y. Kang, Y. Qian, J. Wu, X. Ma, J. Yao, T. Li, Z. Zhang, H. Meng, H. Wang, Y. Deng, J. Li, M. Gu, Additive stabilization of SEI on graphite observed using cryo-electron microscopy, Energy Environ. Sci. 14 (9) (2021) 4882–4889.

[157] H. Cheng, C. Gao, N. Cai, M. Wang, Ag coated 3D-Cu foam as a lithiophilic current collector for enabling Li2S-based anode-free batteries, Chem. Commun. 57 (30) (2021) 3708–3711.

[158] J.-M. Doux, H. Nguyen, D.H.S. Tan, A. Banerjee, X. Wang, E.A. Wu, C. Jo, H. Yang, Y.S. Meng, Stack pressure considerations for room-temperature all-solid-state lithium metal batteries, Adv. Energy Mater. 10 (1) (2020), 1903253.

[159] S. Jiao, J. Zheng, Q. Li, X. Li, M.H. Engelhard, R. Cao, J.-G. Zhang, W. Xu, Behavior of lithium metal anodes under various capacity utilization and high current density in lithium metal batteries, Joule 2 (1) (2018) 110–124.

[160] J. Zheng, P. Yan, D. Mei, M.H. Engelhard, S.S. Cartmell, B.J. Polzin, C. Wang, J.-G. Zhang, W. Xu, Highly stable operation of lithium metal batteries enabled by the formation of a transient high-concentration electrolyte layer, Adv. Energy Mater. 6 (8) (2016), 1502151.

[161] A.J. Louli, M. Genovese, R. Weber, S.G. Hames, E.R. Logan, J.R. Dahn, Exploring the impact of mechanical pressure on the performance of anode-free lithium metal cells, J. Electrochem. Soc. 166 (8) (2019) A1291–A1299.

[162] D. Aurbach, E. Zinigrad, H. Teller, P. Dan, Factors which limit the cycle life of rechargeable lithium (metal) batteries, J. Electrochem. Soc. 147 (4) (2000) 1274.

[163] D.P. Wilkinson, H. Blom, K. Brandt, D. Wainwright, Effects of physical constraints on Li cyclability, J. Power Sources 36 (4) (1991) 517–527.

[164] T. Hirai, I. Yoshimatsu, J.I. Yamaki, Influence of electrolyte on lithium cycling efficiency with pressurized electrode stack, J. Electrochem. Soc. 141 (3) (1994) 611–614.

[165] D.P. Wilkinson, D. Wainwright, In-situ study of electrode stack growth in rechargeable cells at constant pressure, J. Electroanal. Chem. 355 (1) (1993) 193–203.

[166] Z. Xie, Z. Wu, X. An, X. Yue, J. Wang, A. Abudula, G. Guan, Anode-free rechargeable lithium metal batteries: progress and prospects, Energy Storage Mater. 32 (2020) 386–401.

[167] P.P. Paul, E.J. McShane, A.M. Colclasure, N. Balsara, D.E. Brown, C. Cao, B.-R. Chen, P.R. Chinnam, Y. Cui, E.J. Dufek, D.P. Finegan, S. Gillard, W. Huang, Z. M. Konz, R. Kostecki, F. Liu, S. Lubner, R. Prasher, M.B. Preefer, J. Qian, M.-T. F. Rodrigues, M. Schnabel, S.-B. Son, V. Srinivasan, H.-G. Steinrück, T.R. Tanim, M.F. Toney, W. Tong, F. Usseglio-Viretta, J. Wan, M. Yusuf, B.D. McCloskey, J. Nelson Weker, A review of existing and emerging methods for lithium detection and characterization in Li-ion and Li-metal batteries, Adv. Energy Mater. 11 (17) (2021) 2100372.

[168] T. Foroozan, S. Sharifi-Asl, R. Shahbazian-Yassar, Mechanistic understanding of Li dendrites growth by in- situ/operando imaging techniques, J. Power Sources 461 (2020), 228135.

[169] T. Krauskopf, H. Dippel, H. Hartmann, K. Peppler, B. Mogwitz, F.H. Richter, W. G. Zeier, J. Janek, Lithium-metal growth kinetics on LLZO garnet-type solid electrolytes, Joule 3 (8) (2019) 2030–2049.

[170] C.-J. Huang, B. Thirumalraj, H.-C. Tao, K.N. Shitaw, H. Sutiono, T.T. Hagos, T. T. Beyene, L.-M. Kuo, C.-C. Wang, S.-H. Wu, W.-N. Su, B.J. Hwang, Decoupling the origins of irreversible coulombic efficiency in anode-free lithium metal batteries, Nat. Commun. 12 (1) (2021) 1452.

[171] J.H. Cheng, A.A. Assegie, C.-J. Huang, M.-H. Lin, A.M. Tripathi, C.-C. Wang, M.-T. Tang, F.-F. Song, W.-N. Su, B.J. Hwang, Visualization of lithium plating and stripping via in operando transmission X-ray microscopy, J. Phys. Chem. C 121 (14) (2017) 7761–7766.

[172] T. Fuchs, J. Becker, C.G. Haslam, C. Lerch, J. Sakamoto, F.H. Richter, J. Janek, Current-dependent lithium metal growth modes in "anode-free" solid-state batteries at the Cu|LLZO interface, Adv. Energy Mater. 13 (1) (2023), 2203174.

[173] S. Menkin, C.A. O'Keefe, A.B. Gunnarsdóttir, S. Dey, F.M. Pesci, Z. Shen, A. Aguadero, C.P. Grey, Toward an understanding of SEI formation and lithium plating on copper in anode-free batteries, J. Phys. Chem. C 125 (30) (2021) 16719–16732.

[174] F. Geng, Q. Yang, C. Li, M. Shen, Q. Chen, B. Hu, Mapping the distribution and the microstructural dimensions of metallic lithium deposits in an anode-free battery by in situ EPR imaging, Chem. Mater. 33 (21) (2021) 8223–8234.

[175] A.L. Davis, E. Kazyak, D.W. Liao, K.N. Wood, N.P. Dasgupta, Operando analysis of interphase dynamics in anode-free solid-state batteries with sulfide electrolytes, J. Electrochem. Soc. 168 (7) (2021), 070557.

[176] K.N. Shitaw, S.-C. Yang, S.-K. Jiang, C.-J. Huang, N.A. Sahalie, Y. Nikodimos, H. H. Weldeyohannes, C.-H. Wang, S.-H. Wu, W.-N. Su, B.J. Hwang, Decoupling interfacial reactions at anode and cathode by combining online electrochemical mass spectroscopy with anode-free Li-metal battery, Adv. Funct. Mater. 31 (6) (2021), 2006951.

[177] Y. Li, Y. Zhang, Z. Li, Z. Yan, X. Xiao, X. Liu, J. Chen, Y. Shen, Q. Sun, Y. Huang, Operando decoding of surface strain in anode-free lithium metal batteries via optical fiber sensor, Adv. Sci. 9 (26) (2022), 2203247.

[178] V. Shutthanandan, M. Nandasiri, J. Zheng, M.H. Engelhard, W. Xu, S. Thevuthasan, V. Murugesan, Applications of XPS in the characterization of Battery materials, J. Electron. Spectrosc. 231 (2019) 2–10.

[179] Y. Liu, M. Lorenz, A.V. Ievlev, O.S. Ovchinnikova, Secondary ion mass spectrometry (SIMS) for chemical characterization of metal halide perovskites, Adv. Funct. Mater. 30 (35) (2020), 2002201.

[180] A. Gundlach-Graham, D. Günther, Toward faster and higher resolution LA–ICPMS imaging: on the co-evolution of LA cell design and ICPMS instrumentation, Anal. Bioanal. Chem. 408 (11) (2016) 2687–2695.

[181] D. Rettenwander, R. Wagner, A. Reyer, M. Bonta, L. Cheng, M.M. Doeff, A. Limbeck, M. Wilkening, G. Amthauer, Interface instability of Fe-stabilized Li7La3Zr2O12 versus Li metal, J. Phys. Chem. C 122 (7) (2018) 3780–3785.

[182] M. Genovese, A.J. Louli, R. Weber, S. Hames, J.R. Dahn, Measuring the Coulombic efficiency of lithium metal cycling in anode-free lithium metal batteries, J. Electrochem. Soc. 165 (14) (2018) A3321–A3325.

[183] T. Pathirana, R. Kerr, M. Forsyth, P.C. Howlett, Application of super-concentrated phosphonium based ionic liquid electrolyte for anode-free lithium metal batteries, Sustain. Energy Fuels 5 (16) (2021) 4141–4152.

[184] L. Lin, K. Qin, Y.S. Hu, H. Li, X. Huang, L. Suo, L. Chen, A better choice to achieve high volumetric energy density: anode-free lithium-metal batteries, Adv. Mater. 34 (23) (2022) 2110323.

[185] R. Rodriguez, R.A. Edison, R.M. Stephens, H.-H. Sun, A. Heller, C.B. Mullins, Separator-free and concentrated LiNO3 electrolyte cells enable uniform lithium electrodeposition, J. Mater. Chem. A 8 (7) (2020) 3999–4006.

[186] J. He, A. Bhargav, A. Manthiram, High-performance anode-free Li–S batteries with an integrated Li2S–electrocatalyst cathode, ACS Energy Lett. 7 (2) (2022) 583–590.

[187] K. Qin, J.V. Nguyen, Z. Yang, C. Luo, Anion modification for stable solid electrolyte interphase in anode-free lithium metal batteries, Mater. Today Energy 31 (2023), 101199.

[188] J. Zhang, H. Zhang, L. Deng, Y. Yang, L. Tan, X. Niu, Y. Chen, L. Zeng, X. Fan, Y. Zhu, An additive-enabled ether-based electrolyte to realize stable cycling of high-voltage anode-free lithium metal batteries, Energy Storage Mater. 54 (2023) 450–460.

[189] Z. Jiang, C. Li, J. Mo, H. Yang, H.-W. Li, Q. Zhang, Y. Li, A cation-anion synergic additive achieving long-term stability of lithium metal anode, Chem. Eng. J. 451 (2023), 138580.

[190] X. Ye, J. Wu, J. Liang, Y. Sun, X. Ren, X. Ouyang, D. Wu, Y. Li, L. Zhang, J. Hu, Q. Zhang, J. Liu, Locally fluorinated electrolyte medium layer for high-performance anode-free Li-metal batteries, ACS Appl. Mater. Interfaces 14 (48) (2022) 53788–53797.

[191] C. Zhou, L. Zheng, T. He, M.A. Garakani, S. Abouali, Y. Shen, L. Chen, V. Thangadurai, Rational design of a carbonate-glyme hybrid electrolyte for practical anode-free lithium metal batteries, Energy Storage Mater. 42 (2021) 295–306.

[192] Y. Ren, A. Bhargav, W. Shin, H. Sul, A. Manthiram, Anode-free lithium–sulfur cells enabled by rationally tuning lithium polysulfide molecules, Angew. Chem. Int. Edit. 61 (35) (2022), e202207907.

[193] J.B. Bates, N.J. Dudney, B. Neudecker, A. Ueda, C.D. Evans, Thin-film lithium and lithium-ion batteries, Solid State Ionics 135 (1–4) (2000) 33–45.

[194] Y.-H. Lin, C.-Y. Shih, R. Subramani, Y.-L. Lee, J.-S. Jan, C.-C. Chiu, H. Teng, Ternary-salt gel polymer electrolyte for anode-free lithium metal batteries with an untreated Cu substrate, J. Mater. Chem. A 10 (9) (2022) 4895–4905.

[195] Y. Liu, X. Meng, Z. Wang, J. Qiu, Development of quasi-solid-state anode-free high-energy lithium sulfide-based batteries, Nat. Commun. 13 (1) (2022) 4415.

[196] H.H. Weldeyohannes, L.H. Abrha, Y. Nikodimos, K.N. Shitaw, T.M. Hagos, C. J. Huang, C.-H. Wang, S.-H. Wu, W.-N. Su, B.J. Hwang, Guiding lithium-ion flux to avoid cell's short circuit and extend cycle life for an anode-free lithium metal battery, J. Power Sources 506 (2021), 230204.

[197] C.-A. Lo, C.-C. Chang, Y.-W. Tsai, S.K. Jiang, B.J. Hwang, C.-Y. Mou, H.-L. Wu, Regulated Li electrodeposition behavior through mesoporous silica thin film in anode-free lithium metal batteries, ACS Appl. Energy Mater. 4 (5) (2021) 5132–5142.

[198] S.S. Zhang, X. Fan, C. Wang, A tin-plated copper substrate for efficient cycling of lithium metal in an anode-free rechargeable lithium battery, Electrochim. Acta 258 (2017) 1201–1207.

[199] Q. Li, H. Pan, W. Li, Y. Wang, J. Wang, J. Zheng, X. Yu, H. Li, L. Chen, Homogeneous interface conductivity for lithium dendrite-free anode, ACS Energy Lett. 3 (9) (2018) 2259–2266.

[200] W. Chen, R.V. Salvatierra, M. Ren, J. Chen, M.G. Stanford, J.M. Tour, Laser-induced silicon oxide for anode-free lithium metal batteries, Adv. Mater. 32 (33) (2020), 2002850.

[201] T. Kang, J. Zhao, F. Guo, L. Zheng, Y. Mao, C. Wang, Y. Zhao, J. Zhu, Y. Qiu, Y. Shen, L. Chen, Dendrite-free lithium anodes enabled by a commonly used copper antirusting agent, ACS Appl. Mater. Interfaces 12 (7) (2020) 8168–8175.

[202] J.H. Lee, Y.-G. Cho, D. Gu, S.J. Kim, 2D PdTe2 thin-film-coated current collectors for long-cycling anode-free rechargeable batteries, ACS Appl. Mater. Interfaces 14 (13) (2022) 15080–15089.

[203] H. Liu, X. Yue, X. Xing, Q. Yan, J. Huang, V. Petrova, H. Zhou, P. Liu, A scalable 3D lithium metal anode, Energy Storage Mater 16 (2019) 505–511.

[204] Wang, Y.; Liu, Y.; Nguyen, M.; Cho, J.; Katyal, N.; Vishnugopi, B.S.; Hao, H.; Fang, R.; Wu, N.; Liu, P.; Mukherjee, P.P.; Nanda, J.; Henkelman, G.; Watt, J.; Mitlin, D., Stable anode-free all-solid-state lithium battery through tuned metal wetting on the copper current collector. Adv. Mater., 2022, 2206762.

[205] S.K. Merso, T.M. Tekaligne, H.H. Weldeyohannes, Y. Nikodimos, K.N. Shitaw, S.-K. Jiang, C.-J. Huang, Z.T. Wondimkun, B.A. Jote, L. Wichmann, G. Brunklaus, M. Winter, S.-H. Wu, W.-N. Su, C.-Y. Mou, B.J. Hwang, An in-situ formed bifunctional layer for suppressing Li dendrite growth and stabilizing the solid electrolyte interphase layer of anode free lithium metal batteries, J. Energy Storage 56 (2022), 105955.

[206] S. Pyo, S. Ryu, Y.J. Gong, J. Cho, H. Yun, H. Kim, J. Lee, B. Min, Y. Choi, J. Yoo, Y. S. Kim, Lithiophilic wetting agent inducing interfacial fluorination for long-lifespan anode-free lithium metal batteries, Adv. Energy Mater. 13 (4) (2023), 2203573.

[207] P. Liang, H. Sun, C.-L. Huang, G. Zhu, H.-C. Tai, J. Li, F. Wang, Y. Wang, C.-J. Huang, S.-K. Jiang, M.-C. Lin, Y.-.Y. Li, B.-J. Hwang, C.-A. Wang, H. Dai, A nonflammable high-voltage 4.7V anode-free lithium battery, Adv. Mater. 34 (51) (2022), 2207361.

[208] S. Cho, D.Y. Kim, J.-I. Lee, J. Kang, H. Lee, G. Kim, D.-H. Seo, S. Park, Highly reversible lithium host materials for high-energy-density anode-free lithium metal batteries, Adv. Funct. Mater. 32 (47) (2022), 2208629.

[209] S. Koul, Y. Morita, F. Fujisaki, H. Ogasa, Y. Fujiwara, A. Kushima, Effect of liquid metal coating on improved cycle performance of anode-free lithium metal battery, J. Electrochem. Soc. 169 (2) (2022), 020542.

[210] Z. Li, X. Huang, L. Kong, N. Qin, Z. Wang, L. Yin, Y. Li, Q. Gan, K. Liao, S. Gu, T. Zhang, H. Huang, L. Wang, G. Luo, X. Cheng, Z. Lu, Gradient nano-recipes to guide lithium deposition in a tunable reservoir for anode-free batteries, Energy Storage Mater. 45 (2022) 40–47.

[211] Z. Zhang, H. Luo, Z. Liu, S. Wang, X. Zhou, Z. Liu, A chemical lithiation induced Li4.4Sn lithiophilic layer for anode-free lithium metal batteries, J. Mater. Chem. A 10 (17) (2022) 9670–9679.